Mathematical modelling of nanoparticle melting or freezing

Bisheng Wu
University of Wollongong

Mathematical modelling of nanoparticle melting or freezing

A thesis submitted in fulfillment of the

requirements for the award of the degree of

Doctor of Philosophy

from

University of Wollongong

by

Bisheng Wu

University of Wollongong

School of Mathematics and Applied Statistics

2008

CERTIFICATION

I, Bisheng Wu, declare that this thesis, submitted in fulfilment of the requirements for the award of Doctor of Philosophy, in the School of Mathematics and Applied Statistics, University of Wollongong, is wholly my own work unless otherwise referenced or acknowledged. The document has not been submitted for qualifications at any other academic institution.

Bisheng Wu

May, 2008

Acknowledgements

First of all I would like to express my sincere gratitude to my principle supervisor, Professor James M. Hill, for his constant encouragement and guidance over the past three years. He has walked me through all the stages of the writing of this thesis and without his help this thesis could not have reached its present form.

Thanks are also due to my associate supervisors: Dr. Pei Tillman and Dr. Scott W. McCue, whose insightful comments and advice have been a source of inspiration.

Additionally, I'm very fortunate to be studying in the Nanomechanics Group at the University of Wollongong, which provides a good academic atmosphere. In the group there are excellent members who, living like a family, help each other in daily life. Moreover, the weekly impassioned talks and presentations benefit us greatly. It has become a rewarding experience and one that I will treasure all of my life.

Abstract

This thesis presents a mathematical modelling in nanotechnology. Many experiments and molecular dynamics simulations demonstrate that the melting point of nanoparticles shows a size-dependent characteristic in the nanoscale. Based on the assumption that the material is a pure one, the melting process of spherical and cylindrical particles, especially nanoparticles, is treated as a Stefan moving boundary problem. Analytical or semi-analytical approaches, such as small-time perturbation expansions with front-fixing techniques, large Stefan number limit, integral iterative scheme, and numerical methods, such as enthalpy scheme and front-fixing method, are applied to the one- and or two- phase Stefan problem in spherical and cylindrical domains by taking into account the effect of the interfacial or surface tension. The results from these methods are compared and show excellent agreement to some extent. This thesis may provide a possibility of explaining some interesting phenomena occurring in the physical experiments, i.e. superheating and "abrupt melting", or work as a guide for the potential applications of nanoparticles, for example, drug delivery, nanoimprinting and targeted ablation of tumor cells

In Chapter 1, a simply survey of the research background is given. Chapter 2 studies the full classical two-phase Stefan problems without surface or interfacial tension. By using the approach from large Stefan number limit and small-time perturbation methods, long- and short-time solutions are obtained, and the results from these methods are compared with the numerical enthalpy scheme. The limits of zero Stefan-number and slow diffusion in the inner core are also noted. Chapter 3 presents the melting of a spherical or cylindrical nanoparticle by including the effects of surface tension through the Gibbs-Thomson condition. A single-phase melting limit is derived from the general two-phase formulation, and the resulting equations are studied analytically in the limit of small time and large Stefan number. Further analytical approximations for the temperature distribution and the position of the solid-melt interface are found by applying an integral formulation together with an iterative scheme. All these analytical results are compared with numerical solutions obtained using a numerical front-fixing method, and they are shown to provide good approximations in various regimes. In Chapters 4 and 5, the methods used in above sections are extended to the melting problem for spherical and cylindrical

nanoparticles, respectively. The results from these approaches are compared with those from the numerical front-fixing method.

The original contributions of this thesis are: approximate analytical solutions are obtained for the classical two-phase Stefan problems in a spherical domain; a general single-phase limit for the melting of nanoparticles are derived and analyzed with the correct boundary conditions; a critical radius is found to exist for the blow-up of the one-phase melting; the melting process of spherical and cylindrical nanoparticles are studied analytically from the perspective of Stefan moving boundary problem by including the effect of surface tension; some interesting phenomena observed in physical experiments, i.e. superheating and "abrupt melting", are explained in terms of Stefan problems.

Contents

List of Figures

List of Tables

Nomenclature

k_ℓ^*, k_s^* the thermal conductivities of the solid and liquid phases, respectively

$c_\ell{}^*$, c_s^* the specific heat of the solid and liquid phases, respectively

σ_{sv}, σ_{lv} the interfacial tension between the solid and vapor phases and between the liquid and vapor phases, respectively

T_ℓ^*, T_s^* the physical temperatures of the liquid and solid phases, respectively

T_ℓ, T_s the dimensionless temperatures of the liquid and solid phases, respectively

T_a^* the physical temperature of particle surface

V^*, V the physical and dimensionless initial temperatures of the particle

T_m^* the fusion temperature of the bulk material of the particle

R^*, R the physical and dimensionless positions of the solid/liquid interface

a^* the initial radius of the particle

$T_f^*(R^*)$ the equilibrium temperature at the solid/liquid interface

κ the ratio of the thermal conductivities k_s^*/k_ℓ^*

δ the ratio of the specific heat $c_s^*/c_\ell{}^*$

L the latent heat of fusion

λ the interfacial tension coefficient

α the Stefan number $\alpha = L/[c_\ell(T_a^* - T_m^*(1 - \omega/a^*))]$

β the effective Stefan number $\beta = \alpha - \sigma(1 - \delta) - \delta V$

σ the parameter related to the interfacial tension

Chapter 1

Research overview

1.1 Nanoparticle and its applications

1.1.1 Background of nanoparticles

Nanotechnology and nanoscience stimulate great interest in the fields of physics, chemistry, medicine, electronics, electromechanics and so on. As the building blocks for nanotechnology, nanoparticles have become the focus of tremendous research for their interesting and unique properties, such as quantum conductance [1], enhanced mechanical strength and binding energy [2] and thermal stability [3]. Because of these properties, nanoparticles find wide engineering applications, for example switches, catalyst, novel photoluminescent material, sensors [2], drug delivery [4], nanoimprinting [5] and targeted ablation of tumor cells [6].

1.1.2 Size-dependent properties

One of the most interesting phenomena is that some thermal properties of the material in the nanoscale become greatly different from those in the macro scale. This kind of problem can be traced to W. Thomson in 1870 and J.J. Thomson in 1888 (see [7]) who suggested that the melting temperature of a finite particle would depend on the physical and chemical properties of the surface, also known as thermodynamics size effect. It was not until 1909, however, that a theoretical expression of a size-dependent solid-liquid coexistence temperature was first proposed by Pawlow (see [7]). The melting of tin nanoparticles was observed first experimentally by Takagi [8] with reflection electron diffraction and Blackman & Curzon [9] with transmission electron diffraction. In 1960 Hanszen [10] derived an expression for the melting point of a solid sphere by considering the equilibrium between the solid sphere and

a concentric liquid shell and Wronski [11] used this model to account for the experiments on the melting of small tin particles. During the past several decades, a large number of experiments have been carried out on the melting of some metallic nanoparticles, such as lead, bismuth, indium, silver, copper and tin. Two classical experiments were carried out by Kofman [7] and Buffat & Borel [12]. Buffat & Borel [12] studied the melting point lowering of gold particles and accounted for the results by using several melting models. Kofman [7] utilized the dark-field microscopy technique to investigate the melting of small tin particles on SiO_2 substrate and found that, in addition to the melting point depression, an "abrupt melting" phenomena happens. Moreover, molecular dynamics (MD) simulation on the melting, freezing or coalescence of nanoparticles [13, 14, 15, 16, 17] also indicates that the melting temperature of nanoparticles shows size-dependent characteristics at the nanoscale.

In addition to the size-dependent melting point, researchers also found that some other properties of the material, such as the latent heat of fusion [18, 19, 20], cohesive energy [21], melting enthalpy and melting entropy [22], exhibit size-dependent characteristics.

1.1.3 Melting point model

Because of the enhanced effect of the size-dependent melting point on the physical phenomena, much research has been undertaken to relate the melting point temperature to the interfacial tension of the material. Many models, such as the homogeneous melting and growth model [12], the liquid shell model [11, 12], the liquid nucleation and growth model [23, 24] and the surface-phonon instability model [25] have been proposed. For a spherical or cylindrical nanoparticle, the size-dependent models based on theoretical calculations and empirical results generally take the form

$$T_f^*(R^*) = T_m^* \left(1 - \omega/R^*\right), \quad \omega = 2\lambda/\rho_s L, \tag{1.1}$$

which is the Gibbs-Thomson effect mentioned in the Introduction. Here the melting point temperature of a nanoparticle with radius R^* is denoted by $T_f^*(R^*)$, T_m^* is the bulk melting point of the material, L is the latent heat of fusion, ρ_s is the density of the material in the solid state, and λ the interfacial tension coefficient. The homogeneous melting and growth model considers the thermodynamical equilibrium

between the solid particle and the melted liquid phase. In this model, the interfacial tension coefficient of the nanoparticles may be expressed as

$$\lambda_{\mathrm{HGM}} = \sigma_{sv} - \sigma_{lv}(\rho_s/\rho_\ell)^{2/3}, \tag{1.2}$$

where ρ_ℓ denotes the mass density of the material in liquid state, σ_{sv} is the interfacial tension between the solid and vapour phases and σ_{lv} the interfacial tension between the liquid and vapour phases.

Table 1.1 contains values for these physical properties, using the metals gold, bismuth, tin and lead as examples. We see that for gold, with an atomic radius of about 0.135 nm, we have the value $\omega = 0.2396$ nm. This means that when the radius of a gold particle is $R^* = 10$ nm, containing about 200 atoms, the melting point is about 26.9 K less than the bulk melting point. This is a significant reduction.

Table 1.1: Physical properties of some metals

	ρ_s (kg/m^3)	ρ_l (kg/m^3)	σ_{sv} (N/m)	σ_{lv} (N/m)	L (J/kg)	T_m (K)	λ (J/m^2)	ω (nm)
Au	19.30×10^3	17.31×10^3	0.90	0.74	63718	544.4	0.1473	0.2396
Bi	9.80×10^3	10.05×10^3	0.55	0.38	51900	544.4	0.1812	0.7126
Sn	7.27×10^3	6.99×10^3	0.66	0.55	59225	505.8	0.0957	0.4447
Pb	11.34×10^3	10.66×10^3	0.56	0.45	23020	600.6	0.0893	0.6847

From the equation (1.1), we see that the model becomes invalid when the particle size R^* approaches 0 because the sign of $T_f^*(R^*)$ becomes negative. Experiments show that the melting temperature will never be negative. In fact, Kofman [7] investigated the melting of tin small particles approaching 0 diameter and divided the melting process of nanoparticles into two regimes: the mesoscale regime in which the above melting model works well and the molecular regime in which the melting point does not display a monotonic relation with the particle size.

1.2 Classical Stefan problems

1.2.1 An introduction to the Stefan problem

As the melting or freezing process is closely related to phase change, also known as Stefan problem [26, 27], there exists a moving boundary which separates the material into solid, liquid and sometimes plus gas phases. The Stefan problem

happens very often in daily life and in engineering environments, such as diffusion controlled bubble growth and dissolution, melting or freezing of foods [28], crystal growth, melting and solidification of alloys, production of ice, various problems in mechanics of continuous media [29], the penetration of frost into the earth, ice accretion on vehicles and static structures [30]. So it is of interest and importance to study the properties of these problems, i.e. the temperature distribution, solution concentration and interface motion.

The heat conduction in a pure material is assumed to obey the Fourier equation in the solid and liquid phases

$$\rho c \frac{\partial T^*}{\partial t^*} = \bigtriangledown.(k \bigtriangledown T^*), \tag{1.3}$$

where ρ, c and k are the mass density, specific heat and thermal conductivity of the material, respectively, and can be temperature-dependent. When the phase change happens, the temperatures of different phases at the moving boundary are equal to

$$T_1{}^*(x^*, t^*) = T_2^*(x^*, t^*) = T_f^*(X^*), \quad x^* = X^*, \tag{1.4}$$

where 1 and 2 denote different phases, X^* is the coordinate of the moving boundary, $T_f^*(X^*)$ is the equilibrium temperature . Due to conservation of energy at the moving boundary, the Stefan condition takes the form

$$k_1 \frac{\partial T_1{}^*}{\partial x^*} - k_2 \frac{\partial T_2{}^*}{\partial x^*} = q, \quad \text{on} \quad x^* = X^*, \tag{1.5}$$

where q is the interface heat source because of liberation or absorption of the latent heat.

The above equations represent the general formulations for the classical two-phase Stefan problems with appropriate boundary and initial conditions. It is of importance to mention a special case. When melting a particle with the initial temperature at its fusion point, as heat diffuses only in the liquid phase, the temperature in the solid phase remains constant. In this case we only need to consider the liquid phase. This is the classical one-phase melting problem.

There are several differences between classical melting or freezing and nanoparticle melting or freezing. First, for classical melting or freezing problems, the temperature $T_f^*(X^*)$ at the moving boundary is generally a constant, i.e. the bulk melting

point T_m^*, while for the nanoparticle melting, as mentioned in the previous subsection, $T_f^*(X^*)$ is a function of the moving boundary position $X^*(t^*)$. Secondly, the interface heat source for classical Stefan problem is $q = \rho L \upsilon$, where L is the latent heat and υ is the speed of the interface, while for nanoparticle melting or freeezing q should be modified to be

$$q = \rho V[c_1(T_1^* - T_m^*) - c_2(T_2^* - T_m^*) + L], \quad \text{on} \quad x^* = X^*, \tag{1.6}$$

when considering the superheating or supercooling and the effect of interfacial tension. Physically speaking, the right side of the equation (1.6) can be regarded as the difference between the rate of the heat flux which enters and leaves the interface. A detailed derivation of this equation can be found in [31] by Alexiades & Solomon.

1.2.2 Solving methods

Classical Stefan problems have been greatly investigated since the nineteenth century by Lamé and Clapeyron in 1831, Neumann in the 1860s and Stefan in 1889 [32]. The introduction of the moving boundary makes the problem nonlinear and adds much complexity to the solution. Accordingly, very few analytical solutions are available in closed form, and only exist for one-dimensional cases of an infinite or semi-infinite region with simple boundary and initial conditions and constant physical properties. For example, the Neumann solution, found in [32, 33], is obtained for the freezing of a liquid which is initially at a temperature higher than the melting point in a semi-infinite region and takes the form of functions of the single variable $r/t^{\frac{1}{2}}$, known as similarity solutions. Tao [34] studied the analyticity of solutions of the Stefan problem for a semi-infinite body with arbitrarily prescribed initial and boundary conditions, and proved the existence and convergence of the series solutions. Fazio [35] also used the similarity approach to transform some classes of free boundary value problems into initial value problems.

In addition to similarity solutions, some approximate analytical or asymptotic solutions are proposed. For example, after Savino & Siegel [36] proposed an approximate method using an integral iteration scheme to solve the one-phase freezing problem, Shih & Tsay [37] and Shih & Chou [38] applied this method to successfully study the solidification of a saturated liquid in a cylinder or spherical domain.

The applicability of this method for the spherical and cylindrical cases is due to some suitable transformations which change the governing equations into the conventional form. Dewynne [39] also used this approach to investigate the two-phase melting of spherical and cylindrical particles. This approach works well only when the initial temperature is equal to the fusion temperature of the material and needs lengthy calculations if high order iteration results are required. The convergence and stability of this approach are not verified in above references [36, 37, 38, 39].

The heat balance integral method is another approximate approach proposed by Goodman [40] to solve problems involving a change of phase. This method is based on one basic assumption, that the temperature distribution can be expressed by a polynomial or finite trigonometric series in the space variables. Later Goodman & Shea [41], Yuen [42] and Tsai [43] applied this method to determine the melting rate of a finite or semi-infinite slab which is initially at a uniform temperature below the melting point. Riley & Duck [44] applied this method to a three-dimensional problem of the freezing of cuboid. Charach & Zoglin [45] combined the heat balance integral method and the perturbation theory to study a finite, initially overheated slab and the resulting solution is valid uniformly in time. One interesting example is that Konrad et al. [46] investigated the melting and re-solidification of a subcooled metal powder particle subjected to nanosecond laser heating. As the differences arising in the method's implementation may result in quantitatively distinct solutions, Wood [47] gives some guidance for selecting the appropriate implementation of the method.

Asymptotics approaches are widely used to solve the melting or freezing problems. For example, in the one-phase problem for cylindrical or spherical particles, a small-time series approach has been described by Tao [34], Ostrach & McConnell [48], Wu & Chen [49], Wu et al. [50], Davis & Hill [51] and Hill & Kucera [52]. Hill & Kucera [52] also applied this short-time perturbation method to a two-phase solidification problem with arbitrary initial conditions in cylindrical and spherical domains. Comparing the results from this method with those from accurate enthalpy solutions [53], the short-time solutions do not work well when the Stefan number is large. Fortunately, this shortcoming can be overcome by the large Stefan number asympotics approach and there is a great deal of research on this method. One particular problem, i.e. one-phase solidification initially at fusion temperature

in a cylindrical or spherical domain, was considered by a large number of researchers, such as Pedroso & Domoto [54], Riley, Smith & Poots [55], Huang & Shih [56], who applied the regular perturbation method and found that singular points exist at the end of the solidification. Similar work can be found in Stewartson & Waechter [57] and Soward [58] who provided an asymptotic theory which adequately describes the final temperature profile. Weinbaum & Jiji [59] employed a singular perturbation theory with asymptotic matching techniques to obtain long- and short- time scale results for the melting or freezing in a finite domain initially not at the fusion temperature. Other work on the large Stefan number limit can be found in Davis & Hill [51], Jiji [60], Prud'homme & Nguyen [61], Gammon & Howarth [62, 63, 64], Kharche & Howarth [65, 66] and Feltham & Garside [67].

As few analytical solutions are available, a great number of numerical schemes have been developed. In Crank [32] and Hill and Dewynne [68], some numerical approaches are discussed in detail and some of these methods are compared by Furzeland [69]. These numerical methods can be classified into three main types: the front tracking method, the fixed-domain method and the front-fixing method. For the front tracking method, which computes the position of the moving boundary at each time step, fixed, modified grids or adaptive meshes [70, 71] are used. Murray and Landis [72] proposed two new numerical methods, i.e. fixed and variable space network, either of which is applicable to a region with arbitrary initial and boundary conditions. Tao [73] presented general solutions for the problem of freezing a saturated liquid inside a cylindrical or spherical container. Tien and Churchill [74] considered the two-phase freezing outside an isothermal cylinder by using a four-point Lagrangian interpolation at the moving boundary. Multidimensional solidification/melting problem was solved by Lazaridis [75] using a simple numerical technique. Based on the method of lines with invariant imbedding, Womble [76] solved the two-phase or multiphase Stefan problem. Askar [77] combined finite difference and the finite element method to study the two phase freezing problem.

It should be noted that in the fixed domain methods the enthalpy scheme proposed by Eyre et al. [78] received wide applications for Stefan problems. The advantage of this method is that the direct tracking of the moving boundary is not necessary. Voller & Cross [53] described a simple development over the en-

thalpy formulation leading to very accurate solutions. They also developed an enthalpy formulation for problems about convection/diffusion phase change. Wood et al. [79] evaluated the performance of the enthalpy scheme by considering a two-dimensional melting problem. As standard finite difference discretizations of the enthalpy method have a tendency to oscillate numerically in temperature and phase front position, Tacke [80] derived a procedure to discretize explicit enthalpy formulations for one-dimensional planar phase change problems and removed numerical oscillations. Dewynne [39] applied this method to the one-and two- phase melting problems in spherical and cylindrical domains by combining it with integral formulation. Rostami et al. [81] modified the technique so that it is not necessary that the temperature of the mesh containing the interface remains constant at the melting point.

The third type adopts new space coordinates using the Landau transformation [82] to fix the moving boundary. This approach was first used by Crank [83]. Later Furzeland [69] utilized this method to consider a more general, linear equation with constant coefficients for the unknown temperature variable in each phase.

From the references mentioned we know that a great deal of work has been carried out for the classical Stefan problems. However, most of the work focuses on the cases without interfacial tension, meaning that the temperature at the interface is always equal to the bulk melting point. In fact, the interfacial tension plays an important role in the melting or freezing process of material. We also know from equation (1.1) that, for a cylindrical or spherical particle, when the melting or freezing begins, the equilibrium temperature at the solid/liquid interface will be a function of the position of the interface (or the curvature of the interface). In addition to the effect the interfacial tension has on the temperature at the interface, some interesting issues remain to be answered in this thesis and include: what other effects the interfacial tension has on the temperature distributions, what the melting or freezing rate will be like and when the melting or freezing process is complete.

1.3 Plan of the thesis

This thesis consists of 6 chapters. Chapter 1 presents the background of nanoparticles and gives a simple introduction to the classical Stefan problems. Chapter 2 deals

with the classical two-phase freezing Stefan problem for spherical particles without interfacial tension. In Chapter 3 the formulation for one-phase problem of nanoparticle melting is derived and the results from an integral iterative scheme, small-time solution and large Stefan number limit are compared. Following this, in Chapter 4 the two-phase melting problem for spherical nanoparticles will be formulated, analyzed and discussed with small-time series solutions, large Stefan asympotic approaches and numerical front-fixing technique. Chapter 5 presents the two-phase melting problem for cylindrical nanoparticles. Finally, some concluding marks are given in Chapter 6 with Appendices and References at the end of the thesis.

Chapter 2

Classical two-phase Stefan problems

2.1 Introduction

One of the most simple moving boundary problems to pose is the classical Stefan problem for the inward solidification of a spherical-shaped ball of liquid, or, equivalently, the melting of a spherical ice-ball. For the solidification problem, consider a sphere of liquid of radius a^*, initially at some constant temperature V^*, which is greater than, or equal to, the fusion temperature T_m^*. Now suppose the outer surface of the sphere is held at a temperature T_a^*, which is lower than the fusion temperature. The sphere will begin to solidify inwards. The problem to be solved is to obtain the temperature field in both the liquid and solid phases, as well as to track the location of the interface between the two phases. The corresponding melting problem is equivalent (with appropriate trivial adjustments in language), but for clarity we think of the Stefan problem in terms of solidification, and note that all the results and conclusions in this chapter apply equally well for both cases.

The characterising feature of this solidification problem, which holds for all Stefan problems, is the moving solid-melt boundary. Latent heat will be liberated at this interface between the two phases, and for the classical Stefan problem it is assumed to be removed via conduction only. Thus, the model considered here is that the temperature in each phase is governed by the linear heat equation, and coupled via a boundary condition (the Stefan condition) that describes the dependence of the latent heat removal on the speed of the interface.

The thermal diffusivity in the solid and liquid phases is denoted by κ_s^* and κ_ℓ^*, respectively. By scaling all temperatures, lengths and time with respect to $T_m^* - T_a^*$,

a^* and a^{*2}/κ^*, respectively, and by setting the nondimensional fusion temperature to be zero, the dimensionless solidification problem becomes

$$\frac{\partial T_s}{\partial t} = \frac{\partial^2 T_s}{\partial r^2} + \frac{2}{r}\frac{\partial T_s}{\partial r} \quad \text{in} \quad R(t) < r < 1, \tag{2.1}$$

$$\frac{\partial T_l}{\partial t} = \kappa\left(\frac{\partial^2 T_l}{\partial r^2} + \frac{2}{r}\frac{\partial T_l}{\partial r}\right) \quad \text{in} \quad 0 < r < R(t), \tag{2.2}$$

with fixed boundary conditions

$$T_s = -1 \quad \text{on} \quad r = 1, \tag{2.3}$$

$$T_s = 0 \quad \text{on} \quad r = R, \tag{2.4}$$

$$\frac{\partial T_l}{\partial r} = 0 \quad \text{on} \quad r = 0, \tag{2.5}$$

$$T_l = 0 \quad \text{on} \quad r = R, \tag{2.6}$$

the moving boundary condition (the Stefan condition)

$$\frac{\partial T_s}{\partial r} - \kappa\frac{\partial T_l}{\partial r} = \alpha\frac{\mathrm{d}R}{\mathrm{d}t} \quad \text{on} \quad r = R, \tag{2.7}$$

and initial conditions

$$T_l = V \quad \text{at} \quad t = 0, \quad R = 1 \quad \text{at} \quad t = 0. \tag{2.8}$$

Here $T_s(r,t)$ and $T_l(r,t)$ are the temperature fields in the solid and liquid, respectively, r is the radial distance, t represents time, and $r = R(t)$ describes the location of the solid-melt interface. The three parameters in the problem are the dimensionless initial temperature V, the Stefan number $\alpha = L/(c(T_m^* - T_a^*))$, and the ratio of thermal diffusivities $\kappa = \kappa_\ell^*/\kappa_s^*$. Here c is the specific heat of the substance, which is assumed to be the same constant in both phases, and L is the latent heat of fusion.

Care needs to be taken during the initial stages of the solidification process, since the interface behaves like $dR/dt \to -\infty$ as $t \to 0^+$. In Section 2.5 we seek to understand the small time behaviour by refining the analysis of Kucera & Hill [84], which is not accurate for larger values of the Stefan number. All of the analytical results are compared with numerical solutions in Section 2.6, and finally a brief discussion is included in Section 2.7.

2.2 Large Stefan number limit $\alpha \gg 1$

In this section we generalise the large Stefan number analysis of Pedroso & Domoto [54], Riley, Smith & Poots [55], Stewartson & Waechter [57] and Soward [58] to hold for the full two-phase problem (2.1)-(2.8). The main goal is to determine the extent to which the inner liquid phase affects the outer solid phase and the evolution of the solid-melt interface. In doing so, we wish to establish under what circumstances the second phase can be ignored.

For $\alpha \gg 1$ a large amount of latent heat is being produced at the solid-melt interface $r = R(t)$, the result being that generally the interface moves very slowly. The two exceptions are for $1 - R \ll 1$ or $R \ll 1$; in these two regimes the interface speeds up, with $dR/dt \to -\infty$ as $t \to 0^+$ and $t \to t_f^-$, where t_f is the time it takes for the sphere to completely solidify.

In the large Stefan number limit the two-phase problem breaks up into a number of different time-scales, and these are described below.

2.2.1 Time-scale 1, $t = O(1)$

The first time-scale is for $t = O(1)$. On this short time scale (compared to t_f, which turns out to be $t_f = O(\alpha)$), the temperature in the liquid phase is approximately equal to V for most values of r, but rapidly decreases to $T_l = 0$ near the free boundary $r = R(t)$. Thus there are two length-scales to consider: one away from, and one near, the free boundary.

Note that the analysis on this time-scale is not necessary in order to examine the next time-scale, which is for $t = O(\alpha)$, since it happens that on the next time-scale we are able to apply the initial conditions directly (without matching). However, the results for this time-scale do shed light on the coupling between the two phases for small time, which is something we are most interested in.

2.2.1.1 Inner region, $1 - r = O(\alpha^{-1/2})$

For the inner region we scale the spatial variables as $r = 1 - \alpha^{-1/2}\tilde{r}$, $R(t) = 1 - \alpha^{-1/2}\tilde{R}(t)$, and write

$$T_s \sim \tilde{u}_0(\tilde{r}, t) + \frac{1}{\alpha^{1/2}}\tilde{u}_1(\tilde{r}, t) + O(\alpha^{-1}), \quad T_l \sim \tilde{v}_0(\tilde{r}, t) + \frac{1}{\alpha^{1/2}}\tilde{v}_1(\tilde{r}, t) + O(\alpha^{-1}),$$

$$\tilde{R} \sim \tilde{R}_0(t) + \frac{1}{\alpha^{1/2}}\tilde{R}_1(t) + O(\alpha^{-1}) \quad \text{as} \quad \alpha \to \infty.$$

The leading order partial differential equations are

$$\frac{\partial^2 \tilde{u}_0}{\partial \tilde{r}^2} = 0 \quad \text{in} \quad 0 < \tilde{r} < \tilde{R}_0, \quad \frac{\partial^2 \tilde{v}_0}{\partial \tilde{r}^2} = 0 \quad \text{in} \quad \tilde{r} > \tilde{R}_0, \tag{2.9}$$

with boundary conditions

$$\tilde{u}_0 = -1 \quad \text{on} \quad \tilde{r} = 0, \tag{2.10}$$

$$\tilde{u}_0 = 0, \quad \tilde{v}_0 = 0, \quad \frac{\partial \tilde{u}_0}{\partial \tilde{r}} - \kappa \frac{\partial \tilde{v}_0}{\partial \tilde{r}} = \frac{\mathrm{d}\tilde{R}_0}{\mathrm{d}t} \quad \text{on} \quad \tilde{r} = \tilde{R}_0, \tag{2.11}$$

$$\tilde{v}_0 \sim \tilde{a}_0(t)\tilde{r} \quad \text{as} \quad \tilde{r} \to \infty. \tag{2.12}$$

The function $\tilde{a}_0(t)$ in the last condition comes from matching onto the outer region, as described below.

The next order problems are

$$\frac{\partial^2 \tilde{u}_1}{\partial \tilde{r}^2} = 2\frac{\partial \tilde{u}_0}{\partial \tilde{r}} \quad \text{in} \quad 0 < \tilde{r} < \tilde{R}_0, \quad \frac{\partial^2 \tilde{v}_1}{\partial \tilde{r}^2} = 2\frac{\partial \tilde{v}_0}{\partial \tilde{r}} \quad \text{in} \quad \tilde{r} > \tilde{R}_0, \tag{2.13}$$

with boundary conditions

$$\tilde{u}_1 = 0 \quad \text{on} \quad \tilde{r} = 0, \tag{2.14}$$

$$\tilde{u}_1 + \tilde{R}_1 \frac{\partial \tilde{u}_0}{\partial \tilde{r}} = 0, \quad \tilde{v}_1 + \tilde{R}_1 \frac{\partial \tilde{v}_0}{\partial \tilde{r}} = 0, \quad \frac{\partial \tilde{u}_1}{\partial \tilde{r}} - \kappa \frac{\partial \tilde{v}_1}{\partial \tilde{r}} = \frac{\mathrm{d}\tilde{R}_1}{\mathrm{d}t} \quad \text{on} \quad \tilde{r} = \tilde{R}_0, \tag{2.15}$$

$$\tilde{v}_1 \sim \tilde{a}_0(t)\tilde{r}^2 + \tilde{a}_1(t)\tilde{r} \quad \text{as} \quad \tilde{r} \to \infty. \tag{2.16}$$

Again, the function $\tilde{a}_1(t)$ will be determined by matching with the outer region.

In terms of $\tilde{a}_0(t)$ and $\tilde{a}_1(t)$ the solutions to (2.9)-(2.12) and (2.13)-(2.16) are

$$\tilde{u}_0 = -1 + \frac{\tilde{r}}{\tilde{R}_0}, \quad \tilde{v}_0 = \tilde{a}_0(t)(\tilde{r} - \tilde{R}_0),$$

$$\tilde{u}_1 = \frac{1}{\tilde{R}_0}\tilde{r}^2 - \left(1 + \frac{\tilde{R}_1}{\tilde{R}_0^2}\right)\tilde{r}, \quad \tilde{v}_1 = \tilde{a}_0(\tilde{r}^2 - \tilde{R}_0^2 - \tilde{R}_1) + \tilde{a}_1(\tilde{r} - \tilde{R}_0),$$

with $\tilde{R}_0$ and $\tilde{R}_1$ satisfying the differential equations

$$\frac{\mathrm{d}\tilde{R}_0}{\mathrm{d}t} - \frac{1}{\tilde{R}_0} = -\kappa\tilde{a}_0, \quad \frac{\mathrm{d}\tilde{R}_1}{\mathrm{d}t} + \frac{\tilde{R}_1}{\tilde{R}_0^2} = 1 - \kappa(2\tilde{a}_0\tilde{R}_0 + \tilde{a}_1) \tag{2.17}$$

and initial conditions $\tilde{R}_0(0) = 0$, $\tilde{R}_1(0) = 0$.

2.2.1.2 Outer region, $1 - r = O(1)$

The outer region is for $1 - r = O(1)$. Here we write $T_l = \bar{v}(r, t)$, where

$$\frac{\partial \bar{v}}{\partial t} = \kappa \left(\frac{\partial^2 \bar{v}}{\partial r^2} + \frac{2}{r} \frac{\partial \bar{v}}{\partial r} \right) \quad \text{in} \quad 0 < r < 1,$$

$$\bar{v} = 0 \quad \text{on} \quad r = 1, \quad \frac{\partial \bar{v}}{\partial r} = 0 \quad \text{on} \quad r = 0, \quad \bar{v} = V \quad \text{at} \quad t = 0.$$

By using the method of separation of variables, the solution for $\bar{v}$ is

$$\bar{v} = \frac{2V}{\pi r} \sum_{n=1}^{\infty} \frac{(-1)^{n+1}}{n} \sin(n\pi r) \mathrm{e}^{-n^2\pi^2\kappa t}. \tag{2.18}$$

2.2.1.3 Matching between regions

By rewriting (2.18) in inner variables $(\tilde{r}, t)$ and expanding as $\alpha \to \infty$ we find

$$\tilde{v}_0 \to 0, \quad \tilde{v}_1 \sim 2V\tilde{r} \sum_{n=1}^{\infty} \mathrm{e}^{-n^2\pi^2\kappa t} \quad \text{as} \quad \tilde{r} \to \infty.$$

Thus matching between the two regions gives

$$\tilde{a}_0 = 0, \quad \tilde{a}_1 = 2V \sum_{n=1}^{\infty} \mathrm{e}^{-n^2\pi^2\kappa t}, \quad \tilde{v}_0 = 0, \quad \tilde{v}_1 = 2V(\tilde{r} - \tilde{R}_0) \sum_{n=1}^{\infty} \mathrm{e}^{-n^2\pi^2\kappa t}.$$

With $\tilde{a}_0$ and $\tilde{a}_1$ we may now solve (2.17) for the moving boundary location, yielding

$$\tilde{R}_0 = (2t)^{1/2}, \quad \tilde{R}_1 = \frac{2t}{3} + V \sum_{n=1}^{\infty} \left\{ \frac{2\mathrm{e}^{-n^2\pi^2\kappa}}{n^2\pi^2} - \frac{\operatorname{erf}\left(\pi n \sqrt{\kappa t}\right)}{n^3 \pi^{5/2} \kappa^{1/2} t^{1/2}} \right\}.$$

2.2.1.4 Small-time limit of time-scale 1 solution

Although the solutions given in Section 2.2 (2.2.1) (2.2.1.3) involve infinite series, in practice for $t = O(1)$ only a few terms are necessary to give an accurate solution. However, as t decreases, the terms begin to decay much more slowly, so that for $t \ll 1$ many terms are required to give an accurate solution.

This problem with convergence for $t \ll 1$ is overcome by noting that the function

$$\varpi(z) = \sum_{n=1}^{\infty} \mathrm{e}^{-n^2\pi z} \tag{2.19}$$

has the property

$$1 + 2\varpi(z) = z^{-1/2} \left[1 + 2\varpi\left(1/z\right) \right] \tag{2.20}$$

(Whittaker & Watson [85](page 273), thus

$$\sum_{n=1}^{\infty} \mathrm{e}^{-n^2\pi^2\kappa t} = -\frac{1}{2} + \frac{1}{2\sqrt{\pi\kappa t}}\left[1 + 2\sum_{n=1}^{\infty} \mathrm{e}^{-n^2/\kappa t}\right]. \tag{2.21}$$

It follows that in the inner region we have

$$\begin{aligned} T_l &\sim \frac{V}{\alpha^{1/2}}(\tilde{r} - \tilde{R}_0)\left\{-1 + \frac{1}{\sqrt{\pi\kappa t}}\left[1 + 2\sum_{n=1}^{\infty} \mathrm{e}^{-n^2/\kappa t}\right]\right\}, \\ R &\sim 1 - \frac{(2t)^{1/2}}{\alpha^{1/2}} - \frac{1}{\alpha}\left\{\frac{2}{3}(1+\kappa V)t - \frac{V}{\sqrt{\pi}}(\kappa t)^{1/2}\right. \\ &\quad \left. -\frac{2V}{\sqrt{\pi}}\sum_{n=1}^{\infty}\left[(\kappa t)^{1/2}\mathrm{e}^{-n^2/\kappa t} - \frac{n^2}{(\kappa t)^{1/2}}E_1\left(\frac{n^2}{\kappa t}\right)\right]\right\} \quad \text{as} \quad \alpha \to \infty, \end{aligned}$$

where $E_1(z)$ is the exponential integral defined by

$$E_1(z) = \int_z^{\infty} \frac{\mathrm{e}^{-\xi}}{\xi}, \mathrm{d}\xi.$$

The infinite sums in these expressions contain terms which decay very quickly for $t \ll 1$, and in particular, we now see that

$$R \sim 1 - \frac{(2t)^{1/2}}{\alpha^{1/2}} + \frac{1}{\alpha}\left\{\frac{V}{\sqrt{\pi}}(\kappa t)^{1/2} - \frac{2}{3}(1+\kappa V)t + O(t^{3/2}\mathrm{e}^{-1/\kappa t})\right\} + O(\alpha^{-3/2})$$

as $t \to 0^+$, $\alpha \to \infty$. By solving this equation asymptotically for t we find

$$\frac{t}{\alpha} \sim \left[\frac{1}{2} + \frac{V}{\alpha^{1/2}}\sqrt{\frac{\kappa}{2\pi}} + O(\alpha^{-1})\right](1-R)^2 + \left[-\frac{1}{3}(1+\kappa V) + O(\alpha^{-1/2})\right](1-R)^3 \tag{2.22}$$

$+O((1-R)^4)$ as $\alpha \to \infty$, $R \to 1^-$.

2.2.1.5 Summary of time-scale $t = O(1)$

On the time-scale $t = O(1)$ it can be seen that near the moving boundary the temperature in both phases has an algebraic dependence on the small parameter $\alpha^{-1/2}$. Furthermore, the two phases are coupled, although to leading order both the temperature in the solid and location of the free boundary are independent of the liquid phase.

2.2.2 Time-scale 2, $t = O(\alpha)$

The second time-scale is for $t = O(\alpha)$, so we rescale time as $t = \alpha\hat{t}$, where $\hat{t} = O(1)$. As mentioned earlier, this time-scale can be described without reference to

the previous time-scale $t = O(1)$, since we are able to apply the initial conditions (2.8) directly, and thus it is not necessary to match back onto $t = O(1)$.

2.2.2.1 Liquid phase

In the liquid phase we have the heat conduction problem

$$\frac{1}{\alpha}\frac{\partial T_l}{\partial \hat{t}} = \kappa\left(\frac{\partial^2 T_l}{\partial r^2} + \frac{2}{r}\frac{\partial T_l}{\partial r}\right) \quad \text{in} \quad 0 < r < R,$$

with boundary conditions

$$\begin{aligned} \frac{\partial T_l}{\partial r} &= 0 \quad \text{on} \quad r = 0, \\ T_l &= 0 \quad \text{on} \quad r = R, \end{aligned}$$

and initial conditions

$$T_l = V \quad \text{at} \quad \hat{t} = 0,$$

where we may think of R as being a given function of $\hat{t}$.

This problem is similar to one treated in Nayfeh [86](page 150). We set $\rho = r/R$ and look for a solution of the form

$$T_l \sim \mathrm{e}^{-\alpha g(\hat{t})}\left(v_0(\rho) + \frac{1}{\alpha}v_1(\rho, \hat{t}) + \ldots\right) \quad \text{as} \quad \alpha \to \infty.$$

Thus, to leading order, we obtain the eigenvalue problem

$$\frac{\mathrm{d}^2 v_0}{\mathrm{d}\rho^2} + \frac{2}{\rho}\frac{\mathrm{d}v_0}{\mathrm{d}\rho} + \frac{R^2 g'}{\kappa}v_0 = 0 \quad \text{in} \quad 0 < \rho < 1,$$

$$\frac{\mathrm{d}v_0}{\mathrm{d}\rho} = 0 \quad \text{at} \quad \rho = 0, \quad v_0 = 0 \quad \text{at} \quad \rho = 1,$$

where the dash denotes a derivative with respect to $\hat{t}$. By using the method of separation of variables, the eigenvalues must therefore be of the form $g' = n^2\pi^2\kappa/R$, where n is an integer, and so after satisfying the initial condition $T_l = V$ at $\hat{t} = 0$, we find

$$T_l \sim \frac{2VR}{\pi r}\sum_{n=1}^{\infty}\frac{(-1)^{n+1}}{n}\sin\left(\frac{n\pi r}{R}\right)\exp\left\{-n^2\pi^2\kappa\alpha\int_0^{\hat{t}}\frac{\mathrm{d}\hat{t}}{R^2}\right\} \quad \text{as} \quad \alpha \to \infty. \quad (2.23)$$

2.2.2.2 Solid phase and free boundary location

In the solid phase we have

$$\frac{1}{\alpha}\frac{\partial T_s}{\partial \hat{t}} = \frac{\partial^2 T_s}{\partial r^2} + \frac{2}{r}\frac{\partial T_s}{\partial r} \quad \text{in} \quad R < r < 1,$$

with boundary conditions

$$\begin{aligned} T_s &= -1 \quad \text{on} \quad r = 1, \\ T_s = 0, \quad \frac{\partial T_s}{\partial r} - \kappa\frac{\partial T_l}{\partial r} &= \frac{\mathrm{d}R}{\mathrm{d}\hat{t}} \quad \text{on} \quad r = R. \end{aligned} \tag{2.24}$$

From the analysis in the liquid phase we see that

$$\left.\frac{\partial T_l}{\partial r}\right|_{r=R} \sim -\frac{2V}{R}\sum_{n=1}^{\infty}\exp\left\{-n^2\pi^2\kappa\,\alpha\int_0^{\hat{t}}\frac{\mathrm{d}\hat{t}}{R^2}\right\} \quad \text{as} \quad \alpha \to \infty, \tag{2.25}$$

thus, by noting the form of the Stefan condition (2.24), the liquid phase is expected to contribute exponentially small terms to the location of the free boundary.

With this in mind, and noting the large Stefan number analysis for the one-phase problem given in Pedroso & Domoto [54] and Riley, Smith & Poots [55], we treat r and R as being the two independent variables, and write

$$\begin{aligned} T_s &= u_0(r,R) + \frac{1}{\alpha}\,u_1(r,R) + \frac{1}{\alpha^2}\,u_2(r,R) + O(\alpha^{-3}), \\ \hat{t} &= \hat{t}_0(R) + \frac{1}{\alpha}\,\hat{t}_1(R) + \frac{1}{\alpha^2}\,\hat{t}_2(R) + \ldots + \hat{T}(R;\alpha). \end{aligned} \tag{2.26}$$

The ellipses in (2.26) denote terms which are $O(\alpha^{-3})$ *and* independent of V, while the term $\hat{T}(R;\alpha)$ is exponentially small in α (and will depend on V).

We may read off the solutions

$$u_0 = -\frac{1}{r}\left[1 - \left(\frac{1-r}{1-R}\right)\right], \quad u_1 = \frac{1-r}{6rR(1-R)}\left[1 - \left(\frac{1-r}{1-R}\right)^2\right],$$

$$u_2 = -\frac{(1-r)}{rR^3(1-R)}\left\{\frac{1}{36}\left[1 - \left(\frac{1-r}{1-R}\right)^2\right] + \frac{4R-1}{120}\left[1 - \left(\frac{1-r}{1-R}\right)^4\right]\right\},$$

$$\hat{t}_0 = \frac{1}{2}(1-R)^2 - \frac{1}{3}(1-R)^3, \quad \hat{t}_1 = \frac{1}{6}(1-R)^2, \quad \hat{t}_2 = -\frac{(1-R)^2}{45R^2}, \tag{2.27}$$

from Pedroso & Domoto [54] and Riley, Smith & Poots [55] and, given (2.25) and

the initial condition $R = 1$ at $t = 0$, we find from $(2.24)_2$ that

$$\hat{T} \sim 2\kappa V \int_R^1 \xi(1-\xi)^2 \sum_{n=1}^{\infty} \exp\left\{ n^2\pi^2\kappa\,\alpha \int_\xi^1 \frac{1}{R^2}\frac{\mathrm{d}\hat{t}}{\mathrm{d}R}\,\mathrm{d}R \right\} \mathrm{d}\xi \quad \text{as} \quad \alpha \to \infty. \quad (2.28)$$

Substitute $\hat{t}_0$, $\hat{t}_1$ and $\hat{t}_2$ into (2.26) and we may rewrite the integral in the braces as

$$\int_\xi^1 \frac{1}{R^2}\frac{\mathrm{d}\hat{t}}{\mathrm{d}R}\,\mathrm{d}R = 1 - \xi + \ln\xi + \frac{1}{3\alpha}\left(1 - \ln\xi - \xi^{-1}\right) + \ldots. \quad (2.29)$$

The temperature in the inner core is now found by combining (2.23) and (2.29).

2.2.2.3 Small-time limit of time-scale 2 solution

As with many of the expressions given in Section 2.2 (2.2.1) (2.2.1.3), parts of the solutions in Section 2.2 (2.2.2) (2.2.2.2) involve infinite series. For $t = O(\alpha)$ these series contain terms which decay extremely quickly, with the first term being sufficient for practical purposes. However, as $\hat{t} \to 0$ we have $R \to 1^-$, and

$$1 - R + \ln R + \frac{1}{3\alpha}\left(1 - \ln R - R^{-1}\right) + O(\alpha^{-2}) \sim \left[-\frac{1}{2} - \frac{1}{6\alpha} + O(\alpha^{-2})\right](1-R)^2$$

$$+ \left[-\frac{1}{3} - \frac{2}{9\alpha} + O(\alpha^{-2})\right](1-R)^3 + \left[-\frac{1}{4} - \frac{1}{4\alpha} + O(\alpha^{-2})\right](1-R)^4 + O\left((1-R)^5\right)$$

as $R \to 1$, $\alpha \to \infty$. Thus in this limit care must be taken, as an increasing number of terms are required to obtain an accurate solution.

To obtain the limiting behaviour as $R \to 1^-$ ($\hat{t} \to 0$) of our large Stefan number solution, we again use the property (2.20) of the function defined in (2.19). By expanding and then integrating term by term, we find

$$\hat{T} \sim \left[\frac{V}{\alpha^{1/2}}\sqrt{\frac{\kappa}{2\pi}} + O(\alpha^{-1})\right](1-R)^2 + \left[-\frac{\kappa V}{3} + O(\alpha^{-1/2})\right](1-R)^3 + O((1-R)^4)$$

as $R \to 1^-$. Thus, from (2.26) and (2.27) we can derive the expression (2.22).

2.2.2.4 Summary of time-scale $t = O(\alpha)$

On the time-scale $t = O(\alpha)$ we see that the temperature in the solid phase has algebraic dependence on the small parameter α^{-1}, while the temperature in the liquid phase is exponentially small in α. Thus the solid and liquid phases essentially decouple, with the liquid phase contributing only exponentially small contributions to the location of the solid-melt interface (the result is that for $t = O(\alpha)$ the solid

phase and free boundary location look almost identical to that found for the well-studied one-phase problem).

2.2.3 Time-scale 3, $t - t_f = O(1)$

Recall that t_f is the time to complete solidification, and note that $t_f = O(\alpha)$. On the time-scale $t - t_f = O(1)$ (that is, at times close to complete solidification) the interface no longer moves slowly, and so the leading order behaviour in the solid away from the interface is no longer quasi-steady. We expect that at this stage the two phases completely decouple, and that the appropriate analysis coincides with the one-phase problem. The details are given in Riley, Smith & Poots [55], Stewarton & Waechter [57]) and Soward [58].

2.2.4 Time-scale 4, $t - t_f = O(\mathbf{e}^{-2\sqrt{2\pi}\alpha^{1/2}})$

As with the one-phase problem, further analysis is required to remove nonuniformities that arise on the time-scale $t - t_f = O(1)$. This leads to an exponentially short final time-scale, which is for $t - t_f = O(\exp(-2\sqrt{2\pi}\alpha^{1/2}))$. The details are presented by Stewarton & Waechter [57], Soward [58] and Herrero & Velázquez [87], and are not repeated here.

2.2.5 Time to complete solidification

It is of interest to obtain an approximate value for t_f, the time to complete solidification. Unfortunately the expansion (2.26) breaks down before $R = 0$, and thus further analysis is required on the third time-scale $t - t_f = O(1)$, as mentioned above. However, we can read off the value of t_f for the one-phase problem ($V = 0$) from Riley, Smith & Poots [55], Stewarton & Waechter [57] and Soward [58] and simply add the appropriate correction for the second phase.

The leading order behaviour of the additional term is found by considering $\alpha\hat{T}(0;\alpha)$ as $\alpha \to \infty$. This approach works because the second phase contributes algebraic corrections to the solidification time only during the first time-scale $t = O(1)$ (the contributions from the later time-scales are exponentially small, as mentioned

above). The result is that

$$\hat{T}(0;\alpha) \sim \frac{\sqrt{2}V}{\pi^{5/2}\kappa^{1/2}\alpha^{3/2}}\left[1 - \frac{2}{3\pi^{1/2}} + \sum_{n=1}^{\infty}\left(\frac{2e^{-n^2}}{\pi^{1/2}n^2} + \frac{\operatorname{erfc}(n)}{n^3}\right)\right] \tag{2.30}$$

as $\alpha \to \infty$, and thus

$$t_f \sim \frac{\alpha}{6} + \frac{1}{6} - \frac{\sqrt{2}}{\pi^{5/2}\alpha^{1/2}}\left(\zeta(3) - \frac{V}{\kappa^{1/2}}\left[1 - \frac{2}{3\pi^{1/2}} + \sum_{n=1}^{\infty}\left(\frac{2e^{-n^2}}{\pi^{1/2}n^2} + \frac{\operatorname{erfc}(n)}{n^3}\right)\right]\right),$$

where $\zeta(z)$ is the Riemann zeta function. The above result for t_f with $V = 0$ is given by Riley, Smith & Poots [55], Stewarton & Waechter [57] and Soward [58]. The derivation of (2.30) is detailed in Appendix A.

2.2.6 Summary

In summary, for Stefan number $\alpha \gg 1$ the complete solidification time is $O(\alpha)$. On the first time-scale $t = O(1)$ the leading order behaviour near the interface coincides with one-phase problem, with the effects of the liquid phase only coming in at the first correction term. By the second time-scale $t = O(\alpha)$ the liquid phase contributes only exponentially small terms to the location of the solid-melt interface, with the analysis in the solid phase coinciding with the one-phase problem to all algebraic orders. At times close to complete solidification the temperature in the liquid essentially vanishes, and the analysis follows the one-phase problem.

2.3 Zero Stefan number solution $\alpha = 0$

When $\kappa = 1$, there is an exact solution for the case $\alpha = 0$ from the method of separation of variables , namely

$$T_s = T_l = V - \frac{1+V}{r}\sum_{n=0}^{\infty}\left\{\operatorname{erfc}\left(\frac{2n+1-r}{2t^{1/2}}\right) - \operatorname{erfc}\left(\frac{2n+1+r}{2t^{1/2}}\right)\right\}, \tag{2.31}$$

with the location of the moving boundary $r = R(t)$ given implicitly by

$$\frac{RV}{1+V} = \sum_{n=0}^{\infty}\left\{\operatorname{erfc}\left(\frac{2n+1-R}{2t^{1/2}}\right) - \operatorname{erfc}\left(\frac{2n+1+R}{2t^{1/2}}\right)\right\}.$$

Provided $V = O(1)$, the first term in the infinite sums above is usually sufficient, at least for practical purposes.

Using this exact solution we find the complete solidification time t_f to be given

implicitly by

$$\frac{V}{1+V} = \frac{2}{\sqrt{\pi t_f}} \sum_{n=0}^{\infty} \mathrm{e}^{-(2n+1)^2/4t_f}.$$

As $V \to 0$ we have that $t_f \to 0$ (very slowly), and in fact

$$\frac{1}{t_f} \sim 4\ln(1/V) + 2\ln\left(\ln(1/V)\right) + 2\ln(16/\pi) \quad \text{as} \quad V \to 0 \quad (\text{for } \alpha = 0),$$

although this leading order approximation is only accurate for extremely small values of V. Thus the sphere freezes instantly in the zero Stefan number limit of the one-phase problem. This is to be expected, since with $\alpha = 0$ there is no latent heat liberated by the interface, and with $V = 0$ no heat must diffuse out in order to lower the temperature in the core to the fusion temperature.

On the other hand, using a formula similar to (2.21) (see Whittaker & Watson [85] (page 124, with $a = 1/2$), we find

$$\pi^2 t_f \sim \ln V + \ln 2 + V^{-1} \quad \text{as} \quad V \to \infty \quad (\text{for } \alpha = 0),$$

which is of course consistent with the notion that increasing the initial temperature should increase the freezing time.

2.4 Slow diffusion limit $\kappa \ll 1$

In the limit $\kappa \to 0$, which corresponds to slow diffusion in the liquid phase, the two-phase problem reduces to a one-phase problem as described by King & Evans [88, 89], and Struckmeier & Unterreiter [90].

The important point is that in order to derive a leading order model for $V \neq 0$, $\kappa \ll 1$, one cannot simply set $\kappa = 0$ in the Stefan condition (2.7), since putting $\kappa = 0$ into (2.2) suggests that $T_l \equiv$ constant, which is incorrect. The problem is thus singularly perturbed, with an interior layer developing near the solid-melt interface.

The interior layer is for $r = R(t) - \kappa\bar{\rho}$, where $\bar{\rho} = O(1)$. By writing $T_l \sim \bar{V}(\bar{\rho}, t)$ in this region, we have

$$\frac{\partial^2 \bar{V}}{\partial \rho^2} = \frac{\mathrm{d}R}{\mathrm{d}t}\frac{\partial \bar{V}}{\partial \rho},$$

which, provided that $\dot{R} < 0$, implies that $\bar{V} = V(1 - \mathrm{e}^{\dot{R}\bar{\rho}})$, where we have matched with the region away from the sold-melt interface. It follows that for $\kappa \ll 1$, the

approximate one-phase problem is

$$\frac{\partial T_s}{\partial t} = \frac{\partial^2 T_s}{\partial r^2} + \frac{2}{r}\frac{\partial T_s}{\partial r} \quad \text{in} \quad R(t) < r < 1, \tag{2.32}$$

$$T_s = -1 \quad \text{on} \quad r = 1, \tag{2.33}$$

$$T_s = 0 \quad \text{on} \quad r = R, \tag{2.34}$$

$$\frac{\partial T_s}{\partial r} = \frac{\mathrm{d}R}{\mathrm{d}t}(\alpha + V) \quad \text{on} \quad r = R. \tag{2.35}$$

The main point here is that this free boundary problem is the same as the well-studied classical one-phase problem (relevant for $\kappa = O(1)$ and $V = 0$) except that the Stefan number α is replaced by $\alpha + V$. It is now the size of $\alpha + V$ which determines the speed of the solid-melt interface.

2.5 Small-time perturbation $t \ll 1$

In this section we derive an approximate solution to (2.1)-(2.8) which is valid for small time. The approach used is similar to the one outlined in Kucera & Hill [91], however, a number of key refinements have been made, which for certain parameter values lead to a much more accurate approximation.

2.5.1 Review of Kucera & Hill [91]

In Kucera & Hill (1986), a small-time solution to (2.1)-(2.8) is sought by first making the domain-fixing transformation $\xi = (r^{-1} - 1)/(R^{-1} - 1)$, $\tau = R^{-1} - 1$, and then applying the ansatz

$$T_s \sim \tilde{A}_0(\xi) + \tau \tilde{A}_1(\xi) + O(\tau^2), \quad T_l \sim -V + V\left\{\tilde{B}_0(\xi) + \tau \tilde{B}_1(\xi) + O(\tau^2)\right\} \tag{2.36}$$

as $\tau \to 0^+$. With this change of variables, the liquid phase is transformed to $1 \leq \xi < \infty$, the solid phase is for $0 \leq \xi \leq 1$, and the time-domain is $0 < \tau < \infty$ (with $\tau \to 0^+$ as $t \to 0^+$).

There are two main concerns with this approach. The first is that the ansatz (2.36) assumes that to leading order the solution in both the solid and liquid phases is almost self-similar; however, this is only true for the outer solid phase. The result is that with their approach, Kucera & Hill [91] were unable to satisfy the initial condition $(2.8)_1$.

The second concern with using (2.36) is that, as a part of the analysis, a Taylor expansion is employed under the assumption that $\xi\tau \ll 1$ for $\tau \ll 1$. However, the quantity $\xi\tau = r^{-1} - 1$ is independent of τ, and in fact becomes very large close to the centre of the sphere, even for very small time. The result is that the scheme is unlikely to converge in the appropriate regime, regardless of how many extra terms in (2.36) are included.

In Section 6 of Kucera & Hill [91] a second method is proposed, which involves looking at small-time perturbation expansions of the form

$$T_s \sim \bar{A}_0(X) + Y\bar{A}_1(X) + O(Y^2), \quad T_l \sim -V + V\left\{\bar{B}_0(X) + Y\bar{B}_1(X) + O(Y^2)\right\}$$

as $Y \to 0^+$, where

$$X = \frac{1-r}{1-R}, \quad Y = 1 - R. \tag{2.37}$$

With this new transformation the liquid phase is now for $1 \leq X < (1-R)^{-1}$ (it is not fixed), the solid phase is for $0 \leq X \leq 1$, and the time-domain is $0 < Y < 1$ (with $Y \to 0^+$ as $t \to 0^+$). In this case Kucera & Hill [91] were able to satisfy the initial condition $(2.8)_1$, but could not satisfy the no flux condition (2.5).

2.5.2 An alternative method

The small-time approximation derived by Kucera & Hill [91] does not agree well with numerical results for moderate to large values of the Stefan number α (see Figure 1, for example); we endeavour to present an alternative approximation in the present section.

2.5.2.1 A summary of the details

As mentioned above, any small-time expansion which assumes that the leading order solution in the liquid phase is self-similar can never satisfy every one of the boundary conditions (2.3)-(2.7) and initial conditions (2.8). Thus this sort of approach can only be approximate in nature, as one boundary condition must be sacrificed, or satisfied only in the limit $t \to 0^+$.

The starting point for our alternative scheme is to look for solutions of the form

$$T_s \sim \frac{1}{r}\left\{A_0(X) + YA_1(X) + O(Y^2)\right\}, \; T_l \sim V + \frac{1}{r}\left\{B_0(X) + YB_1(X) + O(Y^2)\right\}, \tag{2.38}$$

as $Y \to 0^+$, where X and Y are defined in (2.37). We arrive at this ansatz by taking note of the solutions presented in Section 2.2 and Section 2.3, as well as the small-time perturbation series developed by Davis & Hill [51] for the one-phase problem. After substituting (2.38) in (2.1)-(2.4), (2.6)-(2.8), we find that A_0, A_1, B_0 and B_1 satisfy a series of coupled ordinary differential equations

$$\alpha A_0^{"} = a_0 X A_0^{'}, \quad \alpha A_1^{"} = a_0(X A_1^{'} - A_1) + (a_0 + a_1) X A_0^{'},$$

$$\kappa\alpha B_0^{"} = a_0 X B_0^{'}, \quad \kappa\alpha B_1^{"} = a_0(X B_1^{'} - B_1) + (a_0 + a_1) X B_0^{'},$$

with boundary conditions

$$A_0 = 1, \quad A_1 = 0, \quad \text{on} \quad X = 0,$$

$$A_0 = 0, \quad A_1 = 0, \quad B_0 = -V, \quad B_1 = V \quad \text{on} \quad X = 1,$$

$$B_0 = o(1), \quad B_1 = o(X), \quad \text{as} \quad X \to \infty,$$

where $a_0 = A_0^{'}(1) - \kappa B_0^{'}(1)$ and $a_1 = A_1^{'}(1) - \kappa B_1^{'}(1) + \kappa V$. The leading order solutions are

$$A_0 = 1 - \frac{\operatorname{erf}\left(\sqrt{\frac{\gamma}{2}}\, X\right)}{\operatorname{erf}\sqrt{\frac{\gamma}{2}}}, \quad B_0 = -V\, \frac{\operatorname{erfc}\left(\sqrt{\frac{\gamma}{2\kappa}}\, X\right)}{\operatorname{erfc}\sqrt{\frac{\gamma}{2\kappa}}}, \tag{2.39}$$

where γ is the solution to the transcendental equation

$$\gamma\alpha = \frac{1}{L_\ell} \mathrm{e}^{-\gamma/2} - \frac{\kappa V}{L_s} \mathrm{e}^{-\gamma/2\kappa}, \tag{2.40}$$

with L_ℓ and L_s defined by

$$L_\ell = \sqrt{\frac{\pi}{2\gamma}}\, \operatorname{erf}\sqrt{\frac{\gamma}{2}}, \quad L_s = \sqrt{\frac{\kappa\pi}{2\gamma}}\, \operatorname{erfc}\sqrt{\frac{\gamma}{2\kappa}}.$$

Equation (2.40) also arises in the well known Neumann solution (Carslaw & Jaeger [33] page 285) which is for the two-phase semi-infinite planar case. This means that for small time the solidification process in the neighbourhood of $r = 1$ behaves in the same way as the one-dimensional process in a semi-infinite domain.

The next order solutions are

$$A_1 = c_1\, X \left(1 - \mathrm{e}^{\gamma(1-X^2)/2}\right),$$

$$B_1 = c_2\left[\mathrm{e}^{-\gamma X^2/2\kappa} - \sqrt{\frac{\gamma\pi}{2\kappa}}\,X\,\mathrm{erfc}\left(\sqrt{\frac{\gamma}{2\kappa}}X\right)\right] + c_3\,X\mathrm{e}^{-\gamma X^2/2\kappa}, \tag{2.41}$$

where

$$c_1 = \frac{1}{3\gamma}\left(\gamma - \frac{a_1}{\alpha}\right)\frac{1}{L_\ell}\mathrm{e}^{-\gamma/2},$$

$$c_2 = -\frac{kV}{\gamma L_s}\left[1 - \frac{1}{3\gamma}\left(\gamma - \frac{a_1}{\alpha}\right)\frac{1}{L_s}\mathrm{e}^{-\gamma/2\kappa}\right]\left[1 - \frac{\kappa}{\gamma L_s}\mathrm{e}^{-\gamma/2\kappa}\right]^{-1}, \quad c_3 = \frac{V}{3\gamma L_s}\left(\gamma - \frac{a_1}{\alpha}\right),$$

$$\gamma - \frac{a_1}{\alpha} = \frac{3\gamma + \frac{3\kappa V}{\alpha}\left\{\left[1 - \frac{\kappa}{\gamma L_s}\mathrm{e}^{-\gamma/2\kappa}\right]^{-1} - 1\right\}}{3 + \gamma + \frac{V}{\alpha\gamma L_s}\mathrm{e}^{-\gamma/2\kappa}\left\{\kappa\left[1 - \frac{\kappa}{\gamma L_s}\mathrm{e}^{-\gamma/2\kappa}\right]^{-1} - \kappa\gamma - \kappa + \gamma\right\}}.$$

Note that this approximate solution does not satisfy the boundary condition (2.5), and hence for each value of time $t \ll 1$, there will be a small region near $r = 0$ for which the solution is not appropriate. This point is reviewed in Section 2.5 (2.5.3).

An approximate location of the moving boundary is given by

$$t \approx \int_1^R \frac{\xi(1-\xi)}{\gamma - a_1(1-\xi)/\alpha}\,\mathrm{d}\xi = \frac{\gamma\alpha^2}{a_1^2}(1-R) - \frac{\alpha}{2a_1}(1-R^2)$$
$$+\frac{\gamma\alpha^3}{a_1^3}\left(\gamma - \frac{a_1}{\alpha}\right)\ln\left(1 - \frac{a_1}{\gamma\alpha}(1-R)\right), \tag{2.42}$$

which for small time gives

$$t = \frac{1}{2\gamma}(1-R)^2 - \frac{1}{3\gamma^2}\left(\gamma - \frac{a_1}{\alpha}\right)(1-R)^3 + O((1-R)^4) \quad \text{as} \quad R \to 1^-. \tag{2.43}$$

2.5.2.2 Large Stefan number limit of small-time perturbation

In the limit that $\alpha \to \infty$ we have from (2.40) that $\gamma \to 0$, and in fact

$$\gamma = \frac{1}{\alpha} + V\sqrt{\frac{2\kappa}{\pi}}\frac{1}{\alpha^{3/2}} + \left(-\frac{1}{3} + \frac{2V}{\pi} + \frac{\kappa V^2}{\pi}\right)\frac{1}{\alpha^2} + O(\alpha^{-5/2}) \quad \text{as} \quad \alpha \to \infty.$$

Substituting this expression into (4.13) gives

$$\frac{t}{\alpha} \sim \left[\frac{1}{2} - \frac{V}{\alpha^{1/2}}\sqrt{\frac{\kappa}{2\pi}} + \frac{1}{\alpha}\left(\frac{1}{6} - \frac{V}{\pi} + \frac{\kappa V^2}{2\pi}\right) + O(\alpha^{-3/2})\right](1-R)^2$$
$$+\left[-\frac{1}{3}(1-\kappa V) + \frac{V}{18\alpha^{1/2}}\sqrt{\frac{2\kappa}{\pi}}(4 + 3\pi - 10\kappa V) + O(\alpha^{-1})\right](1-R)^3$$

$+O((1-R)^4)$ as $\alpha \to \infty$, $R \to 1^-$. This statement extends the result (2.22).

Some lengthy calculations confirm that the large Stefan number limit of the present small-time perturbation for the liquid phase agree with the small time limit

of the large Stefan number solutions given in Section 2.2. However, there is not the same level of agreement in the liquid phase, which is not surprising, as the solution in the liquid phase is not self-similar, and the small-time perturbation is not uniformly valid there.

2.5.2.3 Zero Stefan number limit of small-time perturbation

Substituting $\alpha = 0$ and $\kappa = 1$ into (2.40) gives

$$\mathrm{erf}\sqrt{\frac{\gamma}{2}} = \frac{1}{1-V}, \quad \mathrm{erfc}\sqrt{\frac{\gamma}{2}} = -\frac{V}{1-V}.$$

Thus we find that, as $t \to 0^+$,

$$T_s \sim \frac{V}{r} + \frac{1-V}{r}\,\mathrm{erf}\left(\frac{1-r}{2t^{1/2}}\right), \quad T_l \sim V + \frac{1-V}{r}\,\mathrm{erf}\left(\frac{1-r}{2t^{1/2}}\right).$$

These solutions are in close agreement with the exact solutions (2.31), provided that $t \ll 1$.

2.5.2.4 Slow diffusion limit of small-time perturbation

By considering the limiting behaviour of the error function (Abramowitz & Stegun [92], page 298), we find that

$$\frac{\kappa V}{L_s}\mathrm{e}^{-\gamma/2\kappa} \sim \gamma V + O(\kappa) \quad \text{as} \quad \kappa \to 0,$$

which implies that for $\kappa \ll 1$, (2.40) is given approximately by

$$\gamma(\alpha + V) = \frac{1}{L_\ell}\mathrm{e}^{-\gamma/2}.$$

This well known transcendental equation arises in the study of one-phase problems (Carslaw & Jaeger [33], page 286), except that the usual Stefan number has been replaced by $\alpha + V$. The conclusion is that for $\kappa \ll 1$ and $t \ll 1$, the temperature in the solid phase is essentially self-similar and governed by the usual one-phase equations with an adjusted Stefan number $\alpha + V$. These one-phase equations are given by (2.32)-(2.35), and thus the slow diffusion limit of the small-time perturbation solutions are totally consistent with the analysis given in Section 2.4.

2.5.3 Further approximation

The temperature profiles generated by the small time approximation of Section 2.5 (2.5.2) do not satisfy the no flux condition (2.5), and in fact, this approach has the temperature in the liquid phase T_l blowing up in the limit $r \to 0$. In order to satisfy (2.5), $(2.38)_2$ is adjusted by writing

$$T_l \approx V + \frac{1}{r}\left\{B_0(X) - B_0(2Y^{-1} - X) + YB_1(X) - YB_1(2Y^{-1} - X)\right\},$$

where B_0 and B_1 are given by (4.9) and (4.11). Given that $2Y^{-1} - X = (1+r)/(1-R)$, this alteration can be thought of as adding an image solution in the domain $-1 \leq r < 0$. The effect of this change is that the new solution now satisfies (2.1)-(2.5) and (2.8) exactly, but only satisfies (2.6) and (2.7) approximately; however, the errors from (2.6) and (2.7) are exponentially small in Y as $Y \to 0^+$. The result is that we are able to derive an excellent approximate solution to the two-phase Stefan problem, valid for $t \ll 1$.

2.6 Numerical results

The two-phase problem (2.1)-(2.8) is solved numerically using an enthalpy method, which we summarize here. The fundamental idea is to recast (2.1) and (2.2) in the form

$$\frac{\partial h}{\partial t} = \frac{\partial^2 T}{\partial r^2} + \frac{2}{r}\frac{\partial T}{\partial r} \quad \text{in} \quad 0 < r < 1, \tag{2.44}$$

where the enthalpy h is related to the temperature T by

$$T = \begin{cases} h - \alpha, & \text{if} \quad h < 0, \\ 0, & \text{if} \quad 0 \leq h \leq \alpha, \\ \kappa(h - \alpha), & \text{if} \quad h > \alpha. \end{cases} \tag{2.45}$$

and the fixed boundary and initial conditions become $\partial T/\partial r(0,t) = 0$, $T(1,t) = -1$ and and $h(r,0) = V/\kappa + \alpha$. A finite-difference scheme is applied to (2.44) to give

$$h_i^{j+1} = h_i^j + \frac{\delta t}{\delta r^2}\left[\frac{\delta r}{r_i}\left(T_{i+1}^j - T_{i-1}^j\right) + \left(T_{i+1}^j - 2T_i^j + T_{i-1}^j\right)\right] \tag{2.46}$$

where the standard notation is used. After each time step the temperature is updated via (2.46). The location of the solid/melt interface can then be determined, again with the use of (2.46), as described by Voller & Cross [53]. In the present case, $\delta t = 10^{-5}$, $\delta r = 0.01$, then $\delta t/\delta r^2 = 0.1$ which is enough to make the calculations convergent and provides second order accuracy.

Figure 2.1 provides a number of temperature profiles for $\alpha = 10$, $\kappa = 1$ and $V = 1$, which is representative of a large Stefan number solution. Included in the figure are numerical results from the enthalpy method, asymptotic results from Section 2.2 (2.2.2), the small-time approximation from Kucera & Hill [91], and the small-time approximation described in Section 2.5 (2.5.3). In part (a) of this figure, three profiles are drawn, for $R = 0.95$, 0.875 and 0.8, to illustrate small time behaviour, while for part (b) of the figure, profiles are drawn for latter times. In part (b), only the outer solid phase is included, since the temperature in the solid phase for these times is essentially zero for all r (see (2.23) and (2.29)).

Figure 2.1 shows that the asymptotic results derived in Section 2.2 agree extremely well with those from the numerical scheme, especially for smaller values of time. As the solid-melt interface approaches the centre of the sphere we expect this approach to break down, as described in Section 2.2 (2.2.3), and this tendency can be observed from the figure. Further, we see that, at least for these parameter values, the small-time approximation described in Section 2.5 (2.5.3) provides a much closer agreement with the numerical solution than the one given by Kucera & Hill [91], especially in the liquid phase. In the outer solid phase there is even reasonable agreement between our small-time solution and the numerical results for larger values of time.

In Figure 2.2 the dependence of the solid-melt location on time is shown for the same parameter values as those in Figure 2.1. Agreement between the numerical and analytical results is good for small time, while the large Stefan number solution (2.26) also works well for larger times. Note that only the first two terms in (2.26) are included in this figure.

To illustrate the behaviour for small Stefan numbers, temperature profiles are shown in Figure 2.3 for the case $\alpha = 0.1$, $\kappa = 1$ and $V = 1$. In addition to the numerical solution, the exact zero-Stefan-number solution is drawn, as well as

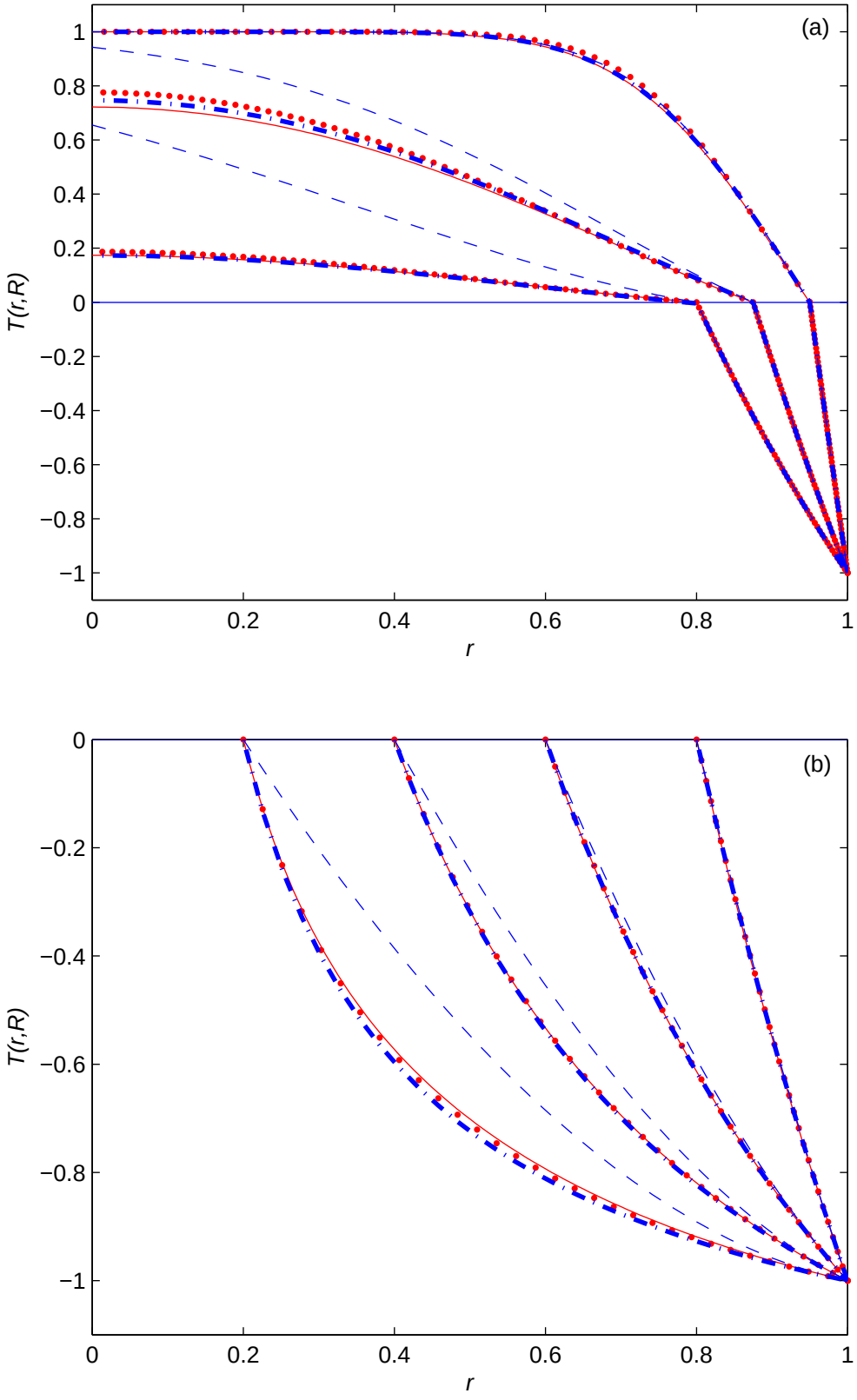

Figure 2.1: Plots of the temperature profiles for the case $\alpha = 10$, $\kappa = 1$, $V = 1$:(a) is for R=0.80, 0.875 and 0.95; (b) is for R=0.2, 0.4, 0.6 and 0.8. The four approaches used are the numerical scheme (solid), the large Stefan number expansion (dots), the small time approximation (dot-dashed) and the small time solution of Kucera & Hill [91] (dashed).

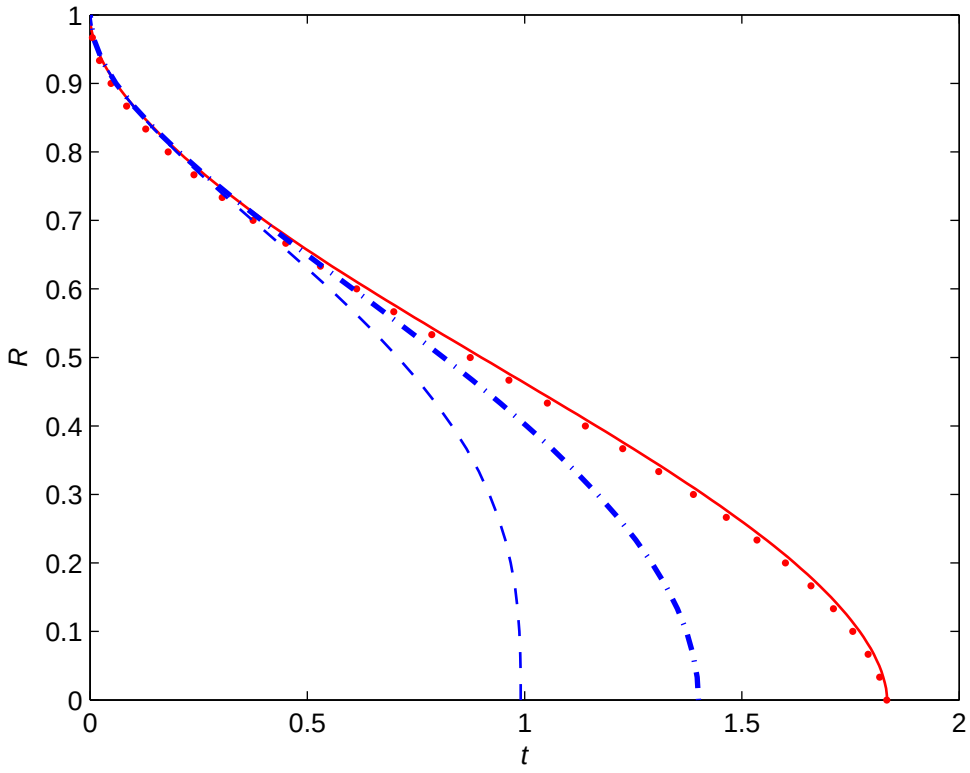

Figure 2.2: Dependence of the interface location on time for the case $\alpha = 10$, $\kappa = 1$, $V = 1$.

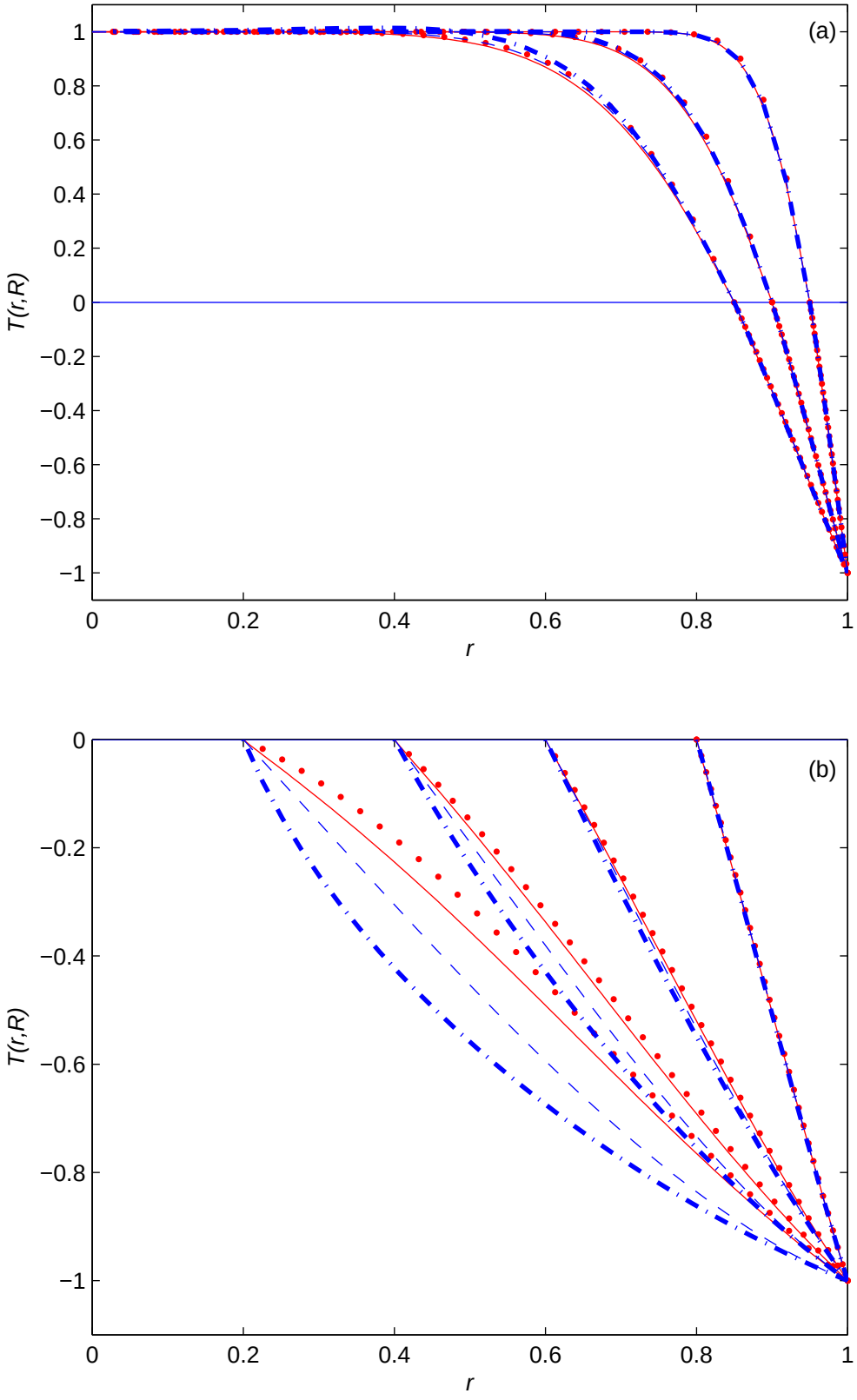

Figure 2.3: Plots of the temperature profiles for the case $\alpha = 0.1$, $\kappa = 1$, $V = 1$: (a) is for R=0.85, 0.90 and 0.95; (b) is for R=0.2, 0.4, 0.6 and 0.8. The four approaches used are the numerical scheme (solid), the zero Stefan number solution (dots), the small time approximation (dot-dashed) and the small time solution of Kucera & Hill [91] (dashed).

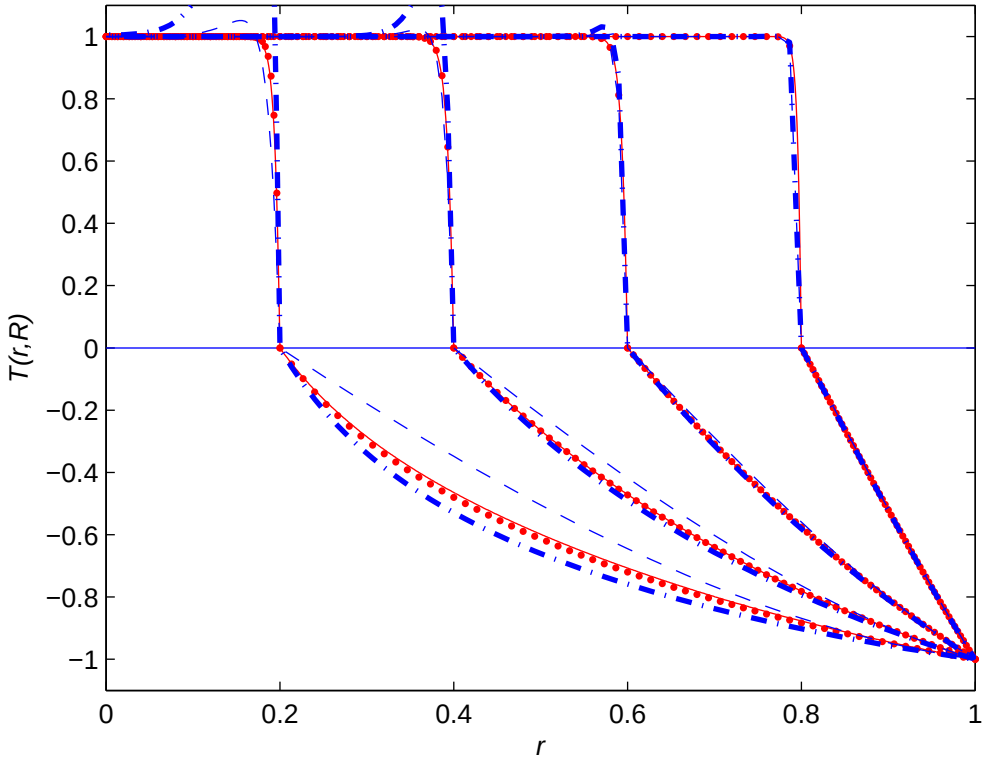

Figure 2.4: Plots of the temperature profiles for the case $\alpha = 1$, $\kappa = 0.01$, $V = 1$ at different positions R=0.2, 0.4, 0.6 and 0.8.. The four approaches used are the numerical scheme (solid), the slow conduction limit (dots), the small time approximation (dot-dashed) and the small time solution of Kucera & Hill [91] (dashed).

the two small-time approximations (from Kucera & Hill [91] and Section 2.5 (2.5.3)). Again, agreement between each approach is good for small times, but it is worthwhile noting that for small values of the Stefan number α, the small-time solutions do not work well for larger times (unlike the case with larger Stefan numbers), which is of course not unexpected.

Finally, to demonstrate the singular behaviour for slow conduction, temperature profiles are shown in Figure 2.4 for $\alpha = 1$, $\kappa = 0.01$ and $V = 1$. In addition to the numerical solution and the two small-time approximations, results are shown from Section 2.4. That is, in the solid phase, the plot shown is the numerical solution to the one-phase problem with α replaced by $\alpha + V$, while in the solid phase, the plot shown is for the interior layer

$$T_l = V(1 - \mathrm{e}^{\dot{R}(R-r)/\kappa}),$$

where $\dot{R}$ is obtained by solving the one-phase problem numerically. It can be seen (in the case of constant V) that the leading order asymptotic solution in the interior layer provides an excellent approximation for the entire liquid phase (including the outer region). Note that the agreement between the small-time results from Section 2.5 (2.5.3) and the numerical solution is very good for early times; however for later times an artifact of the scheme presented in Section 2.5 is that it produces some slightly spurious behaviour in the liquid phase.

2.7 Discussion

It is somewhat surprising that the two-phase Stefan problem for spheres has received such little attention, given the significant amount of literature devoted to the idealised one-phase case. For large values of the Stefan number α, it can be loosely argued that since the solid-melt interface moves slowly relative to the speed at which solidification occurs, the temperature in the inner liquid phase decays very quickly to the fusion temperature. Thus, except for small values of time, the liquid phase does not affect the solidification process, and can be essentially ignored.

Using the method of matched asymptotic expansions this structure has been explored in some detail. We have been able to confirm that on the time-scale at which heat diffuses to the centre of the sphere, the leading order description of both the temperature in the solid phase and the location of the solid-melt interface is independent of the inner liquid phase, although there is a coupling between the phases at higher orders. However, on the much longer time-scale at which solidification occurs, the solid and liquid phases essentially decouple, with the temperature in the liquid phase being exponentially small. This work extends the existing analysis for the one-phase problem.

While the present study is limited to the simple spherical geometry, the scalings for the large Stefan number limit would be expected to carry through to the more general problem of the inward solidification of a truly three-dimensional region of liquid. Thus we might expect the near-complete-solidification results of McCue, King & Riley [93] for the one-phase problem with arbitrary geometry to also hold in the two-phase case.

Consideration has also been given to deriving an approximate solution valid for

small time. In the one-phase problem, this can be done by employing a boundary-fixing transformation and then writing out the temperature T_s in the form $(2.38)_1$, as in Davis & Hill [51]. This small-time solution has been extended to include four terms A_i, $i = 1, 2, 3, 4$ by Hill & Kucera [94]. Adapting this approach to the two-phase problem is not straightforward, since the leading order behaviour for the two-phase problem is not self-similar. However, with the use of an image solution, we have been able to derive an approximate solution which works very well for small values of time.

Chapter 3

Single phase limit for melting nanoparticles

3.1 Introduction

In this chapter we study the effect of surface tension on the one-phase limit of spherical particle melting, and for completeness we consider cylindrical particles as well. In Section 3.2 we follow closely the argument by Evans & King [88, 89], and derive the appropriate one-phase problem with the correct Stefan condition. Solutions to this problem in the limits of small time and large Stefan number are detailed in Sections 3.3 and 3.4, while in Section 3.5 we extend the method presented in [36, 37, 38, 39, 84, 95] (which is for constant melting temperature) to apply to the case in which there is non-zero surface tension. Comparisons are made between the various analytical results and numerical values obtained from both enthalpy and front-fixing schemes in Section 3.6, and finally the results from the study are discussed in Section 3.7.

3.2 Derivation of one-phase limit

3.2.1 Two-phase problem

The geometry for the melting process in question is shown in Fig. 3.1. At time $t^* = 0$ the temperature on the surface is suddenly raised to T_a^*, which is higher than the melting point, and subsequently remains unchanged. The particle begins to melt, with the evolving solid-melt interface position denoted by $r^* = R^*(t^*)$.

The problem to be solved is to obtain the temperature distributions $T_\ell^*(r^*, t^*)$ and $T_s^*(r^*, t^*)$ in the liquid and solid phases, respectively, as well as the location of

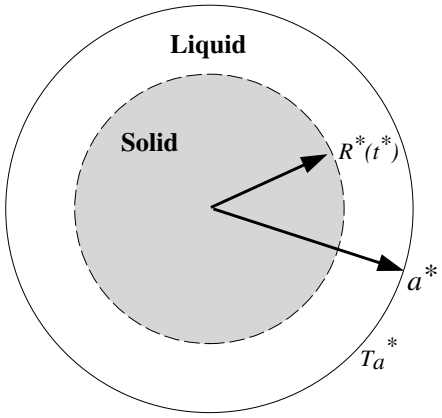

Figure 3.1: Schematic of particle melting

the moving boundary $r^* = R^*(t^*)$. As it is assumed that the heat transfers through both phases via conduction only, the governing equations are

$$\frac{\partial T_\ell^*}{\partial t^*} = \frac{k_\ell}{\rho c_\ell^*}\frac{1}{r^{*m}}\frac{\partial}{\partial r^*}\left(r^{*m}\frac{\partial T_\ell^*}{\partial r^*}\right) \quad \text{in} \quad R^*(t^*) < r^* < a^*, \tag{3.1}$$

$$\frac{\partial T_s^*}{\partial t^*} = \frac{k_s^*}{\rho c_s^*}\frac{1}{r^{*m}}\frac{\partial}{\partial r^*}\left(r^{*m}\frac{\partial T_s^*}{\partial r^*}\right) \quad \text{in} \quad 0 < r^* < R^*(t^*), \tag{3.2}$$

where $m = 1$ is for cylindrical cases and $m = 2$ for spherical cases. The material parameters k_ℓ^* and c_ℓ^* are, respectively, the thermal conductivity and the specific heat capacity of the liquid phase, with the corresponding parameters for the solid phase taking the alternate subscript s. The density ρ of the material is assumed to be the same constant in each phase.

Equations (3.1)-(3.2) are supplemented with the appropriate boundary conditions, which are as follows. On the fixed boundaries we have

$$T_\ell^* = T_a^* \quad \text{on} \quad r = a^* \quad \text{and} \quad \frac{\partial T_s^*}{\partial r^*} = 0 \quad \text{on} \quad r^* = 0. \tag{3.3}$$

At the solid/liquid interface the temperature is equal to the curvature-dependent melting point $T_f^*(R^*)$:

$$T_\ell^* = T_s^* = T_f^*(R^*) \quad \text{on} \quad r^* = R^*(t^*), \tag{3.4}$$

where the form we use for $T_f^*(R^*)$ is given in equation (1.1). Further, the discontinuity in heat flux due to the absorbtion of latent heat L across the interface gives

rise to the Stefan condition (see equations (1.5) and (1.6) in Chapter 1)

$$k_\ell^* \frac{\partial T_\ell^*}{\partial r^*} - k_s^* \frac{\partial T_s^*}{\partial r^*} = -\rho \frac{dR^*}{dt^*} \left[(c_\ell^* - c_s^*)(T_f^* - T_m^*) + L \right] \quad \text{on} \quad r^* = R^*(t^*), \tag{3.5}$$

where T_m^* is the bulk melting point of the material (the melting temperature when the interface is flat). Finally, the initial conditions are that

$$T_s^* = V^*(r^*), \quad R^* = a^*, \quad \text{at} \quad t^* = 0. \tag{3.6}$$

By introducing the following nondimensional variables

$$r = \frac{r^*}{a^*}, \quad R(t) = \frac{R^*(t^*)}{a^*}, \quad t = \frac{k_\ell^*}{\rho c_\ell^* a^{*2}} t^*, \quad \Delta T = T_a^* - T_m^* \left(1 - \frac{\omega}{a^*} \right),$$

$$T_\ell(r,t) = \frac{T_\ell^*(r^*,t^*) - T_m^*(1-\omega/a^*)}{\Delta T}, \quad T_s(r,t) = \frac{T_s^*(r^*,t^*) - T_m^*(1-\omega/a^*)}{\Delta T},$$

the non-dimensional two-phase Stefan problem now reduces to solving the heat conduction equations

$$\frac{\partial T_\ell}{\partial t} = \frac{\partial^2 T_\ell}{\partial r^2} + \frac{m}{r} \frac{\partial T_\ell}{\partial r} \quad \text{in} \quad R(t) < r < 1, \tag{3.7}$$

$$\frac{\partial T_s}{\partial t} = \frac{\kappa}{\delta} \left(\frac{\partial^2 T_s}{\partial r^2} + \frac{m}{r} \frac{\partial T_s}{\partial r} \right) \quad \text{in} \quad 0 < r < R(t), \tag{3.8}$$

where m is a parameter which takes the value $m = 1$ for a cylindrical particle, and $m = 2$ for a spherical one. The governing equations are subject to the boundary conditions

$$T_\ell = 1 \quad \text{on} \quad r = 1, \tag{3.9}$$

$$T_\ell = T_s = \sigma \left(1 - \frac{1}{R} \right) \quad \text{on} \quad r = R(t), \tag{3.10}$$

$$\frac{\partial T_\ell}{\partial r} - \kappa \frac{\partial T_s}{\partial r} = -\frac{dR}{dt} \left[(1-\delta) T_\ell + \alpha - \sigma(1-\delta) \right] \quad \text{on} \quad r = R(t), \tag{3.11}$$

$$\frac{\partial T_s}{\partial r} = 0 \quad \text{on} \quad r = 0, \tag{3.12}$$

and initial conditions

$$T_s(r,0) = V(r), \quad R = 1, \quad \text{at} \quad t = 0. \tag{3.13}$$

The four dimensionless parameters in the problem are defined by

$$\kappa = \frac{k_s^*}{k_\ell^*}, \quad \delta = \frac{c_s^*}{c_\ell^*}, \quad \sigma = \frac{\omega T_m^*}{a^* \Delta T}, \quad \alpha = \frac{L}{c_\ell^* \Delta T}.$$

These are the ratio of thermal conductivities, the ratio of specific heat capacities, the surface tension parameter and the Stefan number, respectively. The other input is the dimensionless initial temperature $V(r)$. For many applications V is considered constant and acts as another dimensionless parameter.

3.2.2 One-phase problem for $\sigma = 0$ and $V(r) \equiv 0$

In Section 3.2.3 we shall be concerned with deriving an approximate one-phase limit from the full two-phase problem (3.7)-(3.13). However, we first note that when the surface tension $\sigma = 0$, an exact one-phase problem arises if the solid is initially at the melting temperature (that is, if $V(r) \equiv 0$). In this case heat flows in the liquid phase only, and the one-phase problem is to solve (3.7) subject to the boundary conditions (3.9) and

$$T_\ell = 0, \quad \frac{\partial T_\ell}{\partial r} = -\alpha \frac{dR}{dt} \quad \text{on} \quad r = R(t), \tag{3.14}$$

together with the initial condition $R(0) = 1$. We observe there is only one parameter in this problem, the Stefan number α, and that this one-phase problem results regardless of κ and δ. The one-phase problem (3.7), (3.9), (3.14) has received considerable attention in the literature, as mentioned in the Introduction. Of particular note, asymptotic solutions for small time [51, 91, 96] and large Stefan number [54, 55, 57, 58] have been derived, and further approximations have been detailed using an iterative scheme [37, 38, 39]. All of these approaches will be extended to include the effects of surface tension in Sections 3.3-3.5 below.

3.2.3 One-phase limit for $\sigma \neq 0$

For the case in which $\sigma \neq 0$, there can never be a true one-phase problem, even if $V(r) \equiv 0$, since the temperature at the solid-melt interface changes as the interface evolves, meaning there will always be temperature gradients in the solid phase. However, in the limit $\kappa \ll 1$, which corresponds to slow conduction in the solid phase, a self-consistent one-phase limit can be derived, as described by Evans & King [89, 88], and repeated below for completeness.

It is worth noting that in the past, a number of researchers have considered one-phase problems with surface tension that arise by simply ignoring (3.8) and setting

$\kappa = 0$ in (3.11). See for example, Wu et al. [50] and Herraiz et al. [97], who both consider one-phase Stefan problems for spheres. As explained in some detail by Evans & King [88, 89], this practice does not conserve heat at the interface, and should be avoided. Further, we reiterate that even if $\sigma = 0$ then the one-phase problem (3.7), (3.9), (3.14) only arises if $V(r) \equiv 0$. If $V(r) \not\equiv 0$ then a one-phase limit can only be derived under the assumption $\kappa \ll 1$ (see Struckmeier & Unterreiter [90]) as described below.

For $\kappa \ll 1$ we have from (3.8) that $T_s \sim V(r)$ in the solid away from the moving boundary $r = R(t)$. This means there must be an interior layer in the solid near $r = R(t)$ where the temperature changes rapidly approximately from $V(r)$ (away from $r = R(t)$) to $\sigma(1 - 1/R)$ (on $r = R(t)$).

The interior layer is for

$$r = R(t) - \kappa\tilde{r},$$

where $\tilde{r} = O(1)$. To leading order we write $T_s \sim \tilde{T}_s(r, t)$, so that

$$\frac{\partial^2 \tilde{T}_s}{\partial \tilde{r}^2} = \delta \frac{dR}{dt} \frac{\partial \tilde{T}_s}{\partial \tilde{r}}.$$

We solve this equation subject to the boundary conditions

$$\tilde{T}_s = T_\ell(R(t), t) \quad \text{on} \quad \tilde{r} = 0, \quad \tilde{T}_s \to V(R(t)) \quad \text{as} \quad \tilde{r} \to \infty, \tag{3.15}$$

where the second condition in (3.15) comes from matching back into the region away from the moving boundary. The result is that

$$\tilde{T}_s \sim V(R(t)) + [T_\ell(R(t), t) - V(R(t))]e^{\delta \dot{R}(t)\tilde{r}}. \tag{3.16}$$

This solution is valid provided $\dot{R}(t) < 0$, which is true in the present melting context (but not in the ill-posed case of crystal growth from a seed in a supercooled liquid). We now have from (3.16) a quantitative description of how the temperature rapidly changes near the moving boundary.

To derive the correct boundary conditions for the liquid phase we note that on the moving boundary $r = R(t)$ we have $\tilde{r} = 0$, and so

$$-\kappa \frac{\partial T_s}{\partial r} = \delta \dot{R}(t)[T_\ell(R(t), t) - V(R(t))]$$

This expression can be directly substituted into (3.11) to eliminate T_s. Thus, in summary, when $\kappa \ll 1$ the appropriate one-phase limit involves solving

$$\frac{\partial T_\ell}{\partial t} = \frac{\partial^2 T_\ell}{\partial r^2} + \frac{m}{r}\frac{\partial T_\ell}{\partial r} \quad \text{in} \quad R(t) < r < 1, \tag{3.17}$$

$$T_\ell = 1 \quad \text{on} \quad r = 1, \tag{3.18}$$

$$T_\ell = \sigma\left(1 - \frac{1}{R}\right) \quad \text{on} \quad r = R(t), \tag{3.19}$$

$$\frac{\partial T_\ell}{\partial r} = -\frac{dR}{dt}\left(T_\ell + \alpha - \sigma(1-\delta) - \delta V\right) \quad \text{on} \quad r = R(t), \tag{3.20}$$

with the initial condition $R(0) = 1$. In the solid region away from the interface we have $T_s \sim V(r)$, while for the interior region the temperature is given by (3.16). As discussed above, the correct Stefan condition (3.20) does not arise by naively setting $\kappa = 0$ in (3.11), and can only be derived by carefully considering the singular limit $\kappa \to 0$.

The following points are worth mentioning. First, we note that this entire one-phase model must break down at times for which $R(t) = O(\kappa)$, when the size of the solid region is of the same order as the interior layer. Furthermore, when $\sigma \neq 0$ the solution to the one-phase problem equations (3.17)-(3.20) ceases to exist before the limit $R = 0$ is reached. From (3.19)-(3.20) we see that the velocity of the interface $dR/dt \to -\infty$ as $R \to R_c$, where the critical radius R_c is the root of the equation

$$R_c = \frac{\sigma}{\sigma\delta + \alpha - \delta V(R_c)}. \tag{3.21}$$

The corresponding temperature on the interface is

$$\lim_{R \to R_c^+} T_\ell(R(t), t) = -[\alpha - \sigma(1-\delta) - \delta V(R_c)],$$

which forms a lower bound on the temperature generally. Thus the model predicts there will be a form of blow-up before the particle melts completely. A phenomenon very similar in nature has been observed experimentally, and is referred to as abrupt melting [7].

Second, while in general the boundary conditions (3.19)-(3.20) depend on σ, α, and $\delta V(r)$, the commonly assumed initial condition $V \equiv$ constant implies that the only important parameters are σ and the combination $\beta = \alpha - \sigma(1-\delta) - \delta V$, where here β acts as an *effective Stefan number*.

Finally, we note that for the case $V \equiv 0$, corresponding to the entire solid being initially at the melting temperature, the limiting one-phase problem (3.17)-(3.20) does not depend on κ (as is the case for the classical one-phase problem (3.7), (3.9), (3.14)), but this parameter is required to describe the interior layer through (3.16).

3.3 Small-time behaviour

The small-time behaviour of the solution to the one-phase problem (3.17)-(3.20) is briefly described here by extending the approach of Davis & Hill [51] and Hill & Dewynne [96], which was applied to the case $\sigma = 0$. An equivalent procedure was detailed in Wu et al. [49] for $\sigma \neq 0$ with different boundary conditions to (3.19)-(3.20).

3.3.1 Spherical geometry

We anticipate self-similar leading order behaviour as $t \to 0$, and look for solutions of the form

$$T_\ell(r,t) \sim \frac{1}{r}\Big\{ A_0(X) + A_1(X)Y \Big\} \qquad \text{as} \quad Y \to 0, \tag{3.22}$$

where

$$X = \frac{1-r}{1-R} \quad \text{and} \quad Y = 1 - R$$

are similarity and time-like variables, respectively. The functions A_0 and A_1 satisfy the following ordinary differential equations

$$A_0'' + \gamma X A_0' = 0, \quad A_1'' + \gamma(XA_1' - A_1) = \frac{a_1 - \gamma\alpha}{\alpha - \sigma(1-\delta)} X A_0',$$

with boundary conditions

$$A_0 = 1, \quad A_1 = 0, \quad \text{on} \quad X = 0,$$

$$A_0 = 0, \quad A_1 = -\sigma, \quad \text{on} \quad X = 1.$$

The solutions are

$$A_0(X) = 1 - \frac{\operatorname{erf}\left(\sqrt{\frac{\gamma}{2}}\, X\right)}{\operatorname{erf}\left(\sqrt{\frac{\gamma}{2}}\right)}, \quad A_1(X) = -\sigma X + c_1 X \left(1 - e^{\gamma(1-X^2)/2}\right), \tag{3.23}$$

where γ is the real root of the well-known transcendental equation [32](page 103)

$$[\alpha - \sigma(1-\delta) - \delta V(1)]\sqrt{\frac{\pi\gamma}{2}}e^{\gamma/2}\text{erf}\left(\sqrt{\frac{\gamma}{2}}\right) = 1,$$

and c_1 is the constant

$$c_1 = \frac{\gamma[\alpha + \delta\sigma - \delta V(1) - \delta V'(1)] + \sigma}{\gamma + 3}.$$

The location of the free boundary is found to be given implicitly by

$$t \sim \frac{1}{2\gamma}(1-R)^2 - \frac{c_2}{\gamma(3+\gamma)}(1-R)^3 + O((1-R)^4), \quad \text{as} \quad R \to 1^-,$$

and where the constant c_2 is given by

$$c_2 = 1 + \frac{(\gamma+1)\sigma - \gamma\delta V'(1)}{\alpha - \sigma(1-\delta) - \delta V(1)}, \tag{3.24}$$

with the dash denoting a derivative with respect to R. Thus it can be seen that for small time the melting process is only weakly dependent on the surface tension σ. In particular, with $\delta = 1$ the effects of σ appear in the correction terms only.

3.3.2 Cylindrical geometry

Again we expect self-similar behaviour at leading order, and thus write

$$T_\ell(r,t) \sim B_0(X) + B_1(X)Y \quad \text{as} \quad Y \to 0,$$

where X and Y are given in (3.23). The function B_0 turns out to be the same function as A_0, given in $(3.23)_1$, while B_1 is

$$B_1(X) = -\sigma X + \frac{X}{6}\left\{3B_0(X) + d_1\left(1 - e^{(1-X^2)\gamma/2}\right)\right\},$$

where d_1 denotes the constant

$$d_1 = \frac{6[\gamma(\sigma - \delta V'(1)) + \sigma]}{\gamma + 3}.$$

The location of the solid-melt interface is found to be given implicitly by

$$t \sim \frac{1}{2\gamma}(1-R)^2 - \frac{c_2 - 1}{\gamma(3+\gamma)}(1-R)^3 + O((1-R)^4), \quad \text{as} \quad R \to 1^-,$$

where the constant c_2 is defined in (3.24). As with the spherical case, it can be seen that the surface tension has a weak effect during the initial stages of the melting

process.

3.4 Large Stefan number limit

We present here a summary of the limiting behaviour of the one-phase problem (3.17)-(3.20) as the Stefan number $\alpha \to \infty$. This limit is particularly relevant for melting nanoscaled particles, since in typical experiments the temperature imposed at the surface of a particle is not much higher than the melting point, leading to high Stefan numbers. In [7], for example, where gold particles (whose radius is of the order of tens to a hundred nanometres) are melted, they have $L = 63718$ J/kg, $c_\ell{}^* = 129$ J/(kg· K), when $\Delta T = 100$ K, which gives $\alpha = 4.94$. Of course smaller values of ΔT produce larger Stefan numbers.

In what follows we have left the initial temperature profile $V(r)$ arbitrary, but we recall that for the situation in which $V =$ constant, the one-phase problem depends only on surface tension σ and the effective Stefan number $\beta = \alpha - \sigma(1-\delta) - \delta V$. Thus, in this special (but frequently assumed) case, $V = 0$, $\delta = 1$ may be set, in the following formulae, and replace α with β.

3.4.1 Time-scale $t = O(\alpha)$

The first time-scale is for $t = O(\alpha)$. Here the details are a simple extension of that given in Pedroso & Domoto [54] and Riley et al. [55]. The appropriate rescaling of time is $t = \alpha\hat{t}$, where $\hat{t} = O(1)$, and so by choosing to employ R as the time-like independent variable, the location of the moving boundary is described by the function $\hat{t}(R)$.

In the limit $\alpha \to \infty$ we seek solutions to (3.17)-(3.20) of the form

$$T \sim \hat{T}_0(r,R) + \frac{1}{\alpha}\hat{T}_1(r,R) + \frac{1}{\alpha^2}\hat{T}_2(r,R) + O(\alpha^{-3}), \tag{3.25}$$

$$\hat{t} \sim \hat{t}_0(R) + \frac{1}{\alpha}\hat{t}_1(R) + \frac{1}{\alpha^2}\hat{t}_2(R) + O(\alpha^{-3}), \tag{3.26}$$

so that the leading order problem is

$$\frac{\partial^2 \hat{T}_0}{\partial r^2} + \frac{m}{r}\frac{\partial \hat{T}_0}{\partial r} = 0 \quad \text{for} \quad R < r < 1, \quad \hat{T}_0 = 1 \quad \text{on} \quad r = 1, \tag{3.27}$$

$$\hat{T}_0 = \sigma\left(1 - \frac{1}{R}\right), \quad \hat{t}_0'\frac{\partial \hat{T}_0}{\partial r} = -1 \quad \text{on} \quad r = R, \tag{3.28}$$

where the dash denotes a derivative with respect to R. We note that (3.27)-(3.28) also describes the radially-symmetric problem of contracting bubbles of air in Hele-Shaw cells ($m = 1$) or in porous media ($m = 2$), otherwise filled with viscous fluid (see [98, 99], for example). In that case the function $\hat{T}_0$ represents fluid pressure, and the (averaged) fluid velocity is recovered by $\mathbf{q} = -\nabla\hat{T}_0$.

The problems for $\hat{T}_1$ and $\hat{T}_2$ are

$$\frac{\partial^2\hat{T}_1}{\partial r^2} + \frac{m}{r}\frac{\partial\hat{T}_1}{\partial r} = \frac{1}{\hat{t}_0'}\frac{\partial\hat{T}_0}{\partial R} \quad \text{for} \quad R < r < 1, \quad \hat{T}_1 = 0 \quad \text{on} \quad r = 1,$$

$$\hat{T}_1 = 0, \quad \hat{t}_1' = \hat{t}_0'\left(\hat{t}_0'\frac{\partial\hat{T}_1}{\partial r} + \hat{T}_0 - \sigma(1-\delta) - \delta V(R)\right) \quad \text{on} \quad r = R,$$

and

$$\frac{\partial^2\hat{T}_2}{\partial r^2} + \frac{m}{r}\frac{\partial\hat{T}_2}{\partial r} = 0 \quad \text{for} \quad R < r < 1, \quad \hat{T}_2 = 0 \quad \text{on} \quad r = 1,$$

$$\hat{T}_2 = 0, \quad \hat{t}_2' = \hat{t}_0'\left(\hat{t}_0'\frac{\partial\hat{T}_2}{\partial r} + \hat{t}_1'\frac{\partial\hat{T}_1}{\partial r}\right) \quad \text{on} \quad r = R,$$

respectively. From (3.27) and (3.28) we obtain $\hat{T}_0$ and $\hat{t}_0$. Then substitute $\hat{T}_0$ and $\hat{t}_0$ into higher order equations for $\hat{T}_1$ and $\hat{T}_2$, we can obtain $\hat{T}_1$,$\hat{T}_2$, $\hat{t}_1$ and $\hat{t}_2$. After some lengthy but straight-forward calculations we find that

$$\hat{T}_0 = \frac{1}{r}\left[1 - \left(\frac{1-r}{1-R}\right)\right] - \frac{\sigma(1-R)}{r}\left(\frac{1-r}{1-R}\right), \tag{3.29}$$

$$\begin{aligned}\hat{t}_0 \;=\; & -\frac{\sigma^2}{(1-\sigma)^3}(1-R) + \frac{1-2\sigma}{2(1-\sigma)^2}(1-R)^2 - \frac{1}{3(1-\sigma)}(1-R)^3 \\ & -\frac{\sigma^2}{(1-\sigma)^4}\ln\left[R + \sigma(1-R)\right],\end{aligned} \tag{3.30}$$

$$\hat{T}_1 = -\frac{R+\sigma(1-R)}{6rR^2}\left(\frac{1-r}{1-R}\right)\left[1 - \left(\frac{1-r}{1-R}\right)^2\right], \tag{3.31}$$

$$\begin{aligned}\hat{t}_1 \;=\; & \frac{\sigma(1-4\sigma)}{3(1-\sigma)^3}(1-R) + \frac{1-\sigma-3\sigma^2}{6(1-\sigma)^2}(1-R)^2 - \frac{\sigma}{3(1-\sigma)}(1-R)^3 \\ & + \frac{\sigma(1-4\sigma)\ln\left[R+\sigma(1-R)\right]}{3(1-\sigma)^4} - \sigma(1-\delta)\hat{t}_0 - \delta\int_R^1 \frac{\xi^2(1-\xi)}{\xi+\sigma(1-\xi)}\,V(\xi)\,\mathrm{d}\xi,\end{aligned} \tag{3.32}$$

for the sphere, with $\hat{T}_2$ and $\hat{t}_2$ given in Appendix A, and

$$\hat{T}_0 = 1 - \frac{[R + \sigma(1-R)]\ln r}{R \ln R}, \tag{3.33}$$

$$\begin{aligned} \hat{t}_0 &= \frac{1 - R^2 + 2R^2 \ln R}{4(1-\sigma)} - \frac{\sigma(1 - R + R\ln R)}{(1-\sigma)^2} \\ &+ \frac{\sigma^2}{(1-\sigma)^3}\left\{\ln\left[\frac{R+\sigma(1-R)}{\sigma}\right] + \mathrm{dilog}\left[\frac{R+\sigma(1-R)}{\sigma}\right]\ln R - \mathrm{dilog}(1/\sigma)\right\}, \end{aligned} \tag{3.34}$$

for cylinders, with $\hat{T}_1$ and $\hat{t}_1$ given in Appendix A. Here $\mathrm{dilog}(z)$ is the dilogarithm function defined by

$$\mathrm{dilog}(z) = \int_1^z \frac{\ln t}{1-t}\,\mathrm{d}t.$$

We recall that for $\sigma \neq 0$, solutions to the full one-phase problem (3.17)-(3.20) have solid-melt interfaces which exhibit blow-up at the critical radius $R = R_c$, given by (3.21). The limiting behaviour of (3.17)-(3.20) as $R \to R_c$ is discussed below in Section 3.4.3, but for now note that the large Stefan number expansions (3.25)-(3.26) do not predict the existence of this critical radius, since $R_c \to 0$ as $\alpha \to \infty$. Instead, as $\alpha \to \infty$, the one-phase problem (3.17)-(3.20) predicts that the temperature on the interface becomes unbounded as $R \to 0$ (which, of course, is not physically realistic).

All the solutions (3.29)-(3.35), (B.2)-(B.4) agree with the corresponding ones given in [54, 55] in the limit $\sigma \to 0$ with r and R fixed, as expected. Furthermore, the leading order behaviour of each of the above solutions is found to be independent of σ as $R \to 1^-$, confirming that the small-time behaviour is only weakly dependent on the surface tension, as established in the previous section. To take an example, for the sphere with V constant we have

$$\begin{aligned} \hat{t}_0 &\sim \frac{1}{2}(1-R)^2 - \frac{1}{3}(1+\sigma)(1-R)^3 + O((1-R)^4), \\ \hat{t}_1 &\sim \left(\frac{1}{6} - \frac{1}{2}\sigma(1-\delta) - \frac{1}{2}\delta V\right)(1-R)^2 - \left(\frac{4}{9}\sigma + \frac{1}{3}(1+\sigma)(\sigma(1-\delta)+\delta V)\right)(1-R)^3 \\ &\quad + O((1-R)^4) \\ \hat{t}_2 &\sim -\frac{1}{45}(1-R)^2 - \frac{1}{45}\left(1 + \frac{1}{3}\sigma\right)(1-R)^3 + O((1-R)^4) \quad \text{as} \quad R \to 1^-, \end{aligned}$$

the surface tension σ appearing in the correction terms only.

On the other hand, for times just before complete melting, the qualitative be-

haviour of the solutions $\hat{T}_i$, $\hat{t}_i$ for $\sigma \neq 0$ is different to that for $\sigma = 0$, even for $\sigma \ll 1$. This is because, for the case in which $\sigma \neq 0$, the melting temperature $T_\ell(R,t) \sim -\sigma/R$ as $R \to 0$, meaning the Gibbs-Thomson model (1.1) predicts the temperature on the interface becomes unbounded in this limit (whereas for $\sigma = 0$ we have $T_\ell(R,t) = 0$, a constant).

Such qualitatively different behaviour manifests itself in the above large-Stefan number expansion when observing the limiting forms of the solutions at each order as $R \to 0$. By taking the limit $R \to 0$ in $\hat{t}_0$, it can be seen that a first approximation for the complete melting time t_f (or the exact extinction time for the corresponding shrinking bubble problem) is given by

$$t_f \approx \beta \hat{t}_0(0) = \beta \left\{ \frac{1 - 5\sigma - 2\sigma^2}{6(1-\sigma)^3} - \frac{\sigma^2 \ln \sigma}{(1-\sigma)^4} \right\}$$

for the sphere, and

$$t_f \approx \beta \hat{t}_0(0) = \beta \left\{ \frac{1 - 5\sigma}{4(1-\sigma)^2} - \frac{\sigma^2 \mathrm{dilog}(1/\sigma)}{(1-\sigma)^3} \right\}$$

for the cylinder. In the limit $\sigma \to 0$, these expressions agree with the $\sigma = 0$ results $\beta \hat{t}_0(0) = \frac{1}{6}\beta$ (sphere) and $\beta \hat{t}_0(0) = \frac{1}{4}\beta$ (cylinder) found in [54, 55], the limiting behaviour

$$\hat{t}_0(0) - \hat{t}_0 \sim \frac{1}{3\sigma} R^3 + O(R^4) \quad \text{as} \quad R \to 0 \tag{3.35}$$

for the sphere, and

$$\hat{t}_0(0) - \hat{t}_0 \sim \frac{1 - 3\ln R}{9\sigma} R^3 + O(R^4 \ln R) \quad \text{as} \quad R \to 0$$

for the cylinder, give different scalings to the case $\sigma = 0$, namely

$$\hat{t}_0(0) - \hat{t}_0 = \frac{1}{4}(1 - 2\ln R)R^2 \quad \text{(sphere)}, \quad \hat{t}_0(0) - \hat{t}_0 = \frac{1}{2}R^2 - \frac{1}{3}R^3 \quad \text{(cylinder)}.$$

In context of the investigating shrinking bubbles in Hele-Shaw cells, these simple results imply that including surface tension in the two- and three-dimensional studies in [98, 99] will lead to very different scalings, and may destroy the elliptic/ellipsoidal nature of the bubble shape just before extinction.

3.4.2 Further time-scales for sufficiently small σ

As detailed in [55, 57, 58], the above expansions (3.25)-(3.26) for the case $\sigma = 0$ fail to provide a valid approximation at times close to complete melting. Physically, the solid-melt interface speeds up as $R \to 0$, and thus there is a limit at which the process is no longer quasi-steady, even though $\alpha \gg 1$. The appropriate time-scale for this behaviour is $t_f - t = O(1)$, where t_f is the complete melting time (recall that $t_f = O(\alpha)$). By considering carefully where the expansion (3.25)-(3.26) breaks down, it can be shown that $R = O(\alpha^{-1/2})$ on this time-scale for the sphere, while $R = O(\epsilon)$ for the cylinder, where here ϵ is a small number related to the Stefan number α by $1 = \alpha\epsilon^2 \ln(1/\epsilon)$ (see [55, 58]).

For sufficiently small surface tension, namely $\sigma \ll \alpha^{-1/2}$ for the sphere and $\sigma \ll \epsilon$ for the cylinder, we expect the same structure to arise on a second time-scale $t_f - t = O(1)$ as the $\sigma = 0$ case mentioned above (we would have $R \gg R_c$ on this time-scale, where R_c is the critical radius given by (3.21)). In a narrow region near the solid-melt interface the temperature will rise very quickly from approximately zero (since $|-\sigma/R|$ will be small on this time-scale) to approximately unity, while away from the interface analysis is required to account for the order-one temporal variations in the temperature field (see [55, 57, 58] for details).

For the case $\sigma = 0$ the analysis on the second time-scale breaks down when R is extremely small, and further treatment is required on a third exponentially short time-scale [57, 58, 87]. When $\sigma \neq 0$, however, we expect a rather different near-complete-melting limit (regardless of how small σ is), as the increasingly large magnitude of the melting temperature as R decreases will eventually dominate the process near the interface. We discuss this phenomenon below in Section 3.4.3.

3.4.3 Generic extinction limit

For larger values of the surface tension ($\sigma = O(\alpha^{-1/2})$ for the sphere and $\sigma = O(\epsilon)$ for the cylinder as $\alpha \to \infty$) we expect the melting process to lose its quasi-steadiness before $R = O(\alpha^{-1/2})$ for the sphere or $R = O(\epsilon)$ for the cylinder, so that the analogy with the $\sigma = 0$ case treated in [55, 57, 58] will no longer be relevant. Furthermore, as mentioned above, the solid-melt interface exhibits finite-time blow-up, meaning that the interface velocity $dR/dt \to -\infty$ as $R \to R_c$, where $R \to R_c$ is the root

to (3.21). Thus for surface tensions with these orders of magnitude we expect completely different scalings in the extinction limit $t \to t_f$ (where now t_f denotes the finite blow-up time) to the previously studied cases for $\sigma = 0$.

Indeed, a generic near-complete-melting analysis, valid for $\alpha = O(1)$ and $\sigma \ll 1$, has been attempted by Herraiz et al. [97]; however, as explained in Section 3.2.3, Herraiz et al. use boundary conditions which do not conserve heat at the solid-melt interface. Herraiz et al. find that $T_\ell \sim -\sigma/r$ for $r - R \ll 1$ as $R \to 0$, with the interface behaving thus

$$t_f - t \sim \frac{\alpha}{3\sigma} R^3 \quad \text{as} \quad R \to 0, \tag{3.36}$$

which agrees with the leading-order large Stefan number result (3.35) for the sphere (the analysis of Herraiz et al. [97] is for both spheres and cylinders, and does not lead to finite-time blow-up). With the more appropriate boundary conditions (3.19)-(3.20), for $\alpha = O(1)$ and $\sigma \ll 1$ we also have $T_\ell \sim -\sigma/r$ for $r - R \ll 1$ as $R \to R_c^+$, but this time the solid-melt interface scales thus

$$t_f - t \sim \frac{1}{2}(R - R_c)^2 \quad \text{as} \quad R \to R_c^+; \tag{3.37}$$

this leading order behaviour being independent of the surface tension, and completely different to that given by Herraiz et al. [97].

3.5 An integral formulation that leads to an iterative scheme

A number of researchers [36, 37, 38, 39] have obtained approximate analytical solutions for one-phase Stefan problems without surface tension through an iteration scheme derived from an integral formulation. Here this approach is extended to the radially symmetric one-phase problem including surface tension effects.

3.5.1 Integral formulation

In what follows we make use of the function $K_m(x, y)$, defined by

$$K_m(x, y) = \int_y^x \xi^{-m} \mathrm{d}\xi, \quad m = 1, 2,$$

where we recall that $m = 1$ corresponds to cylinders while $m = 2$ corresponds to spheres. By multiplying (3.17) by r^m and integrating the resulting equation with respect to r from $R(t)$ to r, we arrive at

$$r^m \frac{\partial T_\ell(r,t)}{\partial r} = R^m \frac{\partial T_\ell(R,t)}{\partial r} + \int_{R(t)}^{r} \xi^m \frac{\partial T_\ell(\xi,t)}{\partial t} \mathrm{d}\xi,$$

which can be simplified to

$$\frac{\partial T_\ell(r,t)}{\partial r} = -\frac{R^m}{r^m}\left(T_\ell(R,t) + \alpha - \sigma(1-\delta) - \delta V(R)\right)\frac{dR}{dt} + \frac{1}{r^m}\int_{R(t)}^{r} \xi^m \frac{\partial T_\ell(\xi,t)}{\partial t}\mathrm{d}\xi$$

by utilising the Stefan condition (3.20). We integrate this equation with respect to r, again from $R(t)$ to r, to yield

$$T_\ell(r,t) - T_\ell(R(t),t) = \frac{\partial}{\partial t}\int_{R(t)}^{r} K_m(r,\xi)\xi^m [T_\ell(\xi,t) + \alpha - \sigma(1-\delta) - \delta V(\xi)]\mathrm{d}\xi, \quad (3.38)$$

and apply the fixed boundary condition (3.18) to give

$$1 - \sigma\left(1 - \frac{1}{R(t)}\right) = \frac{\partial}{\partial t}\int_{R(t)}^{1} K_m(1,\xi)\xi^m [T_\ell(\xi,t) + \alpha - \sigma(1-\delta) - \delta V(\xi)]\mathrm{d}\xi. \quad (3.39)$$

Equations (3.38) and (3.39) represent the key equations in what follows.

It proves useful to again treat R as an independent variable, and describe the moving interface by $t = \bar{t}(R)$. Further, we make use of the dependent variable T defined by $T(r,R) = T_\ell(r,t)$. After applying the chain rule in (3.39) we find

$$\frac{d\bar{t}}{dR} = \frac{\int_R^1 K_m(1,\xi)\xi^m \frac{\partial T(\xi,R)}{\partial R}\mathrm{d}\xi - [\alpha - \sigma(1-\delta) - \delta V(R) + T(R,R)]K_m(1,R)R^m}{1 - \sigma\left(1 - 1/R\right)}, \quad (3.40)$$

which provides an expression for the speed of the interface in terms of the temperature T and R. By again applying the chain rule and eliminating $d\bar{t}/dR$ from (3.38), we find

$$T(r,R) = F(r,R)\left[1 - \sigma\left(1 - \frac{1}{R}\right)\right] + \sigma\left(1 - \frac{1}{R}\right), \quad (3.41)$$

where the function $F(r,R)$ is defined by

$$F(r,R) = \frac{\int_R^r K_m(r,\xi)\xi^m \frac{\partial T(\xi,R)}{\partial R}\mathrm{d}\xi - [\alpha - \sigma(1-\delta) - \delta V(R) + T(R,R)]K_m(r,R)R^m}{\int_R^1 K_m(1,\xi)\xi^m \frac{\partial T(\xi,R)}{\partial R}\mathrm{d}\xi - [\alpha - \sigma(1-\delta) - \delta V(R) + T(R,R)]K_m(1,R))R^m}.$$

Thus, (3.41) provides an equation with the temperature T on both sides. Together with (3.40), this expression will form the basis of an iterative scheme, described in

the following section.

3.5.2 Iterative procedure

The iterative scheme works as follows: given an expression for the temperature distribution at a particular iteration, we can substitute it into (3.41) to obtain the distribution for the next iteration, and into (3.40) to obtain an updated relationship between time $\bar{t}$ and solid-interface position R. Thus for each integer value n we have

$$T_{n+1}(r,R) = F_n(r,R)\left[1-\sigma\left(1-\frac{1}{R}\right)\right]+\sigma\left(1-\frac{1}{R}\right),$$

with $F_n(r,R)$ defined by

$$F_n(r,R) = \frac{\int_R^r K_m(r,\xi)\xi^m \frac{\partial T_n(\xi,R)}{\partial R}\mathrm{d}\xi - [\alpha-\sigma(1-\delta)-\delta V(R)+T_n(R,R)]K_m(r,R)R^m}{\int_R^1 K_m(1,\xi)\xi^m \frac{\partial T_n(\xi,R)}{\partial R}\mathrm{d}\xi - [\alpha-\sigma(1-\delta)-\delta V(R)+T_n(R,R)]K_m(1,R)R^m},$$

and

$$\frac{d\bar{t}_{n+1}}{dR} = \frac{\int_R^1 K_m(1,\xi)\xi^m \frac{\partial T_n(\xi,R)}{\partial R}\mathrm{d}\xi - [\alpha-\sigma(1-\delta)-\delta V(R)+T_n(R,R)]K_m(1,R)R^m}{1-\sigma\,(1-1/R)}.$$

We begin the iteration process by choosing $T_{-1}\equiv 0$.

For the spherical case ($m=2$), the first three results for the temperature are given by

$$\begin{aligned}
T_0 &= \frac{1}{r}\left[1-\left(\frac{1-r}{1-R}\right)\right]-\frac{\sigma(1-R)}{r}\left(\frac{1-r}{1-R}\right), && (3.42)\\
T_1 &= T_0 - \frac{R+\sigma(1-R)}{2rR[3\sigma(R-1)+3(\alpha-\sigma(1-\delta)-\delta V(R))R+1]}\\
&\times \left(\frac{1-r}{1-R}\right)\left[1-\left(\frac{1-r}{1-R}\right)^2\right], && (3.43)\\
T_2 &= T_0 - \frac{[R+\sigma(1-R)]h_1(r,R)}{8rR(R-1)^2h_2(R)}\left(\frac{1-r}{1-R}\right)\left[1-\left(\frac{1-r}{1-R}\right)^2\right], && (3.44)
\end{aligned}$$

where the functions $h_1(r,R)$ and $h_2(R)$ are given by Appendix (C.1)-(C.3) in Appendix C. The corresponding results for the motion of the interface are given by

$$\begin{aligned}
\bar{t}_0 &= (\alpha-\sigma(1-\delta))\hat{t}_0(R)+\int_R^1 \frac{\delta V(\xi)(\xi-1)\xi^2}{(1-\xi)\sigma+\xi}\mathrm{d}\xi,\\
\bar{t}_1 &= (\alpha-\sigma(1-\delta))\hat{t}_0(R)+\hat{t}_1(R),\\
\bar{t}_2 &= \int_R^1 \frac{(1-\xi)h_2(\xi)}{15\xi[(1-\sigma)\xi+\sigma][3(\sigma+\alpha-\sigma(1-\delta)-\delta V(\xi))\xi+1-3\sigma]^2}\mathrm{d}\xi,
\end{aligned}$$

where the functions $\hat{t}_0$ and $\hat{t}_1$ are defined in (3.30) and (3.33), and $h_2(\xi)$ is given in Appendix (C.3). Clearly there is a strong correspondence between these results and the ones derived in Section 3.4. In terms of the solutions $\hat{T}_i$ given in (3.29), (3.31), (B.2), we have $T_0 = \hat{T}_0$,

$$\begin{aligned} T_1 &= \hat{T}_0 + \frac{1}{\alpha}\hat{T}_1 + O(\alpha^{-2}) \quad \text{as} \quad \alpha \to \infty, \\ T_2 &= \hat{T}_0 + \frac{1}{\alpha}\hat{T}_1 + \frac{1}{\alpha^2}\frac{h_3(r,R)\hat{T}_1}{60R^3(R-1)^2} + O(\alpha^{-3}) \quad \text{as} \quad \alpha \to \infty, \end{aligned} \tag{3.45}$$

where the function $h_3(r, R)$ is defined in Appendix (C.3), so that clearly these approaches agree well in that limit. It is hoped that the iteration method also produces accurate analytical results for $\alpha = O(1)$.

For cylindrical particles (m=1) the first two iterations give

$$\begin{aligned} T_0 &= 1 - \frac{[R + \sigma(1-R)]\ln r}{R\ln R}, \\ T_1 &= T_0 + \frac{(-R + \sigma R - \sigma)}{Rh_4(R)}\left\{\left[r^2 - R^2 + \frac{R^2-1}{\ln R}\right]\ln r + 1 - r^2\right\}, \\ \bar{t}_0 &= (\alpha - \sigma(1-\delta))\hat{t}_0(R) + \int_R^1 \frac{\delta V(\xi)\xi^2 \ln\xi}{(1-\xi)\sigma + \xi}\mathrm{d}\xi, \\ \bar{t}_1 &= \int_R^1 \frac{h_4(\xi)}{4\xi(\ln\xi)^2[(\xi-1)\sigma - \xi]}\mathrm{d}\xi. \end{aligned}$$

where $h_4(R)$ is defined in Appendix (C.4) and $\hat{t}_0$ is given in (3.35). Again, there is a strong relationship with the large Stefan number solutions presented in Section 3.4. We have $T_0 = \hat{T}_0$, where $\hat{T}_0$ is the leading order solution (3.33) from the large Stefan number expansion, and furthermore, (3.45) holds with $\hat{T}_1$ given in Appendix (B.3).

In principle, this iterative scheme can be applied to obtain higher order approximations. Indeed, Dewynne [39] found that the second- or third-order approximations can provide reasonable results for the one-phase Stefan problem without surface tension, but lose their validity at times close to complete melting. However, as noted in Dewynne & Hill [95], there is no proof of convergence, and higher order iterations may lead to unphysical singularities. Some numerical results using this method are presented in the following section.

3.6 Results

In this section the analytical results of Sections 3.3-3.5 are compared with numerical solutions found using a front-fixing method given in Appendix D. This numerical scheme is chosen over the commonly used enthalpy method [32, 53], which has proved to be an efficient method for classical Stefan problems without surface tension, since the application of the enthalpy method involves characterising the liquid phase by the value of the temperature (or enthalpy) only. With the addition of surface tension effects, the temperature on the solid-melt interface is not constant, and thus this characterisation is no longer applicable. On the other hand, the front-fixing method, which works by transforming the moving boundary problem to a fixed-boundary problem, is relatively easy to apply, and produces acceptable results provided the timestep is properly chosen according to the Neumann method [100].

Note that only results for the sphere are shown here. It is found that the qualitative behaviour for cylinders was the same as for spheres, and it is only the scalings that are found to differ in some instances.

3.6.1 Check of numerical scheme for $\sigma = 0$, $V \equiv 0$

As a check on the front-fixing scheme used to compute solutions for $\sigma \neq 0$, results obtained using this method for $\sigma = 0$, $V \equiv 0$ were compared with results computed using the enthalpy method (which, as mentioned above, is straightforward to apply for $\sigma = 0$, $V \equiv 0$). It was found that, regardless of the Stefan number, the numerical results produced by the two methods were in excellent agreement, with temperature profiles essentially indistinguishable when plotted on the scale $0 \leq T \leq 1$ with $0 \leq r \leq 1$. As an example, included in Fig. 3.2 are profiles drawn for the two different Stefan numbers $\alpha = 1$ (corresponding to moderately fast melting) and $\alpha = 10$ (corresponding to slow melting). The only exception in this close agreement was for very small values of R (corresponding to times close to complete melting). In this regime, a slight difference between results produced by the two methods was noticed, as can be seen by Fig. 3.3, which contains the dependence of R on time t for Stefan numbers $\alpha = 1$, 2 and 5.

Thus, except for in the very final stages of melting, we are confident that the front-fixing scheme is accurate, provided the proper time-step is chosen to ensure

the stability of the scheme [100]. It may be that for times near complete melting the enthalpy method is more accurate than the front-fixing scheme, and to take an example, it is noted that for the value $\alpha = 10$ used in Fig. 2(b), the calculated time for complete melting using the front-fixing scheme was $t_f = 1.85$, while the corresponding time using the enthalpy method was $t_f = 1.81$. Using the large Stefan number approximation taken from [55, 57, 58], namely

$$t_f \approx \frac{\alpha + 1}{6} - \frac{\sqrt{2}\zeta(3)}{\pi^{5/2}\alpha^{1/2}},$$

where $\zeta(z)$ is the Riemann zeta function, we see that the complete melting time is approximately $t_f \approx 1.80$, which is in closer agreement with that found using the enthalpy scheme. For the reasons given above, however, all numerical solutions for $\sigma \neq 0$ cited in the rest of this section have been computed using the front-fixing scheme.

3.6.2 Comparison of small-time series and large Stefan number expansion with numerical results

In Figs 3.4 and 3.5 typical temperature profiles and interface positions (for $\sigma \neq 0$) computed with the front-fixing scheme are compared with corresponding results from the small time series (Section 3.3.1) and the large Stefan number expansion (Section 3.4.1, including all three terms) for a surface tension value $\sigma = 0.15$. The thin solid curve in Fig. 3.4 denotes the melting temperature (3.19), which for nonzero σ is dependent on both the surface tension σ and the location of the solid-melt interface $r = R$. For these plots the initial temperature V is assumed to be constant, meaning the melting process depends only on the effective Stefan number $\beta = \alpha - \sigma(1 - \delta) - \delta V$.

In Figs 3.4(a) and 3.5(a), which are for effective Stefan number $\beta = 1$, there is very good agreement between the numerical results and the small time solution during the early stages of the melting process, with each of these two methods producing noticeably different results for late times. Of course this behaviour is to be expected, since terms of order Y^2 ignored in (3.22) become more important as R decreases in value. The large Stefan number solution in Fig. 3.4(a) agrees much less favourably with the numerical solution than the small time series, and indeed

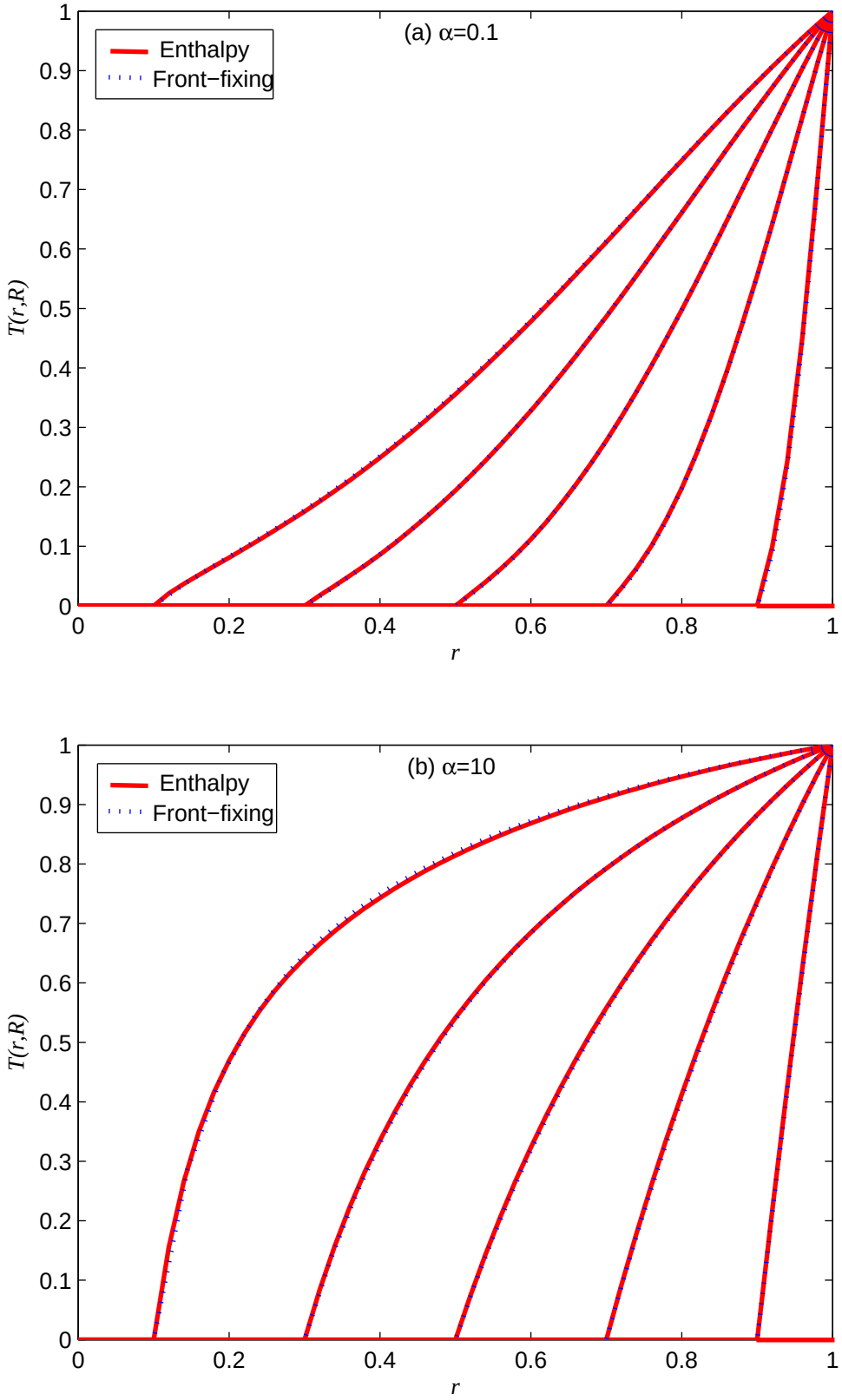

Figure 3.2: Plots of the temperature profiles computed numerically for $\sigma = 0$, $V = 0$ at different positions R=0.1, 0.3, 0.5, 0.7 and 0.9: part (a) is for $\alpha = 0.1$; part (b) is for $\alpha = 10$.

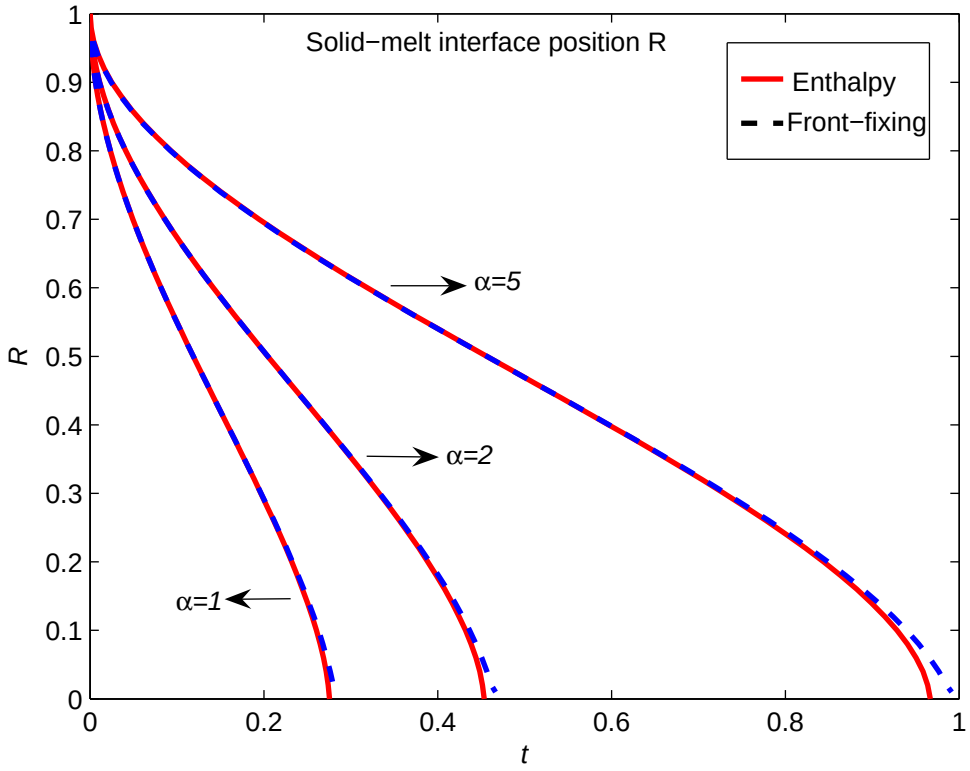

Figure 3.3: Plots of particle radius R versus time t computed numerically for Stefan numbers $\alpha = 1$, 2 and 5. For each curve $\sigma = 0$, $V = 0$.

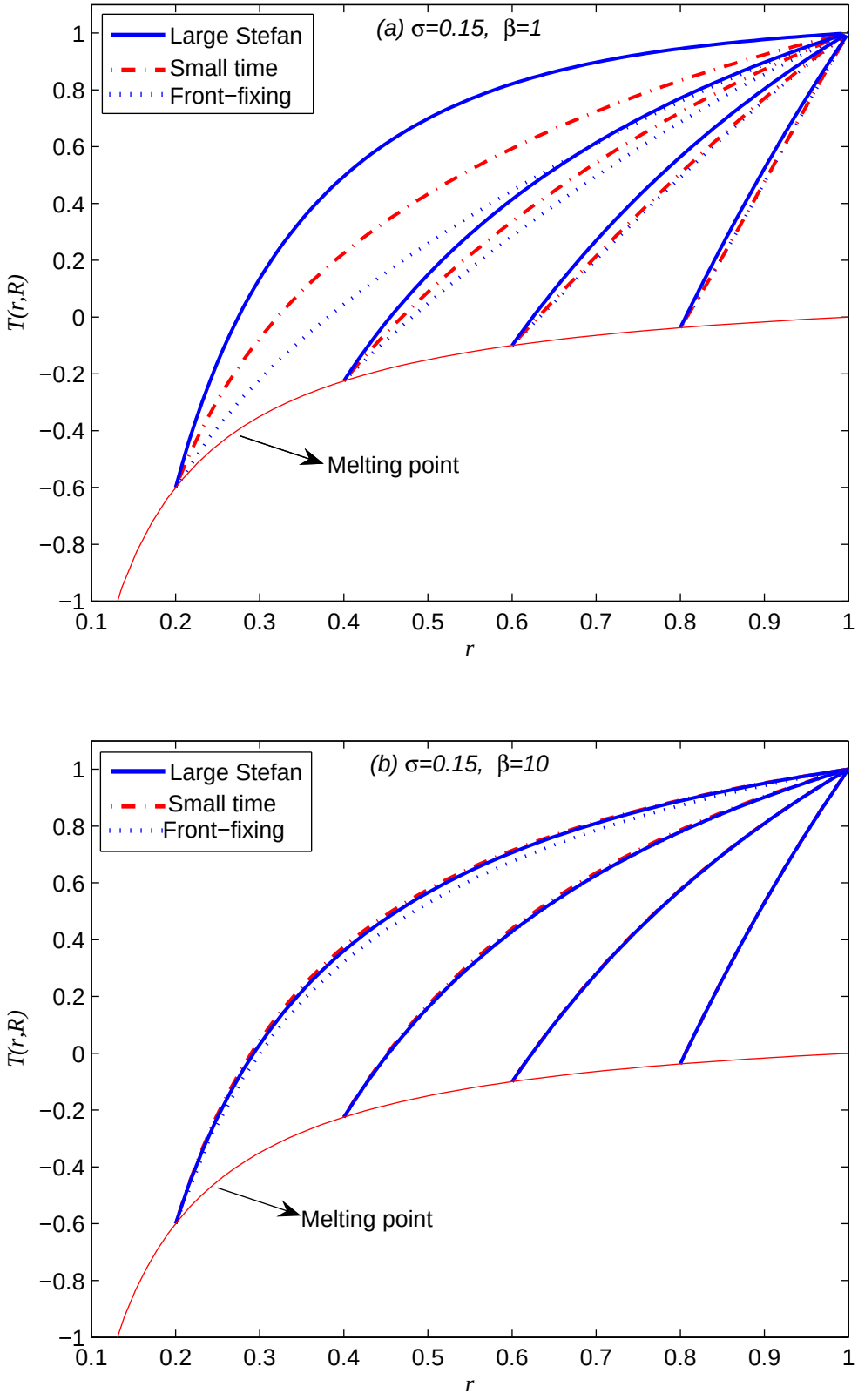

Figure 3.4: Plots of the temperature profiles for surface tension $\sigma = 0.15$ at different positions R=0.2, 0.4, 0.6 and 0.8: part (a) is for $\beta = 1$; part (b) is for $\beta = 10$. The three approaches used are the numerical scheme (dashed), the large Stefan number expansion (solid) and the small time series (dot-dashed). Included as a thin curve is the melting temperature.

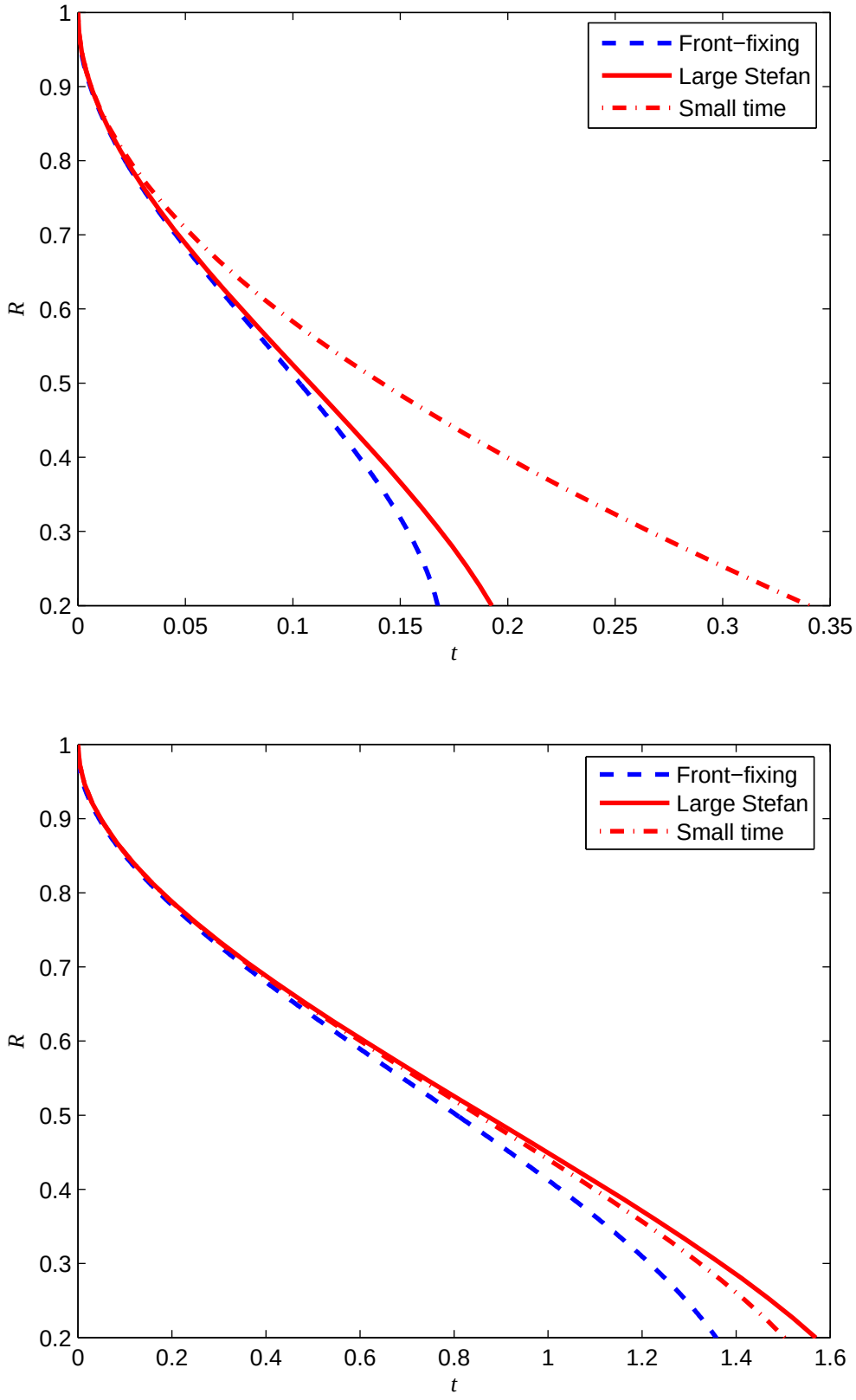

Figure 3.5: Plots of particle radius R versus time t for surface tension $\sigma = 0.15$: part (a) is for $\beta = 1$; part (b) is for $\beta = 10$. The three approaches used are the numerical scheme (dashed), the large Stefan number expansion (solid) and the small time series (dot-dashed).

we have left out the curve for $R = 0.2$ since it does not fit in the scale of the figure. This behaviour is not unsurprising, since the the value $\beta = 1$ is not large.

On the other hand, Figs 3.4(b) and 3.5(b) are drawn for $\beta = 10$, which can be considered large. Here both analytical approximations agree extremely well with the numerical solutions for the temperature profiles, but not quite as well for the interface position. It is remarkable that the small time series produces such accurate results for the temperature profiles, especially for later times. Any disagreement between the large Stefan number approximation and the numerical results for small values of R is due to the nature of the expansion (3.25)-(3.26), which implies that the interface is moving relatively slowly, and is not valid near complete melting (recall that increasing the Stefan number slows the melting process).

3.6.3 Comparison of iterative scheme with numerical results

Fig. 3.6 shows a comparison of the temperature profiles obtained from the three iterations (3.42)-(3.44) and the numerical front-fixing method for an effective Stefan number $\beta = 2$. In Fig. 3.6(a), which is for surface tension $\sigma = 0.05$, the profiles corresponding to each subsequent iteration agree more closely with the numerical result, suggesting the scheme may be converging to the exact solution. Indeed, the results from the third iteration are in excellent agreement with the numerical results for most of the melting process. Temperature profiles for a larger value of surface tension, namely $\sigma = 0.15$, are shown in Fig. 3.6(b). In this case it is evident that, at least for larger times, the iterative scheme is not converging. For $R = 0.2$ we see that the third iteration is much further away from the numerical results than the second. This suggests that the iterative scheme derived in Section 3.5 is a less effective tool for producing analytical results than the small time series and the large Stefan number expansion given in Sections 3.3 and 3.4. Similar conclusions can be drawn by observing plots showing the dependence of the interface position R on time t.

We make the comment that, as well as working better for smaller values of surface tension σ, it was found that the iterative scheme agreed well with numerical results for large values of the Stefan number. Of course this is not unexpected, given that in the limit $\alpha \to \infty$ we have shown in Section 3.5.2 that the iterative

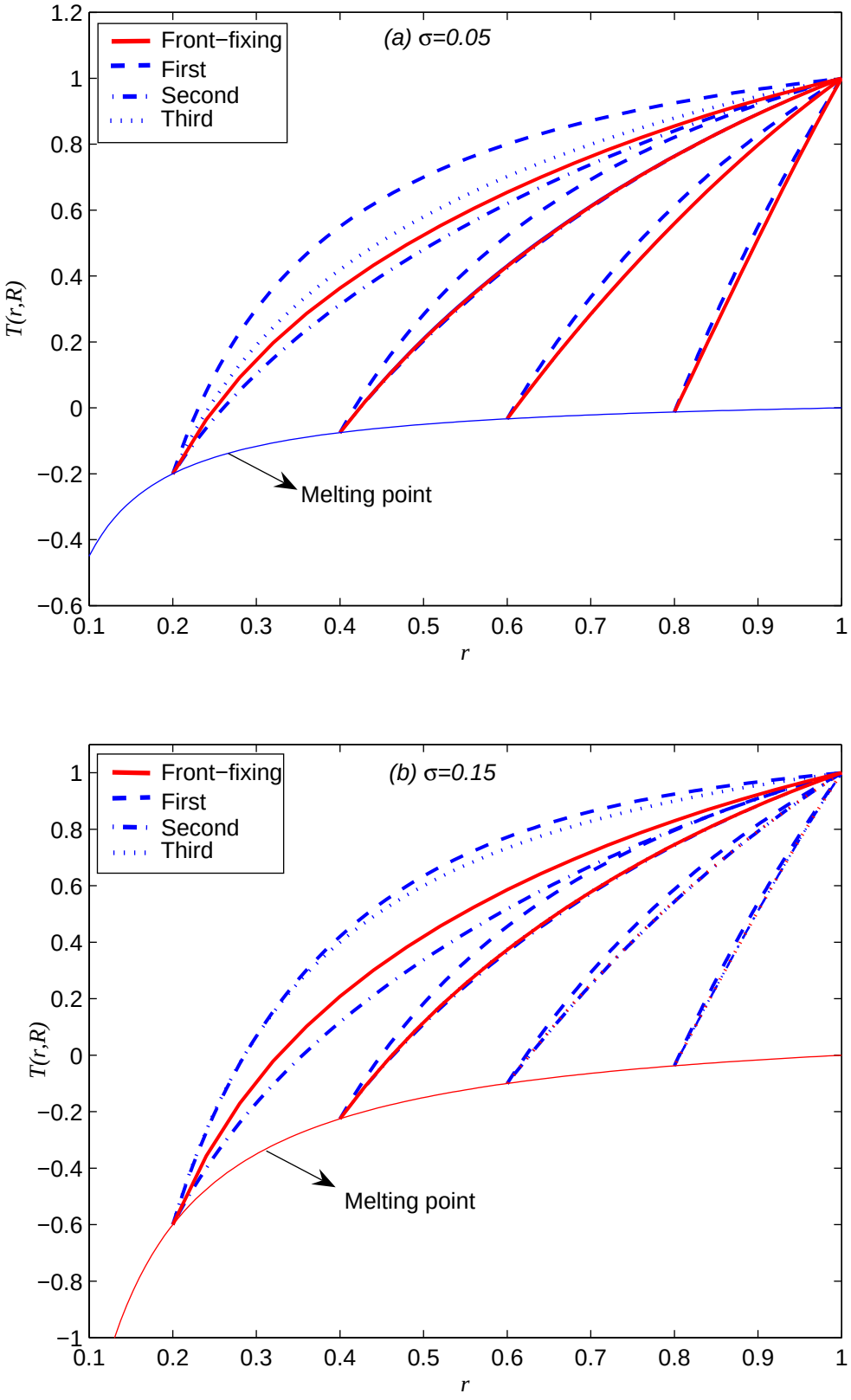

Figure 3.6: Plots of the temperature profiles for effective Stefan number $\beta = 2$ at different positions R=0.2, 0.4, 0.6 and 0.8: part (a) is for $\sigma = 0.05$; part (b) is for $\sigma = 0.15$. The numerical solution is compared with results obtained using the iterative scheme.

scheme approaches the large Stefan number expansion, and in Section 3.6.2 we have seen that the large Stefan number expansion gives an excellent approximation to the numerical results in that limit.

3.6.4 Effect of surface tension on the solid-melt interface

As an illustration of the effect of varying the surface tension parameter σ, the relationship between the velocity of the solid-melt interface dR/dt and the particle radius R is shown in Fig. 3.7 for three typical values of σ (all results are found using the numerical scheme). It is clear that for small time, varying surface tension does not have a significant effect on the curves, which is consistent with the finding that σ does not appear in the leading order term A_0 in the small time series (3.22). However, as R decreases, surface tension becomes more important and has a dramatic effect on the speed of the interface. Of course the critical radius R_c given in (3.21) increases as σ increases, which explains why blow-up occurs for each curve in this figure at different values of R.

More generally, it can be observed that the speed of the solid-melt interface decreases initially, then reaches a minimum when R is approximately a half of the original particle radius. For later times the interface accelerates until blow-up occurs ($dR/dt \to -\infty$ as $R \to R_c^+$).

As noted in Section 3.2.3, while the use of the boundary condition (3.14) instead of (3.20) is commonplace in the literature (see [50] and [97], for example), this approach does not conserve heat at the solid-melt interface, and should be avoided (at least for well-posed melting problems; (3.14) is only appropriate for the ill-posed process of outward solidification into an undercooled melt). In Fig. 3.8 the dependence of the interface velocity dR/dt on the particle radius R is shown for $\alpha = 2$, $\sigma = 0.2$, by applying each boundary condition separately (each solution is found numerically using the front-fixing method). The solid curve denotes the solution with (3.20), while the dashed curve corresponds to (3.14). It can be seen that for small time both solutions are in agreement, but for later times the interface for the correct solution speeds up more quickly, and will eventually blow-up as $R \to R_c^+$. Included in the figure is the thin dot-dashed curve, which shows the asymptotic behaviour (3.37). It is expected that as $R \to R_c^+$ the solid curve will

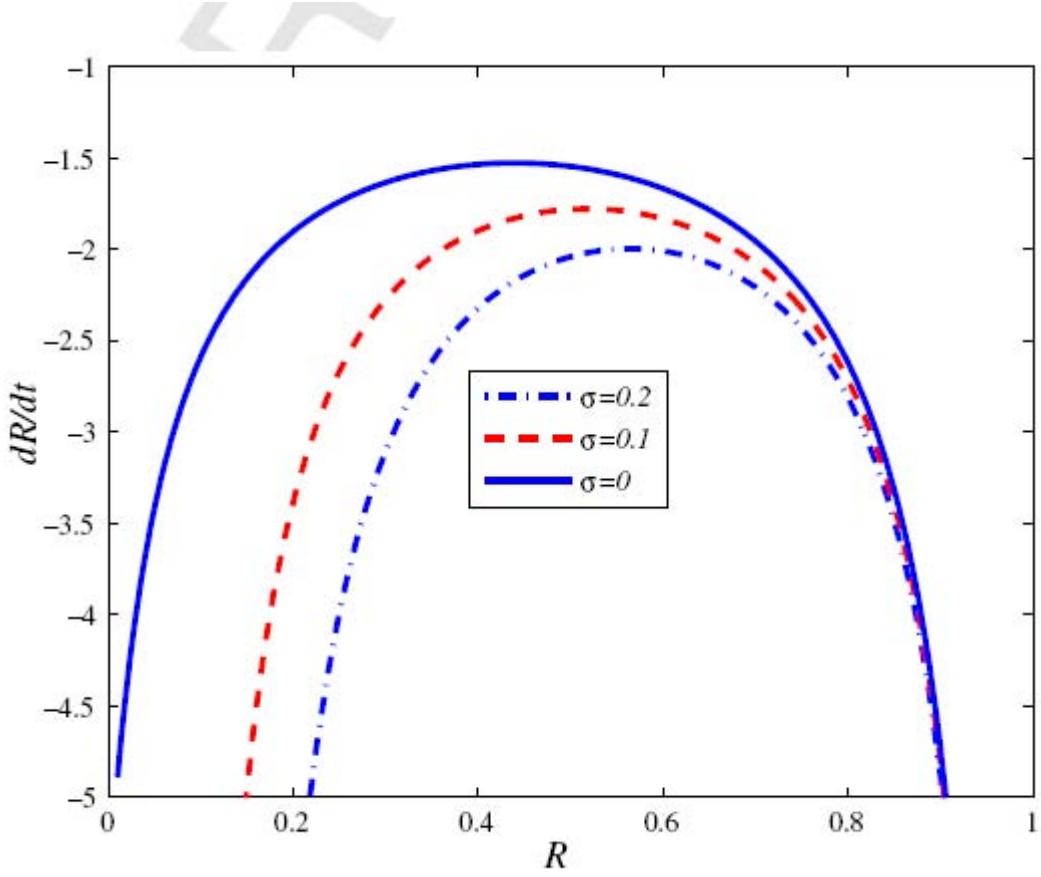

Figure 3.7: Dependence of the interface speed dR/dt on R for $\sigma = 0$ (solid curve), $\sigma = 0.1$ (dashed curve) and $\sigma = 0.2$ (dot-dashed curve). Each curve is drawn for $\beta = 2$.

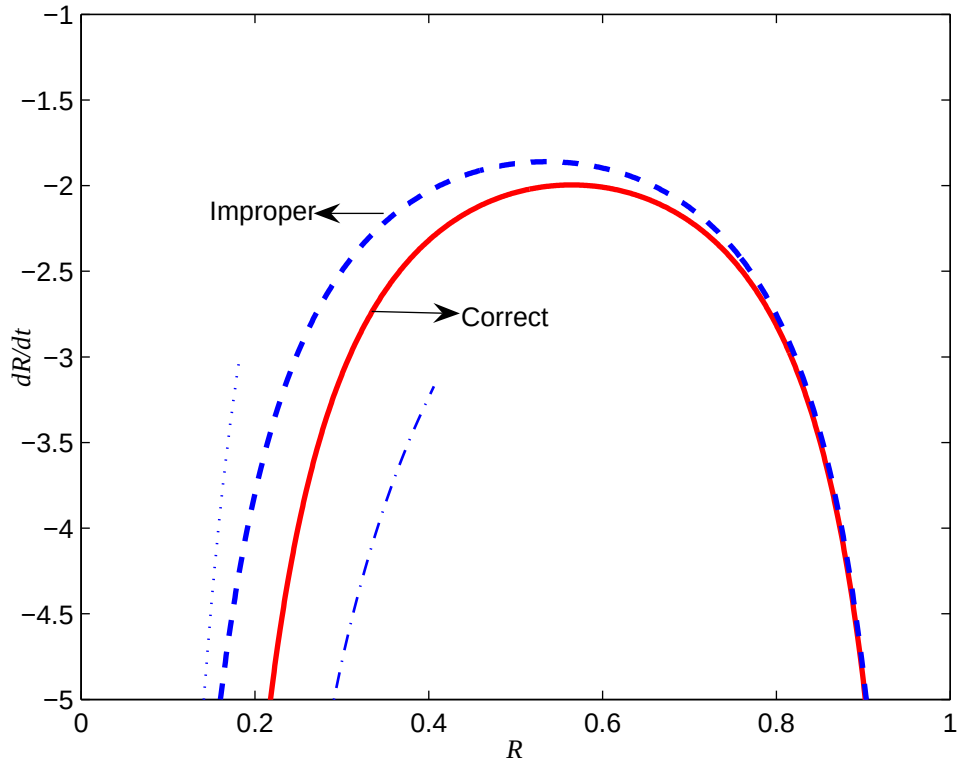

Figure 3.8: Dependence of the interface speed dR/dt on R for $\alpha = 2$, $\sigma = 0.2$, $V = 0$. The solid curve uses the correct boundary condition (3.20) while the dashed curve uses (3.14). Included is the asymptotic behaviours (3.36) (dotted curve) and (3.37) (dot-dashed curve).

approach the dot-dashed curve. Also included in the figure as a dotted curve is the asymptotic behaviour (3.36), derived by [97] using the condition (3.14). We expect the dashed curve to approach the dotted one in the limit $R \to 0$. In closing we note that the difference between the curves drawn for (3.14) and (3.20) will become more obvious for smaller values of the Stefan number.

3.7 Further discussion

This section deals with the one-phase Stefan problem for melting spherical and cylindrical particles with the assumption that the melting temperature depends on both surface tension and particle radius through the Gibbs-Thomson effect (1.1). Analytical solutions for a small-time series, a large Stefan number expansion and an integral iteration scheme are obtained, and they show good agreement with numerical solutions under certain conditions, particularly when melting is slow, which

often happens in real experiments with nanoscaled particles.

It is found that the addition of surface tension tends to accelerate the melting process. This effect is only weak for small time, but increases as the solid-melt interface evolves towards the centre of the particle. We find that the one-phase problem (3.17)-(3.20) predicts that ultimately a form of blow-up will occur, with the speed of the interface becoming infinite at a finite particle radius. This result may be an artifact of the way in which the free boundary problem (3.17)-(3.20) was derived; however, we note with interest that a phenomenon referred to as instant or abrupt melting has been observed in experiments dealing with melting nanoscaled particles [7]. This behaviour is qualitatively consistent with the predictions of our one-phase model.

It is well known that the opposite process to the one considered in this section, namely the outward solidification of an undercooled melt from a solid crystal, is ill-posed, with slight deviations from radial symmetry leading to the formation of tree-like structures or dendrites. Even under the idealised conditions of radial symmetry, the (ill-posed) outward solidification problem is not the time-reversal of the (well-posed) melting problem, due to the temporal derivative in the heat equation and also the fact that in the outward solidification case (3.20) should be replaced with (the more commonly used) $(3.14)_2$. This idealised problem has been treated for small time by Wu & Chen [49], while the more realistic problem which includes the dendrite growth is expected to be significantly more complicated. The reader is referred to [27] for discussions on the physics behind solidification problems with undercooled melts and related modelling issues.

The one-phase problem (3.17)-(3.20) considered in this section is derived in Section 3.2.3 by considering the two-phase problem in the singular limit $\kappa = k_s^*/k_\ell \to 0$. Although this limit may be appropriate for some insulators and semiconductors [101], and also for analogous problems arising in mass transfer, for most metals it is usually the case that $\kappa = O(1)$. However, the problem (3.17)-(3.20) still provides a useful approximation for melting nanoparticles, since in typical experiments the Stefan number α is large, and in the limit $\alpha \gg 1$ the temperature in the liquid phase is only weakly dependent on the solid-phase, even for $\kappa = O(1)$.

As an illustration, we consider the two-phase problem (3.7)-(3.13) for the sphere

with $V \equiv$ constant and $\alpha \gg 1$. On the time-scale $t = O(\alpha)$ we scale time as $t = \alpha\hat{t}$, and apply the expansion (3.25) for the liquid phase. Further, we write

$$T_s = v(r, R; \alpha) + w(r, R; \alpha)$$

for the solid phase, where

$$v \sim \hat{v}_0(r, R) + \frac{1}{\alpha}\hat{v}_1(r, R) + O(\alpha^{-2}), \quad w \sim e^{-\alpha g(R)}\left(\hat{w}_0(r, R) + O(\alpha^{-1})\right)$$

as $\alpha \to \infty$, and describe the location of the solid-melt interface by (3.26). Preliminary calculations reveal that

$$\hat{v}_0 = \sigma\left(1 - \frac{1}{R}\right), \quad \hat{v}_1 = \frac{\sigma\delta(r^2 - R^2)}{6\kappa\hat{t}_0' R^2}, \tag{3.46}$$

$$\hat{w}_0 = \frac{2RU_s}{\pi r}\sin\left(\frac{\pi r}{R}\right), \quad g = -\frac{\pi^2\kappa}{\delta}\int_R^1 \frac{\hat{t}_0'}{R^2}\,\dot{\mathrm{R}}, \tag{3.47}$$

which implies that on the solid-melt interface $\partial T_s/\partial r = O(\alpha^{-1})$, so that, to leading order, the Stefan condition (3.11) is approximated by $(3.28)_2$. Thus, at least for $V \equiv$ constant and for $1 - R = O(1)$, the one-phase problem (3.17)-(3.20) should provide a reasonable approximation to the two-phase problem (3.7)-(3.13) when the Stefan number α is large, even for $\kappa = O(1)$. (Ideas which lead to similar conclusions are stated in the Appendix of [102], where the three different regimes $\alpha \gg 1$ with $\kappa = O(1)$, $\alpha \gg 1$ with $\kappa \ll 1$ and $\alpha = O(1)$ with $\kappa \ll 1$ are noted for the two-phase problem. The resulting boundary conditions given for the latter regime do not conserve heat for well-posed melting problems, and so are only valid for ill-posed crystal growth problems.) For $\alpha = O(1)$ and $\kappa = O(1)$, however, the melting process may be studied more comprehensively by considering the full two-phase problem; such analysis will appear elsewhere.

We close by noting that the melting of genuinely two- and three-dimensional objects may exhibit certain characteristics not displayed in the present study, which has been confined to radially-symmetric particles. For example, a natural question is to ask how the shape of the solid-melt interface evolves when a two- or three-dimensional particle is melted, and for the one-phase limit this question is addressed for the zero surface tension case using large-Stefan-number and near-complete-melting asymptotics in [93, 103, 104]. It is shown there that the interface

evolves to an ellipse or ellipsoid in shape just before complete melting, regardless of the initial geometry. In the present study, we argue in Section 3.4.3 that the final stages of melting are significantly affected by surface tension, to the extent that for the more general two- and three-dimensional problem, the scalings used in [93, 103, 104] would not be appropriate if $\sigma \neq 0$. Furthermore, there is experimental evidence [105, 106] that suggests surface tension acts to force the elliptic or ellipsoidal interfaces to become circular or spherical at very small times just before complete melting. Thus the task of generalising [93, 103, 104] to include the effects of surface tension would seem to provide an interesting and nontrivial problem for future research.

Chapter 4

Two-phase Stefan problem with spherical symmetry, including the effects of surface tension

4.1 Introduction

In Chapter 3, we investigate the one-phase limit for nanoparticle melting with the assumption that $\kappa_s^*/\kappa_\ell^* \to 0$ by including the surface tension effect. However, for many cases in the physical world, the differences between the thermal conductivities of the solid and liquid phases are small. Thus, there is not ideal one-phase problem when considering the effect of the surface tension. The approaches used in Chapter 3 are extended to study the two-phase melting problem for spherical nanoparticle melting in Chapter 4 which is organized as follows. In Section 4.2 the governing equations for the two-phase melting problem for spheres is formulated. This problem is analysed using a small-time perturbation approach in Section 4.3, and then a large Stefan number expansion in Section 4.4. Numerical results are computed using a numerical front-fixing scheme, and these are discussed in Section 4.5. It is shown that the analytic results derived in Sections 4.3 and 4.4 agree well with the numerical results in the appropriate regimes. Further, in the limit of slow conduction in the solid phase, numerical evidence is provided to show that the full two-phase problem does indeed reduce to the one-phase problem derived in [89] and Chapter 3. Finally, the numerical results predict that ultimately the solid becomes superheated and, furthermore, the speed of the solid-melt interface becomes unbounded at some critical time before complete melting takes place. At this time the temperature gradient in the solid phase also becomes unbounded at the interface. This form

of finite-time blow-up and the apparent relationship with the problem of melting a superheated solid particle noted are discussed in Section 4.6.

4.2 Problem description and non-dimensional governing equations

The geometry for the melting process under consideration is illustrated in Fig. 3.1. The relevant independent variables are the radial distance from the centre of the particle, r^*, and time, t^*. We suppose the particle is initially of radius a^*, and at a uniform temperature T_i^*. Then at time $t^* = 0$ the temperature on the surface $r^* = a^*$ is suddenly raised to T_a^*, and subsequently held there at that value. Provided that T_a^* is above the melting temperature, the particle will begin to melt, with a solid-melt interface $r^* = R^*(t^*)$ propagating from $r^* = a^*$ towards the centre of the particle.

From Section 3.2.1 in Chapter 3, when $m = 2$, the non-dimensional governing equations for the spherical nanoparticle melting are

$$\frac{\partial T_\ell}{\partial t} = \frac{\partial^2 T_\ell}{\partial r^2} + \frac{2}{r}\frac{\partial T_\ell}{\partial r} \quad \text{in} \quad R(t) < r < 1, \tag{4.1}$$

$$\frac{\partial T_s}{\partial t} = \frac{\kappa}{\delta}\left(\frac{\partial^2 T_s}{\partial r^2} + \frac{2}{r}\frac{\partial T_s}{\partial r}\right) \quad \text{in} \quad 0 < r < R(t), \tag{4.2}$$

subject to the boundary conditions

$$T_\ell = 1 \quad \text{on} \quad r = 1, \tag{4.3}$$

$$T_\ell = T_s = \sigma\left(1 - \frac{1}{R}\right) \quad \text{on} \quad r = R(t), \tag{4.4}$$

$$\frac{\partial T_\ell}{\partial r} - \kappa\frac{\partial T_s}{\partial r} = -\frac{dR}{dt}\left(-\frac{\sigma(1-\delta)}{R} + \alpha\right) \quad \text{on} \quad r = R(t), \tag{4.5}$$

$$\frac{\partial T_s}{\partial r} = 0 \quad \text{on} \quad r = 0, \tag{4.6}$$

and initial conditions

$$T_s = V, \quad R = 1, \quad \text{at} \quad t = 0. \tag{4.7}$$

The five dimensionless parameters in the problem are defined by

$$\kappa = \frac{{k_s}^*}{{k_\ell}^*}, \quad \delta = \frac{{c_s}^*}{{c_\ell}^*}, \quad \sigma = \frac{\omega T_m^*}{a^*\Delta T^*}, \quad \alpha = \frac{L}{{c_\ell}^*\Delta T^*}, \quad V = \frac{T_i^* - T_m^*(1-\omega/a^*)}{\Delta T^*}.$$

These are the ratio of thermal conductivities, the ratio of specific heat capacities, the interfacial tension parameter, the Stefan number, and the dimensionless initial temperature, respectively.

4.3 Small time limit

In Chapter 3 a small-time perturbation expansion, used in [51] for classical one-phase problems and in Chapter 2 for classical two-phase problems, is extended to the one-phase analysis by taking into account the effects of surface tension. In this section we generalise the above studies to the full two-phase problem with surface tension.

4.3.1 Summary of the details

The idea is to look for solutions of the form

$$u \sim \frac{1}{r}\left\{A_0(X) + YA_1(X) + O(Y^2)\right\}, \; v \sim V + \frac{1}{r}\left\{B_0(X) + YB_1(X) + O(Y^2)\right\}, \tag{4.8}$$

as $Y \to 0^+$, where X and Y are defined by

$$X = \frac{1-r}{1-R}, \quad Y = 1 - R.$$

This change of variables transforms the inner solid phase to $1 \leq X < (1-R)^{-1}$ and the outer liquid phase to the fixed domain $0 \leq X \leq 1$.

After substituting (4.8) into the governing equations (4.1)-(4.2), (4.5), we find that A_0, A_1, B_0 and B_1 satisfy the coupled ordinary differential equations

$$A_0'' + \gamma X A_0' = 0, \quad A_1'' + \gamma(XA_1' - A_1) = \frac{a_1 - \gamma\alpha}{\alpha - \sigma(1-\delta)} XA_0',$$

$$\frac{\kappa}{\delta}B_0'' + \gamma X B_0' = 0, \quad \frac{\kappa}{\delta}B_1'' + \gamma(XB_1' - B_1) = \frac{a_1 - \gamma\alpha}{\alpha - \sigma(1-\delta)} XB_0',$$

where

$$\gamma = -\frac{A_0'(1) - \kappa B_0'(1)}{\alpha - \sigma(1-\delta)}, \quad a_1 = A_1'(1) - \kappa B_1'(1) + \kappa V.$$

From (4.3)-(4.4), (4.7), we have the boundary conditions

$$A_0 = 1, \quad A_1 = 0, \quad \text{on} \quad X = 0,$$

$$A_0 = 0, \quad A_1 = -\sigma, \quad B_0 = -V, \quad B_1 = V - \sigma \quad \text{on} \quad X = 1,$$

$$B_0 = o(1), \quad B_1 = o(X), \quad \text{as} \quad X \to \infty.$$

The leading order solutions are

$$A_0 = 1 - \frac{\operatorname{erf}\left(\sqrt{\frac{\gamma}{2}}\, X\right)}{\operatorname{erf}\sqrt{\frac{\gamma}{2}}}, \quad B_0 = -V\, \frac{\operatorname{erfc}\left(\sqrt{\frac{\delta\gamma}{2\kappa}}\, X\right)}{\operatorname{erfc}\sqrt{\frac{\delta\gamma}{2\kappa}}}, \tag{4.9}$$

where γ is the solution to

$$\gamma(\alpha - \sigma(1-\delta)) = \frac{1}{L_\ell} e^{-\gamma/2} + \frac{\kappa V}{L_s} e^{-\delta\gamma/2\kappa}, \tag{4.10}$$

with L_ℓ and L_s defined by

$$L_\ell = \sqrt{\frac{\pi}{2\gamma}}\operatorname{erf}\sqrt{\frac{\gamma}{2}}, \quad L_s = \sqrt{\frac{\kappa\pi}{2\delta\gamma}}\operatorname{erfc}\sqrt{\frac{\delta\gamma}{2\kappa}}.$$

The solution (4.9) together with the transcendental equation (4.10) is almost identical to the well known Neumann solution (Carslaw & Jaeger [33], page 285), the only difference being that in the Neumann solution (which is for zero surface tension), the term $\alpha - \sigma(1-\delta)$ in (4.10) is replaced by α. The correction terms are

$$A_1 = -\sigma X + c_1\, X\left(1 - e^{\gamma(1-X^2)/2}\right),$$

$$B_1 = c_2\left[e^{-\delta\gamma X^2/2\kappa} - \sqrt{\frac{\delta\gamma\pi}{2\kappa}}\, X \operatorname{erfc}\left(\sqrt{\frac{\delta\gamma}{2\kappa}} X\right)\right] + c_3\, X e^{-\delta\gamma X^2/2\kappa}, \tag{4.11}$$

where

$$c_1 = \frac{1}{3\gamma}\left(\frac{\gamma\alpha - a_1}{\beta}\right)\frac{1}{L_\ell} e^{-\gamma/2}, \quad c_3 = \frac{V}{3\gamma L_s}\left(\frac{\gamma\alpha - a_1}{\beta}\right), \tag{4.12}$$

$$c_2 = \frac{\kappa}{\delta\gamma L_s}\left\{\sigma - V\left[1 - \frac{1}{3\gamma}\left(\frac{\gamma\alpha - a_1}{\beta}\right)\frac{1}{L_s} e^{-\delta\gamma/2\kappa}\right]\right\}\left[1 - \frac{\kappa}{\delta\gamma L_s} e^{-\delta\gamma/2\kappa}\right]^{-1},$$

$$\frac{\gamma\alpha - a_1}{\alpha - \sigma(1-\delta)} = \frac{3\left(\gamma\alpha + \sigma - \kappa V + \kappa(V-\sigma)\left[1 - \frac{\kappa}{\delta\gamma L_s} e^{-\delta\gamma/2\kappa}\right]^{-1}\right)}{(3+\gamma)\beta + \frac{V}{\gamma L_s} e^{-\delta\gamma/2\kappa}\left\{\kappa\left[1 - \frac{\kappa}{\delta\gamma L_s} e^{-\delta\gamma/2\kappa}\right]^{-1} - \kappa\gamma - \kappa + \delta\gamma\right\}}.$$

From the Stefan condition (4.5) we have the small time behaviour

$$t = \frac{1}{2\gamma}(1-R)^2 - \frac{1}{3\gamma^2}\left(\frac{\gamma\alpha - a_1}{\beta}\right)(1-R)^3 + O((1-R)^4) \quad \text{as} \quad R \to 1^-. \tag{4.13}$$

As discussed in Chapter 2, the solution described above does not satisfy the no-

flux condition (4.6) at $r = 0$, and indeed by the very nature of this approach one boundary condition must be sacrificed. However, we can easily derive an excellent approximate solution for $t \ll 1$ by changing $(4.8)_2$ to be

$$v \approx V + \frac{1}{r}\left\{B_0(X) - B_0(2Y^{-1} - X) + YB_1(X) - YB_1(2Y^{-1} - X)\right\},$$

where B_0 and B_1 are given by (4.9) and (4.11). Given that $2Y^{-1} - X = (1+r)/(1-R)$, this alteration can be thought of as adding an image solution in the domain $-1 \leq r < 0$. The effect of this change is that the new solution now satisfies (4.1)-(4.3) and (4.6)-(4.7) exactly, but only satisfies (4.4)-(4.5) approximately; however, the errors from (4.4)-(4.5) are exponentially small in Y as $Y \to 0^+$.

4.3.2 Slow diffusion limit of small-time analysis

In the limit $\kappa \to 0$, the transcendental equation (4.10) becomes

$$\gamma(\alpha - \sigma(1-\delta) - \delta V) = \frac{1}{L_\ell} e^{-\gamma/2}$$

and the constant c_1 in (4.12) becomes

$$c_1 = \frac{\gamma(\alpha + \delta\sigma - \delta V) + \sigma}{3 + \gamma}.$$

These two results agree with the small-time analysis of the one-phase problem studies in Chapter 3, which is as expected.

4.4 Large Stefan number limit

In this section we generalise the large Stefan number analysis used in Chapter 2, which was used for the classical two-phase problem, to allow for surface tension on the solid-melt interface. In this limit the interface moves slowly, because of the large amount of latent heat being absorbed there. For early stages the surface tension has no qualitative effect on the melting process, and the details follow Chapter 2 very closely. For later stages, the temperature in the solid phase decays very quickly to zero for the classical case $\sigma = 0$; however, for $\sigma \neq 0$ the leading order temperature in the solid follows the variable melting temperature, and correction terms ultimately lead to superheating. That is, after some point in time we find the temperature in the solid phase will be everywhere greater than the melting temperature.

4.4.1 Time-scale $t = O(1)$

On the first time-scale, which is $t = O(1)$, heat diffuses a distance $O(1)$ (provided $\kappa = O(1)$), but the interface only propagates a distance $O(\alpha^{-1/2})$. Thus a boundary layer develops near $r = 1$.

4.4.1.1 Inner region, $1 - r = O(\alpha^{-1/2})$

For the inner region we scale the spatial variables as $r = 1 - \alpha^{-1/2}\tilde{r}$, $R(t) = 1 - \alpha^{-1/2}\tilde{R}(t)$, and write

$$u \sim \tilde{u}_0(\tilde{r}, t) + \frac{1}{\alpha^{1/2}}\tilde{u}_1(\tilde{r}, t) + O(\alpha^{-1}), \quad v \sim \frac{1}{\alpha^{1/2}}\tilde{v}_1(\tilde{r}, t) + O(\alpha^{-1}),$$

$$\tilde{R} \sim \tilde{R}_0(t) + \frac{1}{\alpha^{1/2}}\tilde{R}_1(t) + O(\alpha^{-1}) \quad \text{as} \quad \alpha \to \infty.$$

The leading order problem for $\tilde{u}_0$, namely

$$\frac{\partial^2 \tilde{u}_0}{\partial \tilde{r}^2} = 0 \quad \text{in} \quad 0 < \tilde{r} < \tilde{R}_0, \tag{4.14}$$

$$\tilde{u}_0 = 1 \quad \text{on} \quad \tilde{r} = 0, \quad \tilde{u}_0 = 0, \quad \frac{\partial \tilde{u}_0}{\partial \tilde{r}} = -\frac{d\tilde{R}_0}{dt} \quad \text{on} \quad \tilde{r} = \tilde{R}_0, \tag{4.15}$$

has the solution

$$\tilde{u}_0 = 1 - \frac{\tilde{r}}{\tilde{R}_0}, \quad \tilde{R}_0 = \sqrt{2t}. \tag{4.16}$$

Note that the solution is independent of the surface tension σ, and is thus identical to that given in Chapter 2.

The next order problems are

$$\frac{\partial^2 \tilde{u}_1}{\partial \tilde{r}^2} = 2\frac{\partial \tilde{u}_0}{\partial \tilde{r}} \quad \text{in} \quad 0 < \tilde{r} < \tilde{R}_0, \quad \frac{\partial^2 \tilde{v}_1}{\partial \tilde{r}^2} = 0 \quad \text{in} \quad \tilde{r} > \tilde{R}_0, \tag{4.17}$$

with boundary conditions

$$\tilde{u}_1 = 0 \quad \text{on} \quad \tilde{r} = 0, \tag{4.18}$$

$$\tilde{u}_1 + \tilde{R}_1\frac{\partial \tilde{u}_0}{\partial \tilde{r}} = -\sigma\tilde{R}_0, \quad \tilde{v}_1 = -\sigma\tilde{R}_0, \quad \frac{\partial \tilde{u}_1}{\partial \tilde{r}} - \kappa\frac{\partial \tilde{v}_1}{\partial \tilde{r}} = -\frac{d\tilde{R}_1}{dt} \quad \text{on} \quad \tilde{r} = \tilde{R}_0, \tag{4.19}$$

$$\tilde{v}_1 \sim \tilde{a}_1(t)\tilde{r} \quad \text{as} \quad \tilde{r} \to \infty. \tag{4.20}$$

The function $\tilde{a}_1(t)$ will be determined by matching with the outer region, as described below.

In terms of $\tilde{a}_1(t)$ the solutions to (4.17)-(4.20) are

$$\tilde{u}_1 = -\frac{1}{\tilde{R}_0}\tilde{r}^2 + \left(1 - \sigma + \frac{\tilde{R}_1}{\tilde{R}_0^2}\right)\tilde{r}, \quad \tilde{v}_1 = \tilde{a}_1(\tilde{r} - \tilde{R}_0) - \sigma\tilde{R}_0,$$

with $\tilde{R}_0$ given in (4.16) and $\tilde{R}_1$ satisfying the differential equation

$$\frac{d\tilde{R}_1}{dt} + \frac{\tilde{R}_1}{\tilde{R}_0^2} = 1 + \sigma + \kappa\tilde{a}_1 \tag{4.21}$$

and initial condition $\tilde{R}_1(0) = 0$.

4.4.1.2 Outer region, $1 - r = O(1)$

The outer region is for $1 - r = O(1)$. Here we write $v = \bar{v}(r, t)$, where

$$\frac{\partial\bar{v}}{\partial t} = \kappa\left(\frac{\partial^2\bar{v}}{\partial r^2} + \frac{2}{r}\frac{\partial\bar{v}}{\partial r}\right) \quad \text{in} \quad 0 < r < 1,$$

$$\bar{v} = 0 \quad \text{on} \quad r = 1, \quad \frac{\partial\bar{v}}{\partial r} = 0 \quad \text{on} \quad r = 0, \quad \bar{v} = V \quad \text{at} \quad t = 0.$$

The solution for $\bar{v}$ is

$$\bar{v} = \frac{2V}{\pi r}\sum_{n=1}^{\infty}\frac{(-1)^{n+1}}{n}\sin(n\pi r)e^{-n^2\pi^2\kappa t}. \tag{4.22}$$

4.4.1.3 Matching between regions

By rewriting (4.22) in inner variables $(\tilde{r}, t)$ and expanding as $\alpha \to \infty$ we find

$$\tilde{v}_1 \sim 2V\tilde{r}\sum_{n=1}^{\infty}e^{-n^2\pi^2\kappa t} \quad \text{as} \quad \tilde{r} \to \infty.$$

Thus matching between the two regions gives

$$\tilde{a}_1 = 2V\sum_{n=1}^{\infty}e^{-n^2\pi^2\kappa t}, \quad \tilde{v}_1 = 2V(\tilde{r} - \tilde{R}_0)\sum_{n=1}^{\infty}e^{-n^2\pi^2\kappa t} - \sigma\tilde{R}_0. \tag{4.23}$$

By substituting $\tilde{a}_1$ and $\tilde{R}_0$ into equation (4.21) and we obtain the moving boundary location, i.e.

$$\tilde{R}_1 = \frac{2}{3}(1 + \sigma)t + V\sum_{n=1}^{\infty}\left\{\frac{2e^{-n^2\pi^2\kappa t}}{n^2\pi^2} - \frac{\operatorname{erf}\left(\pi n\sqrt{\kappa t}\right)}{n^3\pi^{5/2}\kappa^{1/2}t^{1/2}}\right\}.$$

4.4.1.4 Summary of time-scale $t = O(1)$

On the time-scale $t = O(1)$ we see that near the moving boundary the temperature in both phases has an algebraic dependence on the small parameter $\alpha^{-1/2}$. Furthermore, the two phases are coupled, although to leading order both the temperature in the solid and location of the free boundary are independent of the liquid phase. Note that the inclusion of surface tension has no qualitative effect on the solution on this time-scale.

4.4.2 Time-scale $t = O(\alpha)$

On the time-scale $t = O(\alpha)$ the solid-melt interface moves a distance $O(1)$. We rescale time as $t = \alpha\hat{t}$, where $\hat{t} = O(1)$, and look for solutions of the form

$$T_\ell = \hat{u}_0(r,R) + \frac{1}{\alpha}\hat{u}_1(r,R) + O(\alpha^{-2}), \quad T_s = \hat{v}_0(r,R) + \frac{1}{\alpha}\hat{v}_1(r,R) + \ldots + \hat{w}(r,R;\alpha), \tag{4.24}$$

$$\hat{t} = \hat{t}_0(R) + \frac{1}{\alpha}\,\hat{t}_1(R) + \ldots + \hat{\tau}(R;\alpha) \quad \text{as} \quad \alpha \to \infty. \tag{4.25}$$

The ellipses in (4.24)-(4.25) denote terms which are $O(\alpha^{-2})$ *and* independent of the initial temperature V, while the terms $\hat{w}(r,R;\alpha)$ and $\hat{\tau}(R;\alpha)$ are exponentially small in α (and will depend on V).

The problems for $\hat{u}_i$ and $\hat{v}_i$ $(i = 0, 1)$ are all elliptic (with no initial conditions); they are

$$\frac{1}{r^2}\frac{\partial}{\partial r}\left(r^2\frac{\partial \hat{u}_0}{\partial r}\right) = 0 \quad \text{on} \quad R < r < 1, \quad \frac{1}{r^2}\frac{\partial}{\partial r}\left(r^2\frac{\partial \hat{v}_0}{\partial r}\right) = 0 \quad \text{on} \quad 0 < r < R,$$

$$\hat{u}_0 = 1 \quad \text{on} \quad r = 1, \quad \hat{u}_0 = \hat{v}_0 = \sigma\left(1 - \frac{1}{R}\right) \quad \text{on} \quad r = R, \quad \frac{\partial \hat{v}_0}{\partial r} = 0 \quad \text{on} \quad r = 0,$$

$$\hat{t}_0'\left(\frac{\partial \hat{u}_0}{\partial r} - \kappa\frac{\partial \hat{v}_0}{\partial r}\right) = -1 \quad \text{on} \quad r = R,$$

$$\frac{1}{r^2}\frac{\partial}{\partial r}\left(r^2\frac{\partial \hat{u}_1}{\partial r}\right) = \frac{1}{\hat{t}_0'}\frac{\partial \hat{u}_0}{\partial R} \quad \text{on} \quad R < r < 1,$$

$$\frac{1}{r^2}\frac{\partial}{\partial r}\left(r^2\frac{\partial \hat{v}_1}{\partial r}\right) = \frac{1}{\hat{t}_0'}\frac{\partial \hat{v}_0}{\partial R} \quad \text{on} \quad 0 < r < R,$$

$$\hat{u}_1 = 0 \quad \text{on} \quad r = 1 \quad \hat{u}_1 = \hat{v}_0 = 0 \quad \text{on} \quad r = R, \quad \frac{\partial \hat{v}_1}{\partial r} = 0 \quad \text{on} \quad r = 0,$$

$$\hat{t}_1'\left(\frac{\partial \hat{u}_0}{\partial r} - \kappa\frac{\partial \hat{v}_0}{\partial r}\right) + \hat{t}_0'\left(\frac{\partial \hat{u}_1}{\partial r} - \kappa\frac{\partial \hat{v}_1}{\partial r}\right) = \frac{(1-\delta)\sigma}{R} \quad \text{on} \quad r = R.$$

By solving the ordinary differential equations (ODEs) with appropriate boundary conditions involving $\hat{u}_0$ and $\hat{v}_0$, we can obtain $\hat{u}_0$. $\hat{v}_0$ and $\hat{t}_0$. Then substitute $\hat{u}_0$. $\hat{v}_0$ and $\hat{t}_0$ into the other ODEs and we can obtain $\hat{u}_1$. $\hat{v}_1$ and $\hat{t}_1$. Based on this ideas, we obtain the solutions

$$\hat{u}_0 = \frac{1}{r}\left[1-\left(\frac{1-r}{1-R}\right)\right]+\sigma\left(1-\frac{1}{r}\right), \tag{4.26}$$

$$\hat{v}_0 = \sigma\left(1-\frac{1}{R}\right) \tag{4.27}$$

$$\hat{t}_0 = -\frac{\sigma^2(1-R)}{(1-\sigma)^3}+\frac{(1-2\sigma)(1-R)^2}{2(1-\sigma)^2}-\frac{(1-R)^3}{3(1-\sigma)}-\frac{\sigma^2\ln\left[R+\sigma(1-R)\right]}{(1-\sigma)^4} \tag{4.28}$$

$$\hat{u}_1 = -\frac{R+\sigma(1-R)}{6rR^2}\left(\frac{1-r}{1-R}\right)\left[1-\left(\frac{1-r}{1-R}\right)^2\right], \tag{4.29}$$

$$\hat{v}_1 = -\frac{\sigma\delta[R+\sigma(1-R)]}{6\kappa R^4(1-R)}\left(r^2-R^2\right) \tag{4.30}$$

$$\hat{t}_1 = \frac{1-\delta\sigma-3\sigma(1-\delta)}{3}\left\{\frac{\sigma(1-R)}{(1-\sigma)^2}+\frac{(1-R)^2}{2(1-\sigma)}+\frac{\sigma\ln\left[R+\sigma(1-R)\right]}{(1-\sigma)^3}\right\} \tag{4.31}$$

The function $\hat{w}(r,R;\alpha)$ satisfies

$$\frac{1}{\alpha}\frac{\partial\hat{w}}{\partial\hat{t}}=\frac{\kappa}{\delta}\left(\frac{\partial^2\hat{w}}{\partial r^2}+\frac{2}{r}\frac{\partial v}{\partial\hat{w}}\right) \quad \text{in} \quad 0<r<R,$$

$$\frac{\partial\hat{w}}{\partial r}=0 \quad \text{on} \quad r=0, \quad \hat{w}=0 \quad \text{on} \quad r=R,$$

and an initial condition which comes from matching with the first time-scale. For this problem we may think of R as being a given function of $\hat{t}$. As explained in Chapter 2, in the limit $\alpha\to\infty$ we may write $\hat{w}\sim e^{-\alpha g(\hat{t})}\left(\hat{w}_0(\rho)+O(\alpha^{-1})\right)$, where $\rho=r/R$ to derive an eigenvalue problem for $\hat{w}_0$. The result is that

$$\hat{w}\sim\frac{kR}{r}\sin\left(\frac{\pi r}{R}\right)\exp\left\{-\frac{\pi^2\kappa\alpha}{\delta}\int_0^{\hat{t}}\frac{d\hat{t}}{R^2}\right\} \quad \text{as} \quad \alpha\to\infty, \tag{4.32}$$

where k is a constant determined as follows. By writing out T_s (given by (4.24), (4.27)-(4.30) and (4.32)), in the variables used on the first time-scale, we find

$$T_s\sim\frac{1}{\alpha^{1/2}}\left(-\sigma\tilde{R}+k\pi(\tilde{r}-\tilde{R})e^{-\pi^2\kappa\tilde{R}^2/2\delta}\right),$$

so by matching with $\tilde{v}_1$ in (4.23) we conclude that $k=2V/\pi$. Finally, we calculate

$\hat{\tau}$ via the condition

$$\frac{d\hat{\tau}}{dR} \sim -\kappa \left(\frac{\partial \hat{u}_0}{\partial r} \right)^{-2} \frac{\partial \hat{w}}{\partial r} \quad \text{on} \quad r = R,$$

which gives

$$\hat{\tau} \sim 2\kappa V \int_R^1 \frac{\xi^3 (1-\xi)^2}{[\xi + \sigma(1-R)]^2} \exp\left\{ \frac{\pi^2 \kappa \alpha}{\delta} \left[\frac{1-\xi}{1-\sigma} + \frac{\ln[\xi + \sigma(1-\xi)]}{(1-\sigma)^2} \right] \right\} d\xi, \quad \text{as} \quad \alpha \to \infty. \tag{4.33}$$

4.4.2.1 Summary of time-scale $t = O(\alpha)$

On the time-scale $t = O(\alpha)$ we see that the temperature in both phases has an algebraic dependence on the small parameter α^{-1}, although the terms involving V are exponentially small in α. The implication is that for large Stefan numbers the melting process ultimately 'forgets' the initial condition $v = V$, and henceforth the temperature in the solid phase is driven by surface tension alone. Furthermore, given that $\hat{v}_0 + \hat{v}_1/\alpha$ is parabolic in shape with a maximum at $r = 0$, the solid becomes superheated, with the temperature everywhere greater than the melting temperature.

4.5 Numerical results

The problem (4.1)-(4.7) is solved numerically with a front-fixing method [32]. As a test of the scheme, solutions for the classical case $\sigma = 0$ are computed using an enthalpy method, with the two different numerical approaches agreeing quite well over the full range of parameter values. Note that the enthalpy method cannot be applied to the more general problem with $\sigma \neq 0$.

Typical temperature profiles are drawn in Fig. 4.1 for the case $\alpha = 1$, $\kappa = 1$, $\delta = 1$, $V = -1$, $\sigma = 0.1$. In part (a), numerical solutions are compared with the small-time approximation derived in Section 4.3, and they are seen to agree well with each other. On this time-scale the melting temperature is almost constant, and so the surface tension has no significant qualitative effect on the solutions. For later times, numerical profiles are drawn in part (b) using the same parameters. We see that as the melting temperature decreases, there is a point in time after which the solid is superheated, with the temperature everywhere greater than the melting temperature. We believe that this phenomenon is followed by a form of blow-up

with $\partial T_s/\partial r(R,t) \to -\infty$, $\dot{R} \to -\infty$ as $R \to R_c^+$ (with $t < \infty$), where $R_c > 0$ is some critical radius. This point is further discussed below.

A representative solution for large Stefan number is presented in Fig. 4.2. Here the Stefan number is $\alpha = 10$, and the other parameters are the same as in Fig. 4.1. Included in the figure is the numerical solution, as well as the large Stefan number approximation given in Section 4.4. We see the asymptotic solution agrees extremely well with the numerical solution, except for late times in the liquid phase. Note the parabolic shape of the temperature in the solid phase for the profile with $R = 0.1$. Although not entirely clear on this scale, the curve is concave down, meaning the solid is superheated at that stage. Again, we predict the solution will cease to exist before complete melting takes place, however we have observed that the critical radius R_c decreases as the Stefan number increases. We expect that $R_c \to 0^+$ as $\alpha \to \infty$, since the infinite latent heat limit implies the interface will always be able to absorb the surrounding heat energy, thereby preventing blow-up. See Section 4.6 for a related discussion.

It is of interest to compare numerical solutions of (4.1)-(4.7) for a small value of κ to the corresponding solutions of the one-phase problem derived in Chapter 3 (see also Evans & King [89]) via the singular limit $\kappa \to \infty$. This is done in Fig. 4.3 using the same parameters as Fig. 4.1, except that $\kappa = 0.05$. In this figure the dot-dashed curves in the liquid phase represent numerical solutions to the one-phase problem, while dot-dashed curves in the solid phase are drawn using asymptotic results given in [89] and Chapter 3, namely

$$\tilde{T}_s \sim V + \left[\sigma\left(1 - \frac{1}{R}\right) - V\right] \exp\left(\frac{\delta \dot{R}(R-r)}{\kappa}\right),$$

where the interface speed $\dot{R}$ is taken from the numerical solution to the one-phase problem. The agreement between these two approaches is excellent. Again, it is worth noting how superheating develops in the solid phase, which we expect leads to blow-up, as described above. In Chapter 3, it is suggested that in the limit $\kappa \to 0$, the blow-up will occur at the critical radius $R_c = \sigma/(\alpha + \sigma - V)$. Using the parameter values used for this figure, that would be approximately $R_c = 0.048$. The profile drawn in the figure for $R = 0.05$ appears to be very close to blow-up, which is consistent with the one-phase prediction.

In order to illustrate a solution for a small Stefan number, and also to indicate more clearly the behaviour of the melting process for late times, Fig. 4.4 presents temperature profiles for $\alpha = 0.1$, $\kappa = 1$, $\delta = 1$, $V = -1$ and $\sigma = 0.05$. For these parameter values, the numerical results suggest that finite-time blow-up will occur approximately between $R = 0.12$ and 0.13. A characterising feature of the solutions with small Stefan number is that blow-up appears to occur very soon after the solid becomes superheated. We see this in part (b) of this figure, where a approximately flat profile for $R = 0.2$ evolves very quickly to one which appears to have an unbounded temperature gradient in the blow-up limit. Figure 4.5 illustrates the dependence of the interface speed $\dot{R}$ on the particle radius R for the same parameters. The figure shows that $|\dot{R}|$ appears to blow up at approximately between $R = 0.12$ and 0.13.

4.6 Discussion

We have considered the Stefan problem for spheres, including the effects of surface tension, motivated in some part by experimental observations concerning the melting of nanoparticles, as reported by Kofman et al. [7]. By setting up experiments based on dark-field electron microscopy, Kofman et al. [7] found that once the temperature of the particle reached a certain value, the remaining solid core melted abruptly. It may be that our prediction of superheating in the solid particles offers a possible explanation for these peculiar observations.

A most interesting result of our study is that the addition of surface tension in the full two-phase Stefan model leads to superheating in the solid phase, and in fact our numerical computations suggest that the solution will cease to exist when the particle radius reaches some critical value R_c (with $t < \infty$). This form of finite-time blow-up is well-known to occur in some one-dimensional Stefan problems with superheating. For example, consider the ill-posed one-phase problem (without surface tension)

$$\frac{\partial T_s}{\partial t} = \frac{\kappa}{\delta}\frac{\partial T_s}{\partial x} \quad \text{in} \quad 0 < x < s(t), \tag{4.34}$$

$$T_s = 0, \quad \kappa\frac{\partial T_s}{\partial x} = \alpha\frac{ds}{dt} \quad \text{on} \quad x = s(t), \quad \frac{\partial T_s}{\partial x} = 0 \quad \text{on} \quad x = 0, \tag{4.35}$$

with the initial condition $T_s = V(x) > 0$. It is known (see Fasano & Primicerio

[107], Fasano et al. [108] and Fasano et al. [109], for example) that blow-up will occur with $\dot{s} \to -\infty$ as $s \to s_c$, where s_c is some critical size of the domain, if

$$Q = \int_0^1 (V(x) - \alpha)\, dx > 0.$$

In this case there is initially more heat energy in the solid than is required by the solid-melt interface to melt the solid completely. Furthermore, this form of blow-up is still possible for $Q \leq 0$ if, for example, the initial condition $V(x)$ has a sufficiently high peak near $x = 1$. Here the situation is that there is a large amount of heat energy concentrated near the interface, and this heat cannot be conducted away fast enough to prevent blow-up. In a similar vein, for our own problem it may be that the melting temperature decays sufficiently quickly so that blow-up will always occur, regardless of the initial temperature, as there will come a time when too much heat energy is concentrated near the interface. The exception will be the limiting case $\alpha \to \infty$, for which there can never be more heat in the solid than is required to melt it, and presumably blow-up will not occur. We leave these issues to be dealt with elsewhere.

We note that the complete asymptotic structure of (4.34)-(4.35) near blow-up has been documented by King & Evans [88] and Herrero & Velázquez [110], for example, with the use of a Baiocchi transform. The inclusion of surface tension in our model prevents such an approach here, and it is expected that the corresponding analysis for our problem will be more complicated. Again, we leave this aspect of the problem for further research.

It is worth emphasising that the motivation for including surface tension in some other studies has been to regularise the ill-posed problem of melting a superheated solid (or, equivalently, freezing a supercooled liquid), with the goal of smoothing (unphysical) singularities, or preventing blow-up from occuring. In contrast, the present melting problem (with zero surface tension) is well-posed, and it is in fact the inclusion of surface tension that drives the superheating, and hence is responsible for the blow up of solutions so that complete melting can take place. This appears to be a novel feature of the model. It may be that the addition of some other form of regularisation mechanism (such as kinetic undercooling) in our problem would enable the blow-up to be suppressed, so that the solution could be continued past

the blow-up region in the classical sense.

A number of points regarding one-phase models are worth repeating. First, when the effects of surface tension are included at the solid-melt interface, there can never be a true one-phase problem, as there will be always be temperature variations in both phases. However, Evans & King [89] derived a one-phase problem that arises by taking the singular limit of slow conduction in the solid phase ($\kappa \to 0$), and this problem was analysed in Chapter 3 for radially symmetric geometries. The present chapter provided numerical results that show strong agreement between the one-phase model and the full two-phase model for small values of κ. As mentioned in the Introduction, it is noteworthy that some authors treat the one-phase problem that arises by setting $\kappa = 0$ in (4.5) and ignoring (4.2), however this problem does not conserve heat at the interface. For example, Herraiz et al. [97] analysed the near-complete-melting limit of that (unphysical) one-phase problem. There is no finite-time blow-up for that problem, and the scalings derived by Herraiz et al. [97] are not appropriate to either the one-phase problem treated in Chapter 3 or the full two-phase problem studied presently.

It would be particularly interesting to generalise the current study to the problem of melting an arbitrary shaped three-dimensional particle. For the classical case with zero surface tension, the one-phase problem has been considered by McCue et al. [93] and Andreucci et al. [104] . In that case the solution continues to exist right up to complete melting, and these authors show that in general, the solid-melt interface approaches an ellipsoid in shape in the near-complete-melting limit. However, given the numerical results presented in the present chapter, one may expect the solution for the more general three-dimensional problem to blow-up in a similar manner, and it may be that the surface tension drives the melting process to be radially symmetric just before blow-up, regardless of the initial geometry. These questions remain unanswered, and are left for future research.

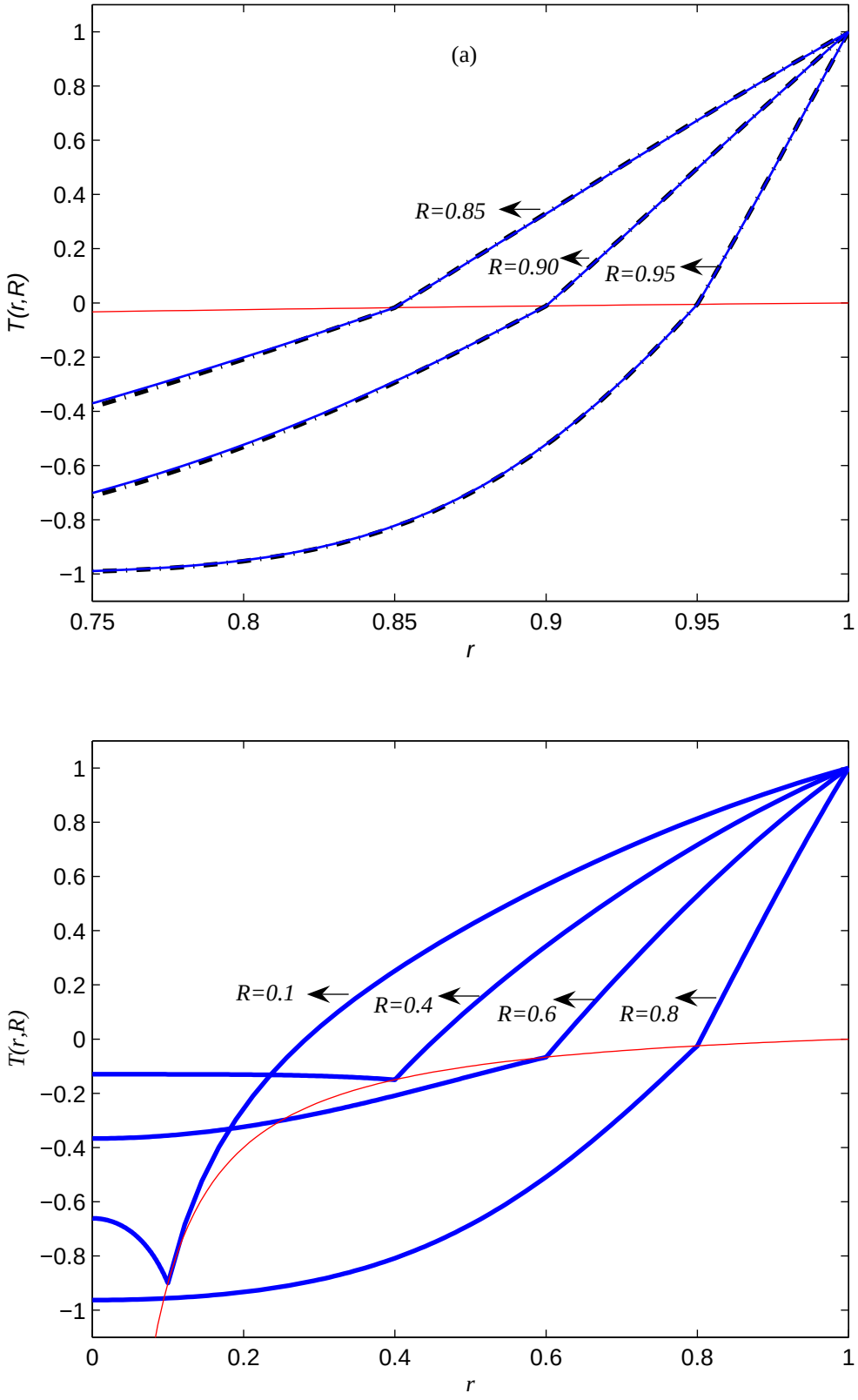

Figure 4.1: Temperature profiles for $\alpha = 1$, $\kappa = 1$, $\delta = 1$, $V = -1$, $\sigma = 0.1$. In part (a) the solid curves represent the numerical solution, while the dot-dashed curves are the small-time approximations. Part (b) shows only numerical solutions. The very thin curve in both parts denotes the melting temperature.

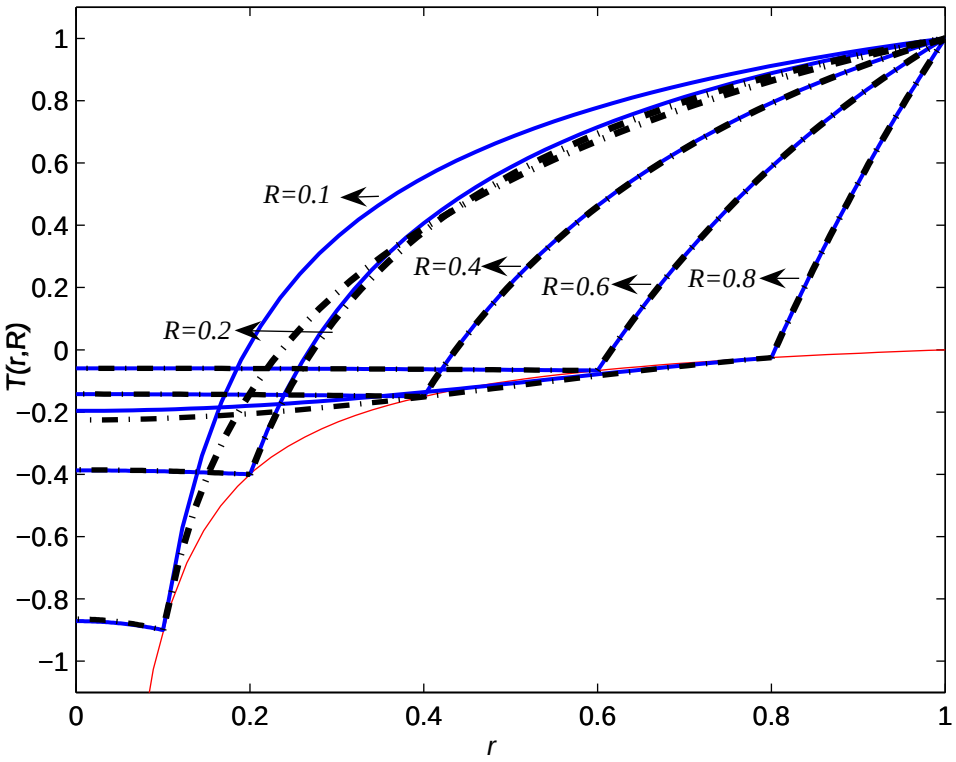

Figure 4.2: Temperature profiles for $\alpha = 10$, $\kappa = 1$, $\delta = 1$, $V = -1$, $\sigma = 0.1$. The solid curves represent the numerical solution, while the dot-dashed curves come from the large Stefan number asymptotics. The very thin curve denotes the melting temperature.

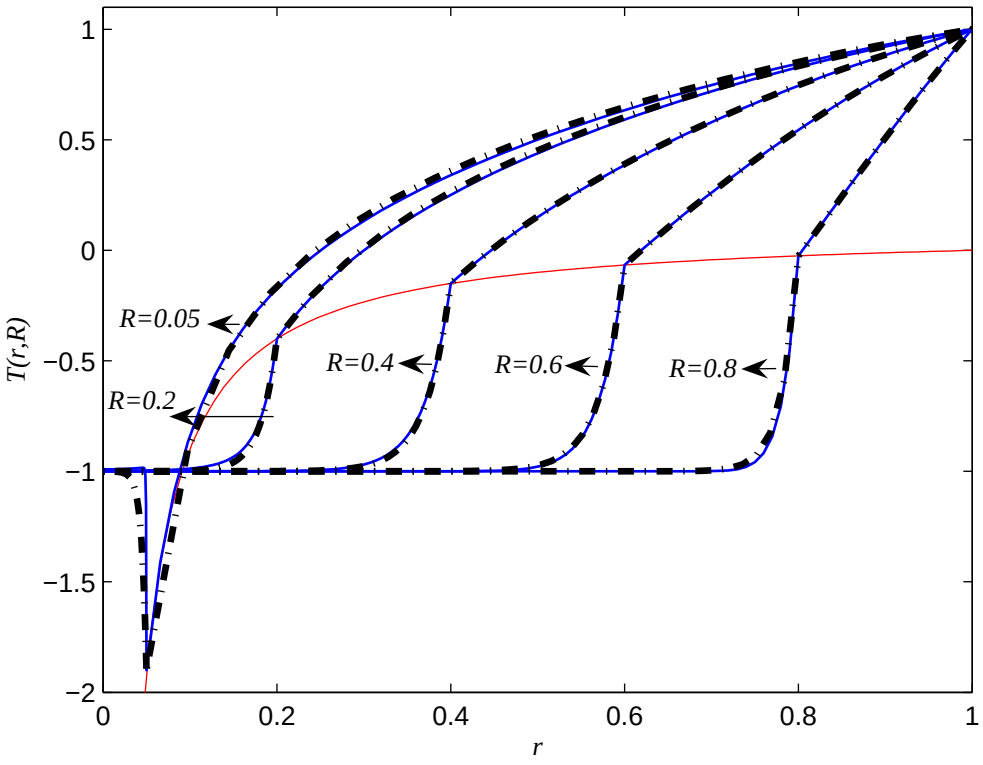

Figure 4.3: Temperature profiles for $\alpha = 1$, $\kappa = 0.05$, $\delta = 1$, $V = -1$, $\sigma = 0.1$. The solid curves indicate the numerical solution to the full two-phase problem (4.1)-(4.7), while the dot-dashed curves represent numerical solutions to the limiting the one-phase problem derived in Chapter 3.

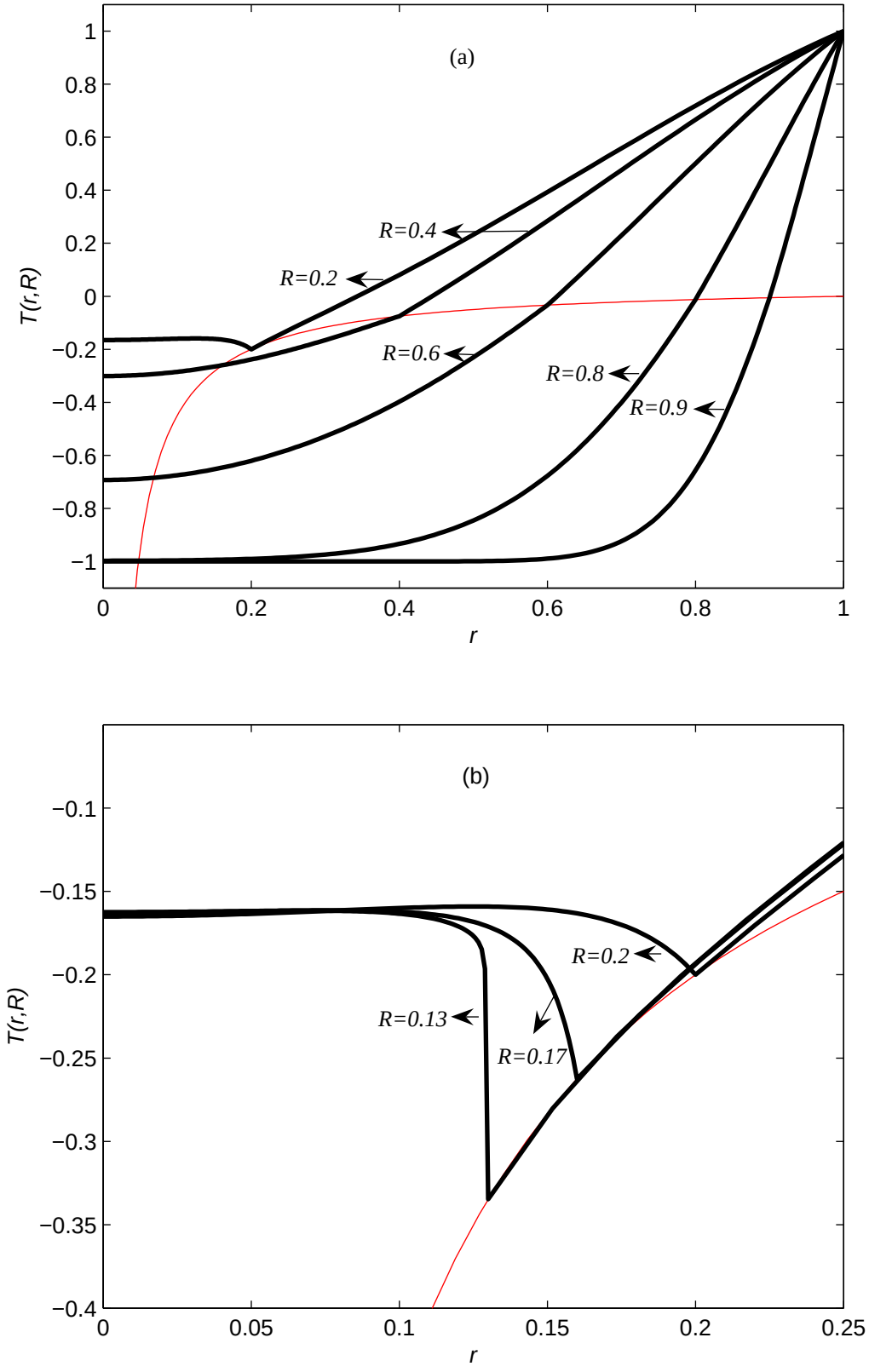

Figure 4.4: Temperature profiles for $\alpha = 0.1$, $\kappa = 1$, $\delta = 1$, $V = -1$, $\sigma = 0.05$. The thick curves represent the numerical solution, while the thin curve denotes the melting temperature. Part (a) is drawn for $R = 0.2$, 0.4, 0.6, 0.8 and 0.9, while part (b) is for $R = 0.13$, 0.17 and 0.2.

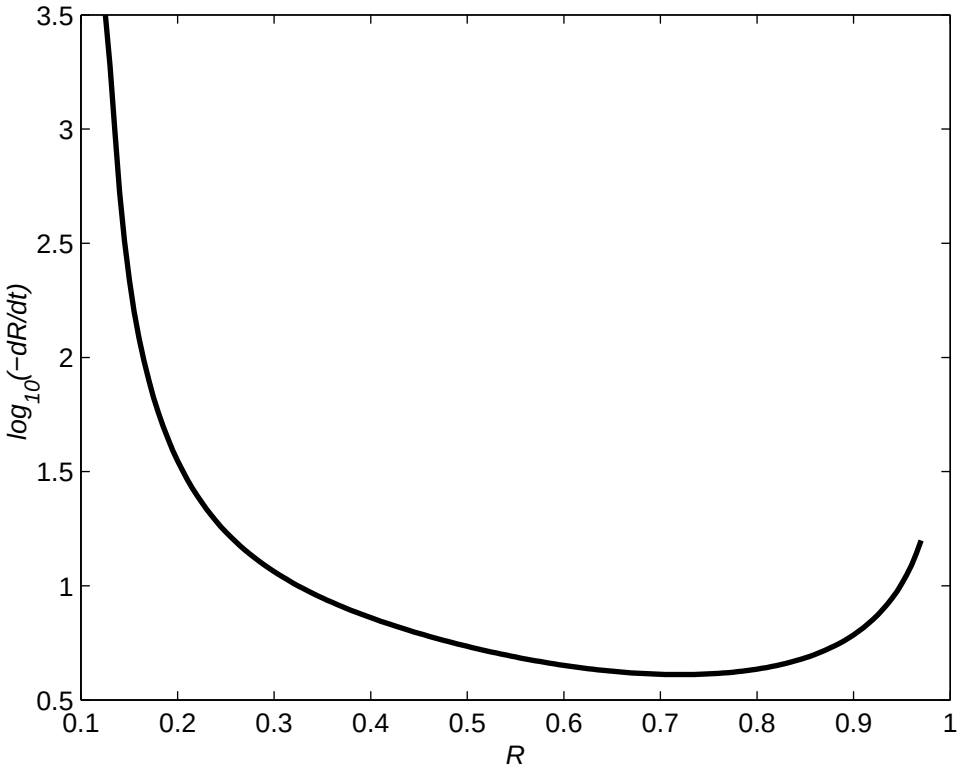

Figure 4.5: Plot of the interface speed $\dot{R}$ versus R for $\alpha = 0.1$, $\kappa = 1$, $\delta = 1$, $V = -1$, $\sigma = 0.05$.

Chapter 5

Two-phase Stefan problem with cylindrical symmetry, including the effects of surface tension

5.1 Introduction

The goal of this chapter is to present, for the first time, analytical and numerical results for the full two-phase Stefan problem of melting a cylindrical particle, including the effects of interfacial or surface tension through a Gibbs-Thomson condition (1.1) applied on the solid-melt interface. We note that the motivation for including surface tension in many other studies has been to regularise the ill-posed problem of freezing a supercooled liquid, for example in the context of crystal formation (Gupta [27]). However, the present melting problem is well-posed, and here the motivation comes from understanding size-dependent thermal effects on the nanoscale, with the goal of explaining some peculiar experimental observations such as abrupt melting of nanoparticles.

Chapter 5 is divided into six sections. In Section 5.2 the problem for the two-phase melting of cylindrical nanoparticle is described, and these are analysed using a small-time perturbation expansion in Section 5.3, and then using a large Stefan asympototics in Section 5.4. The numerical results and a short discussion are presented in Sections 5.5 and 5.6.

5.2 Problem description and governing equations

The geometry for the melting process under consideration is illustrated in Fig. 3.1. We suppose the cylindrical nanoparticle is initially of radius a^*, and at a uniform

temperature T_i^*. Then at time $t^* = 0$ the temperature on the surface $r^* = a^*$ is suddenly raised to T_a^*, and subsequently held there at that value. Provided that T_a^* is above the melting temperature, the particle will begin to melt, with a solid-melt interface $r^* = R^*(t^*)$ propagating from $r^* = a^*$ towards the centre of the particle.

By introducing the same dimensionless variables and parameters defined in Chapters 3 and 4, the two-phase Stefan problem for the melting of cylindrical nanoparticles reduces to solving the heat conduction equations

$$\frac{\partial T_\ell}{\partial t} = \frac{\partial^2 T_\ell}{\partial r^2} + \frac{1}{r}\frac{\partial T_\ell}{\partial r} \quad \text{in} \quad R(t) < r < 1, \tag{5.1}$$

$$\frac{\partial T_s}{\partial t} = \frac{\kappa}{\delta}\left(\frac{\partial^2 T_s}{\partial r^2} + \frac{1}{r}\frac{\partial T_s}{\partial r}\right) \quad \text{in} \quad 0 < r < R(t), \tag{5.2}$$

subject to the the same boundary conditions given in equations (4.3)-(4.7).

5.3 Small time limit

In [49] and [51], one small-time perturbation method is applied to the one-phase Stefan problem, and in Chapters 2 and 4 another small-time approaches are utilized to obtain the analytical solutions for the Stefan problem in a spherical domain. In this section we generalise the above studies to the full two-phase problem with surface tension in a cylindrical domain.

5.3.1 Method 1

Our analysis follows Section 4.3.1 closely by using the same variables u, v, X, Y, A_0, A_1, B_0 and B_1.

After substituting u, v, X and Y into the governing equations (5.1)-(5.2) and (4.5), we find that A_0, A_1, B_0 and B_1 satisfy the coupled ordinary differential equations

$$A_0'' + \gamma X A_0' = 0, \quad A_1'' + \gamma(XA_1' - A_1) = \frac{a_1 - \gamma\alpha}{\alpha - \sigma(1-\delta)} X A_0' - A_0',$$

$$\frac{\kappa}{\delta}B_0'' + \gamma X B_0' = 0, \quad \frac{\kappa}{\delta}B_1'' + \gamma(XB_1' - B_1) = \frac{a_1 - \gamma\alpha}{\alpha - \sigma(1-\delta)} X B_0' - \frac{\kappa}{\delta}B_0',$$

where

$$\gamma = -\frac{A_0'(1) - \kappa B_0'(1)}{\alpha - \sigma(1-\delta)}, \quad a_1 = A_1'(1) - \kappa B_1'(1) + \kappa V.$$

From (4.6)-(4.4), (4.7), we have the boundary conditions

$$A_0 = 1, \quad A_1 = 0, \quad \text{on} \quad X = 0,$$

$$A_0 = 0, \quad A_1 = -\sigma, \quad B_0 = -V, \quad B_1 = V - \sigma \quad \text{on} \quad X = 1,$$

$$B_0 = o(1), \quad B_1 = o(X), \quad \text{as} \quad X \to \infty.$$

We obtain the same leading order solutions and transcendental equation as (4.9) and (4.10) in Section 4.3. This means that the melting process of cylindrical particles is similar to that of spherical ones in a small time. The correction terms for the cylindrical case are

$$A_1 = -\sigma X + c_1 X \left(1 - e^{\gamma(1-X^2)/2}\right) - \frac{X \int_X^1 \mathrm{e}^{-\gamma t^2/2}}{2L_l},$$

$$B_1 = c_2 \left[e^{-\delta\gamma X^2/2\kappa} - \sqrt{\frac{\delta\gamma\pi}{2\kappa}}\, X \operatorname{erfc}\left(\sqrt{\frac{\delta\gamma}{2\kappa}} X\right)\right] + \left(c_3 X + \frac{3\kappa}{2\delta}\right) e^{-\delta\gamma X^2/2\kappa}, \quad (5.3)$$

where

$$c_1 = \frac{1}{3\gamma}\left(\frac{\gamma\alpha - a_1}{\beta}\right)\frac{1}{L_\ell} e^{-\gamma/2}, \quad c_3 = \frac{V}{3\gamma L_s}\left(\frac{\gamma\alpha - a_1}{\beta}\right), \quad (5.4)$$

$$c_2 = \frac{\kappa}{\delta\gamma L_s}\left\{\sigma - V\left[1 - \frac{1}{3\gamma}\left(\frac{\gamma\alpha - a_1}{\beta} + \frac{3\kappa}{2\delta}\right)\frac{1}{L_s} e^{-\delta\gamma/2\kappa}\right]\right\}\left[1 - \frac{\kappa}{\delta\gamma L_s} e^{-\delta\gamma/2\kappa}\right]^{-1},$$

$$\frac{\gamma\alpha - a_1}{\beta} = \frac{3\left(\gamma\alpha + \sigma - \kappa V + \kappa(V - \sigma)\left[1 - \frac{\kappa}{\delta\gamma L_s} e^{-\delta\gamma/2\kappa}\right]^{-1}\right)}{(3+\gamma)\beta + \frac{V}{\gamma L_s} e^{-\delta\gamma/2\kappa}\left\{\kappa\left[1 - \frac{\kappa}{\delta\gamma L_s} e^{-\delta\gamma/2\kappa}\right]^{-1} - \kappa\gamma - \kappa + \delta\gamma\right\}}.$$

From the Stefan condition (4.5) we have the small time behaviour

$$t = \frac{1}{2\gamma}(1-R)^2 - \frac{1}{3\gamma^2}\left(\frac{\gamma\alpha - a_1}{\beta}\right)(1-R)^3 + O((1-R)^4) \quad \text{as} \quad R \to 1^-. \quad (5.5)$$

As discussed in Section 4.3.1 of Chapter 4, the solution described above does not satisfy the no-flux condition (4.6) at $r = 0$. By using the same approach, we obtain the image solutions which satisfies (5.1)-(5.2),(4.3) and (4.6)-(4.7) exactly, but only satisfies (4.4)-(4.5) approximately; however, the errors from (4.4)-(4.5) are exponentially small in Y as $Y \to 0^+$.

5.3.2 Method 2

The key first step in the analysis is to transform the moving boundary problem to one in which the domain is fixed. Following Kucera & Hill [91] the following change of variables are made

$$\xi = \frac{\ln r}{\ln R}, \quad \tau = \ln R, \tag{5.6}$$

with the result being that the liquid and solid phases are fixed into the domains $0 \leq \xi \leq 1$ and $1 \leq \xi < \infty$, respectively. The temperature in each of the phases is expressed in terms of the new independent variables as

$$T_\ell(r,t) = \phi(\xi,\tau), \quad T_s(r,t) = V\left(1-\theta(\xi,\tau)\right). \tag{5.7}$$

Substituting (5.7) into the governing equations (5.1)-(5.2), together with the application of the Stefan conditions (4.5), leads to the partial differential equations

$$\frac{\partial^2\phi}{\partial\xi^2} = \frac{e^{(2\xi-1)\tau}}{\alpha e^\tau - \sigma(1-\delta)}\left[\frac{\partial\phi}{\partial\xi}(1,\tau) + \kappa V\frac{\partial\theta}{\partial\xi}(1,\tau)\right]\left[\xi\frac{\partial\phi}{\partial\xi} - \tau\frac{\partial\phi}{\partial\tau}\right], \tag{5.8}$$

$$\frac{\kappa}{\delta}\frac{\partial^2\theta}{\partial\xi^2} = \frac{e^{(2\xi-1)\tau}}{\alpha e^\tau - \sigma(1-\delta)}\left[\frac{\partial\phi}{\partial\xi}(1,\tau) + \kappa V\frac{\partial\theta}{\partial\xi}(1,\tau)\right]\left[\xi\frac{\partial\theta}{\partial\xi} - \tau\frac{\partial\theta}{\partial\tau}\right], \tag{5.9}$$

which are subject to the following boundary and initial conditions

$$\phi(1,\tau) = \sigma(1-e^{-\tau}), \quad \phi(0,\tau) = 1, \tag{5.10}$$

$$\theta(1,\tau) = 1 - \frac{\sigma}{V}(1-e^{-\tau}), \quad \frac{\partial\theta}{\partial\xi} \to 0 \quad \text{as} \quad \xi \to \infty, \tag{5.11}$$

$$\theta \to 0 \quad \text{as} \quad \xi \to \infty, \quad \tau \to 0. \tag{5.12}$$

The Stefan condition becomes

$$\left[\frac{\partial\phi}{\partial\xi}(1,\tau) + \kappa V\frac{\partial\theta}{\partial\xi}(1,\tau)\right]\left[\tau(\sigma(1-\delta) - \alpha e^\tau)\right]^{-1} = \frac{dR}{dt}, \tag{5.13}$$

from which, given the solutions for ϕ and θ, the location of the solid-melt interface can be obtained.

The next step in the perturbation process is to express the functions $\phi(\xi,\tau)$ and $\theta(\xi,\tau)$ in the power series form

$$\phi(\xi,\tau) = \sum_{n=0}^{\infty} A_n(\xi)\tau^n, \quad \theta(\xi,\tau) = \sum_{n=0}^{\infty} B_n(\xi)\tau^n, \tag{5.14}$$

noting that the limit $\tau \to 0$ is equivalent to the small-time limit $t \to 0$. The expres-

sions for $\phi(\xi,\tau)$ and $\theta(\xi,\tau)$ in (5.14) are substituted into the governing equations (5.8)-(5.9) and, after replacing the exponential terms with their Taylor series expansions, the result is a pair of ordinary differential equations at each order in τ. The resulting leading order equations are

$$A_0^{''} + \mu\xi A_0^{'} = 0, \quad B_0^{''} + \gamma\xi B_0^{'} = 0, \tag{5.15}$$

while the correction terms satisfy

$$A_n^{''} + \mu\left[\xi A_n^{'} - nA_n\right] = \frac{1}{\beta}\sum_{j=1}^{n}\Gamma_j(\xi)\left[\xi A_{n-j}^{\prime} - (n-j)A_{n-j}\right], \tag{5.16}$$

$$B_n^{''} + \gamma\left[\xi B_n^{'} - nB_n\right] = \frac{\delta}{\kappa\beta}\sum_{j=1}^{n}\Gamma_j(\xi)\left[\xi B_{n-j}^{\prime} - (n-j)B_{n-j}\right], \tag{5.17}$$

where $\beta = \alpha - \sigma(1-\delta)$ and the functions $\Gamma_j(\xi)$ are defined as

$$\Gamma_j(\xi) = \sum_{k=0}^{j} a_k P_{j-k}(\xi) \quad \text{for} \quad j = 1, 2, \ldots \tag{5.18}$$

In the above the constants a_n, μ and γ are given by

$$a_n = A_n^{'}(1) + \kappa V B_n^{'}(1), \quad \mu = \frac{-a_0}{\alpha - \sigma(1-\delta)}, \quad \gamma = \frac{\delta}{\kappa}\,\mu, \tag{5.19}$$

and the functions $P_n(\xi)$ are defined as coefficients of the Taylor series expansion

$$\frac{[\alpha - \sigma(1-\delta)]\, e^{(2\xi-1)\tau}}{\alpha e^{\tau} - \sigma(1-\delta)} = \sum_{n=0}^{\infty} P_n(\xi)\tau^n.$$

For the first few values of n these functions are

$$P_0 = 1, \quad P_1 = 2\xi - 1 - \lambda, \quad P_2 = \frac{1}{2}(2\xi - 1 - \lambda)^2 + \frac{1}{2}\lambda(\lambda - 1),$$

where the constant λ is defined by

$$\lambda = \frac{\alpha}{\alpha - \sigma(1-\delta)}.$$

If $\sigma = 0$ (no surface tension) then the constant $\lambda = 1$ and the system of equations for the A_n and B_n described above reduces to that given in Kucera & Hill [91], as expected. Furthermore, since σ appears in each case as part of a product with $1-\delta$, the same reduction occurs if $\delta = 1$ (specific heat capacity is the same in both liquid and solid phases). That is to say if we are studying the effect of nonzero surface

tension, but take the (often reasonable) assumption that $\delta = 1$, then the format of the governing ordinary differential equations does not change. The boundary conditions, however, will change, and these will alter the solutions for the A_n and B_n at each order.

The appropriate boundary conditions for (5.15)-(5.17), which are derived by applying (5.10)-(5.12), are

$$A_0(1) = 0, \quad A_n(1) = \frac{\sigma(-1)^{n+1}}{n!} \quad \text{for} \quad n \geq 1, \tag{5.20}$$

$$B_0(1) = 1, \quad B_n(1) = \frac{\sigma(-1)^n}{n!V} \quad \text{for} \quad n \geq 1, \tag{5.21}$$

$$A_0(0) = 1, \quad A_n(0) = 0 \quad \text{for} \quad n \geq 1, \tag{5.22}$$

$$B_0(\xi) \to 0, \quad B_n^{'}(\xi) \to 0 \quad \text{as} \quad \xi \to \infty \quad \text{for} \quad n \geq 0. \tag{5.23}$$

Finally, from the Stefan condition (5.13) we obtain the speed of the liquid/solid interface in terms of a_n as

$$[\tau(\sigma(1-\delta) - \alpha e^{\tau})]^{-1} \sum_{n=0}^{\infty} a_n \tau^n = \frac{dR}{dt}. \tag{5.24}$$

Thus the perturbation approach has reduced the two-phase Stefan problem with surface tension into one of determining the solutions to the systems of coupled ordinary differential equations (5.15) and (5.16) and (5.17), which are subject to the boundary conditions (5.20)-(5.23).

The leading order solutions, found by solving the homogeneous equations (5.15) together with the appropriate boundary conditions, are given by

$$A_0(\xi) = \frac{1}{L_\ell} \int_{\xi}^{1} e^{-\mu \upsilon^2/2} d\upsilon, , \qquad B_0(\xi) = \frac{1}{L_s} \int_{\xi}^{\infty} e^{-\gamma \upsilon^2/2} d\upsilon, \tag{5.25}$$

where the error function $\text{erf}(z)$ and constants L_ℓ and L_s are defined as

$$\text{erf}(z) = \frac{2}{\sqrt{\pi}} \int_0^z e^{-z^2} dz, \quad L_\ell = \int_0^1 e^{-\mu \upsilon^2/2} d\upsilon, \quad L_s = \int_1^{\infty} e^{-\gamma \upsilon^2/2} d\upsilon, \tag{5.26}$$

and from $(5.19)_3$ we find that the constant μ satisfies the transcendental equation

$$\frac{e^{-\mu/2}}{L_\ell} + \kappa V \frac{e^{-\delta \mu/2\kappa}}{L_s} = [\alpha - \sigma(1-\delta)]\, \mu. \tag{5.27}$$

After solving the above equation, we know $A_0(\xi)$ and $B_0(\xi)$ and then a_0. In a similar way, we can calculate a_1, a_2,...a_n. By substituting a_1, a_2,...a_n into (5.24), we obtain

the interface speed dR/dt and the relation between the interface position R and the time t.

A method for solving (5.16)-(5.17) for each of the correction terms is described in Davis & Hill [51]. Essentially each of the homogeneous equations is solved by making the substitution $z = -\mu\xi^2/2$ for the A_n and $z = -\gamma\xi^2/2$ for the B_n, leading to the hypergeometric equation. Given the well-known linearly independent solutions to this equation, a particular solution is found in the usual way by applying variation of parameters. Here we only consider $n = 1$, for which the details are straightforward. In this case (5.16) and (5.17) are

$$\begin{aligned} A_1^{''} + \mu\left[\xi A_1^{'} - A_1\right] &= \frac{1}{\alpha - \sigma(1-\delta)}\left[2a_0\xi - a_0(1+\lambda) + a_1\right]\xi A_0', \qquad (5.28)\\ B_1^{''} + \gamma\left[\xi B_1^{'} - B_1\right] &= \frac{\delta}{\kappa\left[\alpha - \sigma(1-\delta)\right]}\left[2a_0\xi - a_0(1+\lambda) + a_1\right]\xi B_0', \end{aligned}$$

which are solved together with the boundary conditions (5.20) and (5.22) to give

$$\begin{aligned} A_1(\xi) &= \frac{\xi}{6L_\ell}\Bigg[6\sigma L_\ell + \left(\frac{2a_1}{a_0} + 1 - 2\lambda\right)e^{-\mu/2} - 3\int_\xi^1 e^{-\mu\upsilon^2/2}d\upsilon \qquad (5.29)\\ &+ \left(2\lambda - 1 - \frac{2a_1}{a_0} + 3(1-\xi)\right)e^{-\mu\xi^2/2}\Bigg],\\ B_1(\xi) &= \frac{1}{6L_s}\Bigg\{\frac{\frac{2a_1}{a_0} + 1 - 2\lambda + \frac{3}{\gamma} - 6\sigma_1 e^{\gamma/2}L_s}{1 - \gamma L_s e^{\gamma/2}}\left[e^{-\frac{\gamma\xi^2}{2}} - \sqrt{\frac{\gamma\pi}{2}}\mathrm{erf}\left(\sqrt{\frac{\gamma\pi}{2}}\xi\right)\right]\\ &- \left[3\xi^2 + \left(\frac{2a_1}{a_0} - 2 - 2\lambda\right)\xi + \frac{3}{\gamma}\right]e^{-\gamma\xi^2/2}\Bigg\},\\ A_1^{'}(1) &= \sigma - \frac{e^{-\mu/2}\{2a_1 + \mu[\alpha + \sigma(1-\delta)]\}}{6L_l[\alpha - \sigma(1-\delta)]}, \qquad (5.30)\\ B_1^{'}(1) &= \frac{-\mu}{6(\kappa/\delta - \mu L_s e^{\gamma/2})}\left[\frac{2a_1}{a_0} + 1 - 2\lambda + \frac{3}{\gamma} - 6\sigma_1 L_s e^{\gamma/2}\right]\\ &- \frac{e^{-\gamma/2}}{6L_s}(\gamma - 1)\left[2\lambda - 1 - \frac{2a_1}{a_0}\right]. \end{aligned}$$

From (5.19) and above results a_1 is solved to be

$$\begin{aligned} a_1 &= \frac{a_0}{2}\left\{\frac{(2\lambda-1)M - \frac{6\sigma}{\mu} + \frac{3\delta V}{1-\gamma L_s e^{\gamma/2}}\left(\frac{1}{\gamma} - 2\sigma_1 L_s e^{\gamma/2}\right)}{M + 3[\alpha - \sigma(1-\delta)]}\right\}, \qquad (5.31)\\ M &= \frac{e^{-\mu/2}}{L_l} + \frac{\kappa V e^{-\gamma/2}}{L_s}\left(\frac{\delta}{\kappa} - \frac{1}{\mu}\right) - \frac{\delta V}{(1 - \gamma e^{\gamma/2}L_s)}. \end{aligned}$$

Equations $(5.25)_1$ and $(5.29)_1$ give reasonable results for the temperatures in the liquid phase. However, from $(5.25)_2$ and $(5.29)_2$, we see that there is a singular

point $r = 0$. When $r = 0$, $\xi \to \infty$, $B_0(\xi) \to 0$, $B_1(\xi) \to 0$, this means $T_s(0,t) \equiv V$. In order to avoid this problem, we use another fucntions and variables

$$\psi_\ell(X,Y) = \phi(\xi,\tau), \quad \psi_s(X,Y) = \theta(\xi,\tau), \quad X = \frac{1-r}{1-R}, \quad Y = 1-R, \tag{5.32}$$

where $\psi_\ell(X,Y)$ and $\psi_s(X,Y)$ are also assumed to have series solutions

$$\psi_\ell(X,Y) \;=\; \sum_{n=0}^{\infty} \bar{A}_n(X)Y^n, \quad \psi_s(X,Y) = \sum_{n=0}^{\infty} \bar{B}_n(X)Y^n. \tag{5.33}$$

Then ξ, τ, $\phi(\xi,\tau)$ and $\theta(\xi,\tau)$ can be expressed by the new variables X and Y. By comparing the coefficients of Y, $\bar{A}_n(X)$ and $\bar{B}_n(X)$ can be expressed in terms of $A_n(X)$ and $B_n(X)$.

$$\begin{aligned} &\tilde{A}_0(X) = A_0(X), \quad \tilde{A}_1(X) \simeq -A_1(X) + \frac{A_0^{'}(X)X(X-1)}{2}, \\ &\tilde{B}_0(X) = B_0(X), \quad \tilde{B}_1(X) \simeq -B_1(X) + \frac{B_0^{'}(X)X(X-1)}{2}, \end{aligned} \tag{5.34}$$

from which we obtain

$$\begin{aligned} \tilde{A}_1(X) \;&=\; -\frac{X}{6L_\ell}\left[6\sigma L_\ell + \left(\frac{2a_1}{a_0} + 1 - 2\lambda\right)e^{-\mu/2} - 3\int_X^1 e^{-\mu\upsilon^2/2}d\upsilon \right. \\ &+\; \left. \left(2\lambda - 1 - \frac{2a_1}{a_0} + 3(1-X)\right)e^{-\mu X^2/2}\right] - \frac{X(X-1)e^{-\mu X^2/2}}{2L_l}, \\ \tilde{B}_1(X) \;&=\; -\frac{1}{6L_s}\left\{\frac{\frac{2a_1}{a_0} + 1 - 2\lambda + \frac{3}{\gamma} - 6\sigma_1 e^{\gamma/2}L_s}{1 - \gamma L_s e^{\gamma/2}}\left[e^{-\frac{\gamma X^2}{2}} - \sqrt{\frac{\gamma\pi}{2}}\mathrm{erf}\left(\sqrt{\frac{\gamma\pi}{2}}X\right)\right]\right. \\ &-\; \left.\left[3X^2 + \left(\frac{2a_1}{a_0} - 2 - 2\lambda\right)X + \frac{3}{\gamma}\right]e^{-\gamma X^2/2}\right\} - \frac{X(X-1)e^{-\gamma X^2/2}}{2L_s} \end{aligned} \tag{5.35}$$

The speed of the interface and time can be obtained from (5.24) and (5.6)

$$\frac{dR}{dt} \simeq \frac{a_0 + a_1\ln(R)}{[\sigma(1-\delta) - \alpha R]\ln(R)}, \quad t \simeq \int_1^R \frac{[\sigma(1-\delta) - \alpha\xi]\ln(\xi)}{a_0 + a_1\ln(\xi)}d\xi. \tag{5.36}$$

Here, we use only the first two terms a_0 and a_1 to approximately obtain the interface speed dR/dt. Note that dR/dt is singular at both $R = 1$ and $R = \sigma(1-\delta)/\alpha$, meaning the solid-melt moves with infinite speed at $t = 0$ ($R = 1$), slows down until a minimum speed is reached, and then speeds up again. When $\delta = c_s/c_l \geq 1$, the speed will increase until the Gibbs-Thomson model (1.1) loses its validity. If $\delta = c_s/c_l < 1$, $R = \sigma(1-\delta)/\alpha$. By integration we obtain the relation $(5.36)_2$ between

the interface position R and time t .

As mentioned above, in principle it is possible to solve (5.16)-(5.17) for each n, however as n increases the calculations become lengthy, and we have not attempted them.

5.4 Large Stefan number limit

In this section we applied the large Stefan number analysis used in Chapters 2-4 to the two-phase melting problem for cylindrical nanoparticles including the surface tension on the solid-melt interface.

5.4.1 Time-scale $t = O(1)$

On the first time-scale, which is $t = O(1)$, heat diffuses a distance $O(1)$ (provided $\kappa = O(1)$), but the interface only propagates a distance $O(\alpha^{-1/2})$. Thus a boundary layer develops near $r = 1$. The details follow Section 4.4.1 very closely.

5.4.1.1 Inner region, $1 - r = O(\alpha^{-1/2})$

For the inner region we scale the spatial variables as $r = 1 - \alpha^{-1/2}\tilde{r}$, $R(t) = 1 - \alpha^{-1/2}\tilde{R}(t)$, and write

$$u \sim \tilde{u}_0(\tilde{r}, t) + \frac{1}{\alpha^{1/2}}\tilde{u}_1(\tilde{r}, t) + O(\alpha^{-1}), \quad v \sim \tilde{v}_0(\tilde{r}, t) + \frac{1}{\alpha^{1/2}}\tilde{v}_1(\tilde{r}, t) + O(\alpha^{-1}),$$

$$\tilde{R} \sim \tilde{R}_0(t) + \frac{1}{\alpha^{1/2}}\tilde{R}_1(t) + O(\alpha^{-1}) \quad \text{as} \quad \alpha \to \infty.$$

The leading order problem for $\tilde{u}_0$, namely

$$\frac{\partial^2 \tilde{u}_0}{\partial \tilde{r}^2} = 0 \quad \text{in} \quad 0 < \tilde{r} < \tilde{R}_0, \quad \frac{\partial^2 \tilde{v}_0}{\partial \tilde{r}^2} = 0 \quad \text{in} \quad \tilde{r} > \tilde{R}_0, \tag{5.37}$$

$$\tilde{u}_0 = 1 \quad \text{on} \quad \tilde{r} = 0, \quad \tilde{u}_0 = 0, \quad \tilde{v}_0 = 0, \quad \frac{\partial \tilde{u}_0}{\partial \tilde{r}} - \frac{\partial \tilde{v}_0}{\partial \tilde{r}} = -\frac{d\tilde{R}_0}{dt} \quad \text{on} \quad \tilde{r} = \tilde{R}_0, \tag{5.38}$$

has the solution

$$\tilde{u}_0 = 1 - \frac{\tilde{r}}{\tilde{R}_0}, \quad \tilde{v}_0 = \tilde{a}_0(t)(\tilde{r} - \tilde{R}) \quad \text{as} \quad \tilde{r} \to \infty. \tag{5.39}$$

The next order problems are

$$\frac{\partial^2 \tilde{u}_1}{\partial \tilde{r}^2} = \frac{\partial \tilde{u}_0}{\partial \tilde{r}} \quad \text{in} \quad 0 < \tilde{r} < \tilde{R}_0, \quad \frac{\partial^2 \tilde{v}_1}{\partial \tilde{r}^2} = \frac{\partial \tilde{v}_0}{\partial \tilde{r}} \quad \text{in} \quad \tilde{r} > \tilde{R}_0, \tag{5.40}$$

with boundary conditions

$$\tilde{u}_1 = 0 \quad \text{on} \quad \tilde{r} = 0, \tag{5.41}$$

$$\tilde{u}_1 + \tilde{R}_1 \frac{\partial \tilde{u}_0}{\partial \tilde{r}} = -\sigma \tilde{R}_0, \quad \tilde{v}_1 + \tilde{R}_1 \frac{\partial \tilde{v}_0}{\partial \tilde{r}} = -\sigma \tilde{R}_0, \quad \frac{\partial \tilde{u}_1}{\partial \tilde{r}} - \kappa \frac{\partial \tilde{v}_1}{\partial \tilde{r}} = -\frac{d\tilde{R}_1}{dt} \quad \text{on} \quad \tilde{r} = \tilde{R}_0, \tag{5.42}$$

$$\tilde{v}_1 \sim \tilde{a}_0(t)\tilde{r}^2 + \tilde{a}_1(t)\tilde{r} \quad \text{as} \quad \tilde{r} \to \infty. \tag{5.43}$$

The function $\tilde{a}_1(t)$ will be determined by matching with the outer region, as described below.

In terms of $\tilde{a}_1(t)$ the solutions to (5.40)-(5.43) are

$$\tilde{u}_1 = -\frac{1}{2\tilde{R}_0}\tilde{r}^2 + \left(\frac{1}{2} - \sigma + \frac{\tilde{R}_1}{\tilde{R}_0^2}\right)\tilde{r}, \quad \tilde{v}_1 = \tilde{a}_0(\tilde{r}^2 - \tilde{R}_0^2 - \tilde{R}_1) + \tilde{a}_1(\tilde{r} - \tilde{R}) - \sigma\tilde{R}_0,$$

with $\tilde{R}_0$ given in (5.39) and $\tilde{R}_1$ satisfying the differential equation

$$\frac{d\tilde{R}_0}{dt} + \frac{1}{\tilde{R}_0} = \kappa a_0, \quad \frac{d\tilde{R}_1}{dt} + \frac{\tilde{R}_1}{\tilde{R}_0^2} = \frac{1}{2} + \sigma + \kappa(2a_0R_0 + a_1) \tag{5.44}$$

and initial condition $\tilde{R}_0(0) = 0$, $\tilde{R}_1(0) = 0$.

5.4.1.2 Outer region, $1 - r = O(1)$

The outer region is for $1 - r = O(1)$. Here we write $v = \bar{v}(r, t)$, where

$$\frac{\partial \bar{v}}{\partial t} = \kappa\left(\frac{\partial^2 \bar{v}}{\partial r^2} + \frac{1}{r}\frac{\partial \bar{v}}{\partial r}\right) \quad \text{in} \quad 0 < r < 1,$$

$$\bar{v} = 0 \quad \text{on} \quad r = 1, \quad \frac{\partial \bar{v}}{\partial r} = 0 \quad \text{on} \quad r = 0, \quad \bar{v} = V \quad \text{at} \quad t = 0.$$

The solution for $\bar{v}$ is

$$\bar{v} = 2V \sum_{n=1}^{\infty} e^{-\kappa\beta_n{}^2 t} \frac{J_0(\beta_n r)}{\beta_n J_1(\beta_n)}, \tag{5.45}$$

where J_0 and J_1 are the Bessel functions of the order 0 and 1 of the first kind, respectively, and the β_n value is the positive roots of the equation $J_0(\beta_n) = 0$.

5.4.1.3 Matching between regions

By rewriting (5.45) in inner variables $(\tilde{r}, t)$ and expanding as $\alpha \to \infty$ we find

$$\tilde{v}_0 \sim 0, \quad \tilde{v}_1 \sim 2V\tilde{r} \sum_{n=1}^{\infty} e^{-\kappa\beta_n^2 t} \quad \text{as} \quad \tilde{r} \to \infty.$$

Thus matching between the two regions gives

$$\tilde{a}_0 = 0, \quad \tilde{a}_1 = 2V\sum_{n=1}^{\infty} e^{-\kappa\beta_n^2 t}, \quad \tilde{v}_1 = 2V(\tilde{r}-\tilde{R}_0)\sum_{n=1}^{\infty} e^{-\kappa\beta_n^2 t} - \sigma\tilde{R}_0. \tag{5.46}$$

We may now solve (5.44) for the moving boundary location, yielding

$$\tilde{R}_1 = \frac{1}{3}(1+2\sigma)t + V\sum_{n=1}^{\infty}\left\{\frac{\sqrt{\pi}\mathrm{erf}\left(\beta_n\sqrt{\kappa t}\right)}{\beta_n^3\kappa^{1/2}t^{1/2}} - \frac{2e^{-\kappa\beta_n^2 t}}{\beta_n^2}\right\}.$$

5.4.1.4 Summary of time-scale $t = O(1)$

On the time-scale $t = O(1)$ we see that near the moving boundary the temperature in both phases has an algebraic dependence on the small parameter $\alpha^{-1/2}$. Furthermore, the two phases are coupled, although to leading order both the temperature in the solid and location of the free boundary are independent of the liquid phase. Note that the inclusion of surface tension has no qualitative effect on the solution on this time-scale.

5.4.2 Time-scale $t = O(\alpha)$

The solutions are assumed to be the form

$$T_\ell = \hat{u}_0(r,R) + \frac{1}{\alpha}\hat{u}_1(r,R) + O(\alpha^{-2}), \quad T_s = \hat{v}_0(r,R) + \frac{1}{\alpha}\hat{v}_1(r,R) + \ldots + \hat{w}(r,R;\alpha), \tag{5.47}$$

$$\hat{t} = \bar{t}_0(R) + \frac{1}{\alpha}\bar{t}_1(R) + \cdots + \hat{\tau}(R;\alpha) \quad \text{as} \quad \alpha \to \infty \tag{5.48}$$

The problem for $\bar{u}_i$ and $\bar{v}_i$ are

$$\frac{1}{r}\frac{\partial}{\partial r}\left(r\frac{\partial\bar{u}_0}{\partial r}\right) = 0 \quad \text{on} \quad R < r < 1, \quad \frac{1}{r}\frac{\partial}{\partial r}\left(r\frac{\partial\bar{v}_0}{\partial r}\right) = 0 \quad \text{on} \quad 0 < r < R,$$

$$\bar{u}_0 = 1, \quad \text{on} \quad r = 1, \quad \bar{u}_0 = \bar{v}_0 = \sigma\left(1 - \frac{1}{R}\right) \quad \text{on} \quad r = R, \quad \frac{\partial\bar{v}_0}{\partial r} = 0 \quad \text{on} \quad r = 0,$$

$$\bar{t}_0'\left(\frac{\partial\bar{u}_0}{\partial r} - \kappa\frac{\partial\bar{v}_0}{\partial r}\right) = -1 \quad \text{on} \quad r = R,$$

$$\frac{1}{r}\frac{\partial}{\partial r}\left(r\frac{\partial\bar{u}_1}{\partial r}\right) = \frac{1}{\bar{t}_0'}\frac{\partial\bar{u}_0}{\partial R} \quad \text{on} \quad R < r < 1, \quad \frac{1}{r}\frac{\partial}{\partial r}\left(r\frac{\partial\bar{v}_1}{\partial r}\right) = \frac{1}{\bar{t}_0'}\frac{\partial\bar{v}_0}{\partial R} \quad \text{on} \quad 0 < r < R,$$

$$\bar{u}_1 = 0 \quad \text{on} \quad r = 1 \quad \bar{u}_1 = \bar{v}_1 = 0 \quad \text{on} \quad r = R, \quad \frac{\partial\bar{v}_1}{\partial r} = 0 \quad \text{on} \quad r = 0,$$

$$\bar{t}_1'\left(\frac{\partial\bar{u}_0}{\partial r} - \kappa\frac{\partial\bar{v}_0}{\partial r}\right) + \bar{t}_0'\left(\frac{\partial\bar{u}_1}{\partial r} - \kappa\frac{\partial\bar{v}_1}{\partial r}\right) = \frac{(1-\delta)\sigma}{R} \quad \text{on} \quad r = R.$$

We use the same ideas mentioned in Section 4.4.2 and the solutions for the first order are

$$\bar{u}_0 = \frac{(R-1)\sigma \ln r}{R \ln R} + \frac{(\ln R - \ln r)R}{R \ln R}, \tag{5.49}$$

$$\bar{v}_0 = \sigma\left(1 - \frac{1}{R}\right), \tag{5.50}$$

$$\hat{t}_0 = \frac{1 - R^2 + 2R^2 \ln R}{4(1-\sigma)} - \frac{\sigma(1 - R + R\ln R)}{(1-\sigma)^2} + \frac{\sigma^2}{2(1-\sigma)^3} \tag{5.51}$$
$$\times \left\{2\ln\left[\frac{R+\sigma(1-R)}{\sigma}\right]\ln R + 2\mathrm{dilog}\left[\frac{R+\sigma(1-R)}{\sigma}\right] + 2\mathrm{dilog}(\sigma) + (\ln\sigma)^2\right\},$$

and the solutions for the next order are

$$\hat{u}_1 = \frac{R+\sigma(1-R)}{4R^4 \ln^2 R}\left[\frac{R+\sigma(1-R)}{\ln R} + \sigma\right] \tag{5.52}$$
$$\times \left\{1 - r^2 + \left[r^2 - R^2 - \frac{1-R^2}{\ln R}\right]\ln r\right\},$$

$$\hat{v}_1 = -\frac{\sigma\delta(R+\sigma(1-R))}{4\kappa R^4 \ln(R)}(r^2 - R^2), \tag{5.53}$$

$$\hat{t}_1 = \int_R^1 \{[(2\xi^2 - 2\delta\xi^2)(\ln\xi)^3 + 2\xi^3(\ln\xi)^2 + (1 - 2\xi^3 + \xi^2)\ln\xi + 1 + \xi^3 - \xi - \xi^2]\sigma$$
$$- \xi[-1 - 2\xi^2 \ln\xi + \xi^2 + 2\xi^2(\ln\xi)^2]\}\frac{d\xi}{4\xi(\ln\xi)^2[\xi + \sigma(1-\xi)]}. \tag{5.54}$$

The function $\hat{w}(r, R; \alpha)$ satisfies

$$\frac{1}{\alpha}\frac{\partial \hat{w}}{\partial \hat{t}} = \frac{\kappa}{\delta}\left(\frac{\partial^2 \hat{w}}{\partial r^2} + \frac{1}{r}\frac{\partial v}{\partial \hat{w}}\right) \quad \text{in} \quad 0 < r < R,$$

$$\frac{\partial \hat{w}}{\partial r} = 0 \quad \text{on} \quad r = 0, \quad \hat{w} = 0 \quad \text{on} \quad r = R,$$

and an initial condition which comes from matching with the first time-scale discussed in Section 5.4.1. For this problem we may think of R as being a given function of $\hat{t}$. As explained in Chapter 2, in the limit $\alpha \to \infty$ we may write $\hat{w} \sim e^{-\alpha g(\hat{t})}\,(\hat{w}_0(\rho) + O(\alpha^{-1}))$, where $\rho = r/R$ to derive an eigenvalue problem for $\hat{w}_0$. The result is that

$$\bar{w} = 2V \sum_{n=1}^{\infty} \frac{J_0(\gamma_n r/R)}{\gamma_n J_1(\gamma_n)} \exp\left\{-\frac{\alpha\kappa{\gamma_n}^2}{\delta}\int_0^{\hat{t}} \frac{d\hat{t}}{R^2}\right\}, \tag{5.55}$$

where

$$\int_0^{\hat{t}} \frac{d\hat{t}}{R^2} \sim \frac{2\mathrm{dilog}\left\{\frac{\sigma(1-R)+R}{\sigma}\right\} + 2\mathrm{dilog}(\sigma) + 2\ln R \ln\left\{\frac{\sigma(1-R)+R}{\sigma}\right\} + (\ln\sigma)^2}{2(\sigma-1)},$$

and the γ_n value is the positive roots of the equation $J_0(\gamma_n) = 0$. Finally, we calculate $\hat{\tau}$ via the condition

$$\frac{d\hat{\tau}}{dR} \sim -\kappa \left(\frac{\partial \hat{u}_0}{\partial r} \right)^{-2} \frac{\partial \hat{w}}{\partial r} \quad \text{on} \quad r = R,$$

which gives

$$\begin{aligned} \hat{\tau} &\sim 2\kappa V \int_R^1 \frac{\xi^3 (\ln \xi)^2}{[\xi + \sigma(1-\xi)]^2} \exp\left\{ \frac{\gamma_1^2 \kappa \alpha}{2\delta(\sigma - 1)} \left[2\text{dilog}\left(\frac{\sigma(1-\xi)+\xi}{\sigma} \right) \right. \right. \\ &+ \left. \left. 2\text{dilog}(\sigma) + 2 \ln \xi \ln \left(\frac{\sigma(1-\xi)+\xi}{\sigma} \right) + (\ln \sigma)^2 \right] \right\} d\xi \quad \text{as} \quad \alpha \to \infty. \end{aligned} \tag{5.56}$$

5.4.2.1 Summary of time-scale $t = O(\alpha)$

It can be seen that the melting of cylindrical nanoparticle displays similar behaviours to spherical nanoparticle melting studied in Chapter 4. on the time-scale $t = O(\alpha)$ the temperature in the two phases has an algebraic dependence on the small parameter α^{-1}, although the terms involving V are exponentially small in α. This means that for large Stefan numbers, the initial condition has little effect on the later melting stage and the melting process is is driven by surface tension alone. Furthermore, given that $\hat{v}_0 + \hat{v}_1/\alpha$ is parabolic in shape with a maximum at $r = 0$, the solid becomes superheated, with the temperature everywhere greater than the melting temperature.

5.5 Numerical results

The two-phase melting problem (5.1)-(5.2) is solved numerically using a front-fixing method [32]. For the cases without surface tension (σ=0), this method agrees well with the accurate enthalpy approach [53] in a large range. It should be noted that the enthalpy method cannot be applied to the cases when the surface tension exists ($\sigma \neq 0$).

The temperature profiles for medium Stefan number ($\alpha = 1$) are shown in Fig. 5.1 and Fig. 5.2. Fig. 5.1(a) compares the results from the numerical method and the small-time solution derived in Section 5.3.1. In this time scale, the two methods agree very well in the liquid and solid phase. With the solid/liquid interface moving forward, the small-time solution does not work well for the solid phase and thus the temperature profiles are not shown. From Fig. 5.1(b) it can be seen that during

the initial melting stage, the particle absorbs heat and the temperatures in the two phases increase with time. However, the temperature in the solid phase decreases when the solid/liquid interface comes very close to the centre of the particle. A local temperature plot for R=0.4 is shown in Fig. 5.2 from which we see that the temperature in the solid phase has a maximum when r is about 0.29. When the melting point decreases again, there exists a point after which the particle is superheated with all the temperature inside the particle larger than the melting point. A blow-up is expected to happen when $R \to R_c^+$ with $\partial T_s/\partial r \to -\infty$, $dR/dt \to -\infty$.

Fig. 5.3 gives typical temperature plots for large Stefan numbers. In this case, $\alpha = 10$ and other parameters are the same as those in Fig. 5.1. The short- and long-time solutions from the numerical front-fixing method are compared with those from the large Stefan number limit derived in Section 5.4.2. From part (a), for a short-time scale, the temperatures in the liquid phase obtained from both methods agree well while the temperatures in the solid phase do not. When the solid/liquid interface moves forward, the discrepancy between the temperatures in the solid phase from the two methods reduces. In part (b) the two approaches are in excellent agreement for the two phases at a large-time scale except the solid phase at a later stage. We note that when $R = 0.1$ the temperature gradient at the interface is much less than that in Fig. 5.1 but a blow-up is still expected to happen when $R \to R_c^+$. By comparing Fig. 5.3(b) with Fig. 5.1(b), we know that when the Stefan number increases, the critical radius R_c decreases and the the superheating in the solid phase occurs earlier.

In Fig. 5.4, the two-phase results from the front-fixing method for very small κ are compared with those from the one-phase numerical solutions derived in Chapter 3. In the present example, $\kappa = 0.05$ and other parameters are the same as those in Fig. 5.1. The solid curves show the two-phase numerical solutions, while the dashed curves for the liquid phase represent the one-phase numerical solutions and the dashed curves for the solid phase is drawn from the approximations derived in Chapter 3. It can be seen that the two-phase and one-phase limiting models are in good agreement. Except the sudden jump for the temperature near the solid/liquid interface, the temperature in the inner solid particle, especially near the center of the particle, does not have great change. From Chapter 3, the critical radius

is $R_c = \alpha/[\sigma\delta + \alpha - \delta V]$=0.048. It should be also noted that when $R = 0.05$, $\partial T_s/\partial r \to -\infty$, a blow-up is likely to occur. The critical radius predicted by the two- and one-phase solutions agree very well.

In order to study the melting behaviour more closely, the case with small Stefan numbers is also considered and the numerical results are shown in Fig. 5.5. The plots is drawn for $\alpha = 0.1$, $\kappa = 1$, $\delta = 1$, $V = -1$, $\sigma = 0.05$. Part (b) shows the temperature evolution in the solid phase near the interface $R = 0.13, 0.16$ and 0.20. It can be seen clearly that the blow-up phenomena happens near $R = 0.13$. Fig. 5.6 presents the speed of the solid/liquid interface. We see that when $R > 0.2$ the speed of the interface is relatively smooth and slow while there is large jump especially when R is about 0.13. This kind of change is reflected by the sudden increase of the temperature gradient in the solid phase near the interface.

5.6 Discussion

In this chapter we treated the melting of cylindrical nanoparticle as a two-phase Stefan problem including the effect of the surface tension, triggered by a great deal of research which indicates that the melting point of nanoparticles shows a size-dependent characteristic [11, 24, 25, 111, 112], that it is very difficult to measure the temperature distribution of the particle in the and that some interesting phenomena, such as abrupt melting [7], may occur in the nanoscale. Kofman et al. [7] found that when the radius of the solid particle arrives at a certain value, the melting process of gold nanoparticle is complete "suddenly". The analysis of this chapter may provide a possible explanation for these phenomena.

One aim of this chapter is to obtain the temperature distribution in the two phases of cylindrical nanoparticles. As the size is very small, it is very difficult to measure the temperature distribution of the particle in the micro- or nano- scale. For the short-time scale we can use the small-time perturbation approach to calculate the temperature distribution while for the large time scale the large Stefan asymptotics can be utilized to study the melting/freezing of the particle in a cylindrical domain.

In addition to the temperature reduction at the solid/liquid interface when the particle size becomes small, the inclusion of the surface tension also has a considerable effect on the temperature distribution in the particle, especially in the solid

phase, leading to superheating in the solid phase. Of course, as the heat exchange in the particle requires finite time to finish, the abrupt melting does not take place suddenly. The numerical solutions have shown that when $R \to R_c^+$, $\partial T_s/\partial r \to -\infty$, $dR/dt \to -\infty$ leading to the blow-up in the solid phase.

It should be noted that, generally speaking, the melting point of metallic nanoparticles will never be negative. This means that equation (1.1) will lose its validity when the solid/liquid interface position R^* (or R) is very small. The issue when the Gibbs-Thomson model does not work is left to be determined by other research.

One interesting potential application of nanoparticles is targeted ablation of tumor cells [111]. Melted particles will release the drug molecules faster than solid particles because of their higher diffusion coefficient of the drug molecules inside the liquid carrier. When the nanoparticles enclosing drug molecules arrives at a site where the temperature is higher than the melting point of the nanoparticle, they will melt quickly and release the drug load. Note that in physical world, the liquid phase will flow away when the particle melts, thus in the present chapter the condition of constant temperature at the outside liquid surface is a ideal state. Therefore, it is very important to describe the nanoparticle melting dynamically.

It is also of great interest to extend our analysis to other melting or freezing problems for nanoparticle with different shapes. Cylindrical nanoparticle can be nanodisk, nanofilm, nanorod or nanowire. As the melting or freezing is sometimes related to the orientation, it is very important to generalize our study to the problems of melting an arbitrary shaped three-dimensional particles. This will be tackled in the future research.

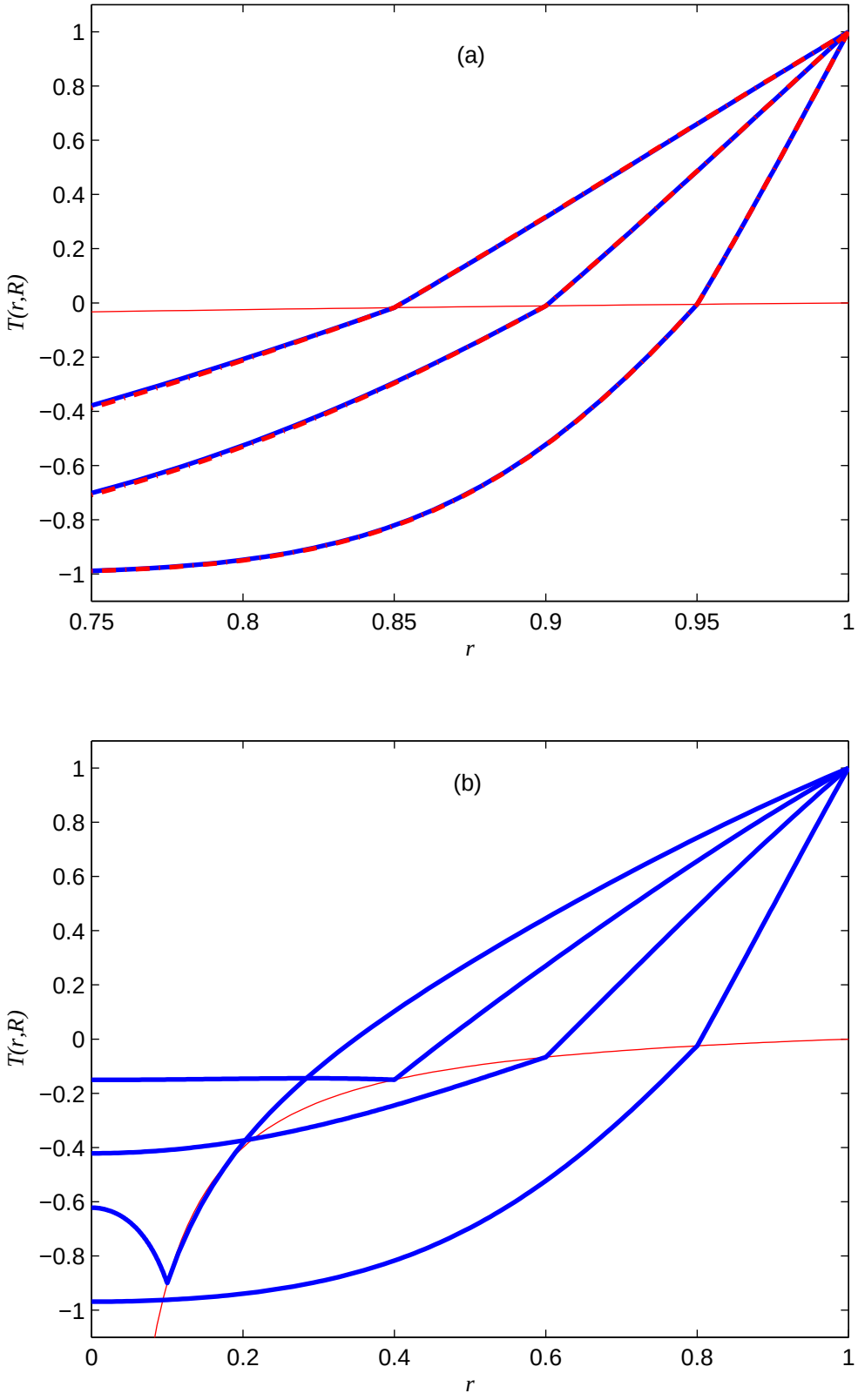

Figure 5.1: Temperature profiles for $\alpha = 1$, $\kappa = 1$, $\delta = 1$, $V = -1$, $\sigma = 0.1$ at different positions: (a) is for R=0.85, 0.90 and 0.95; (b) is for R=0.1, 0.4, 0.6 and 0.8. In part (a), the solid curves represent the numerical solution, while the dashed curves are the small-time approximations. Part (b) shows only numerical solutions. The very thin curve in both parts denotes the melting temperature.

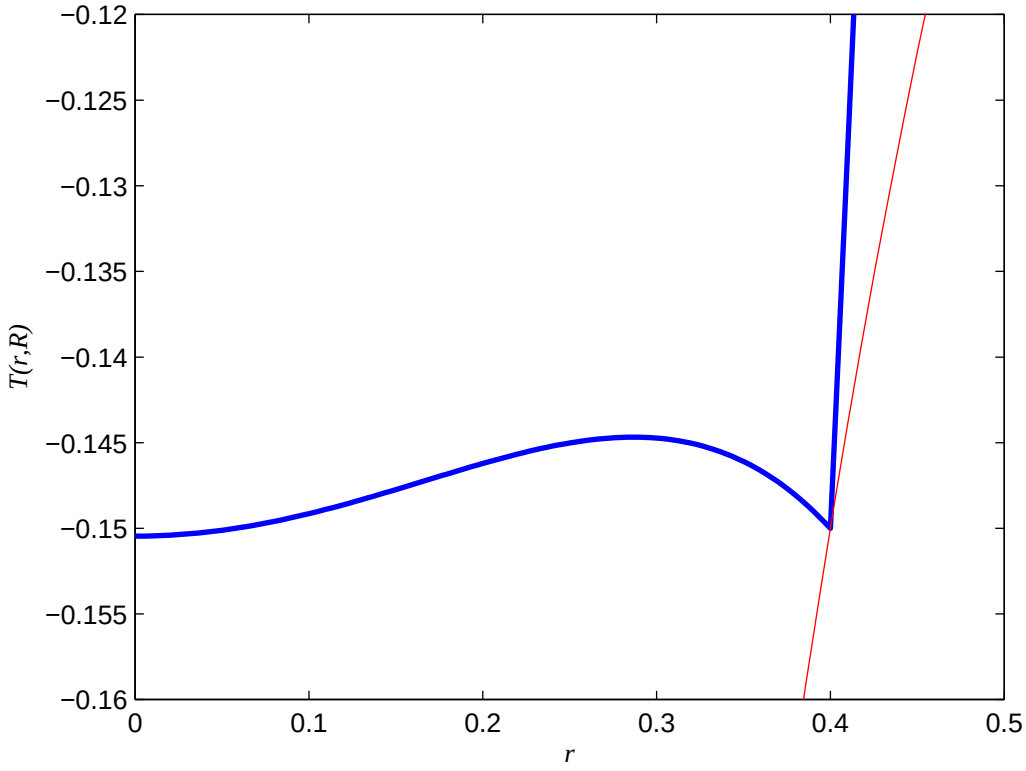

Figure 5.2: Local temperature plot when $R = 0.4$ for the case $\alpha = 1$, $\kappa = 1$, $\delta = 1$, $V = -1$, $\sigma = 0.1$. The thick curves represent the numerical solution, while the very thin curve denotes the melting temperature.

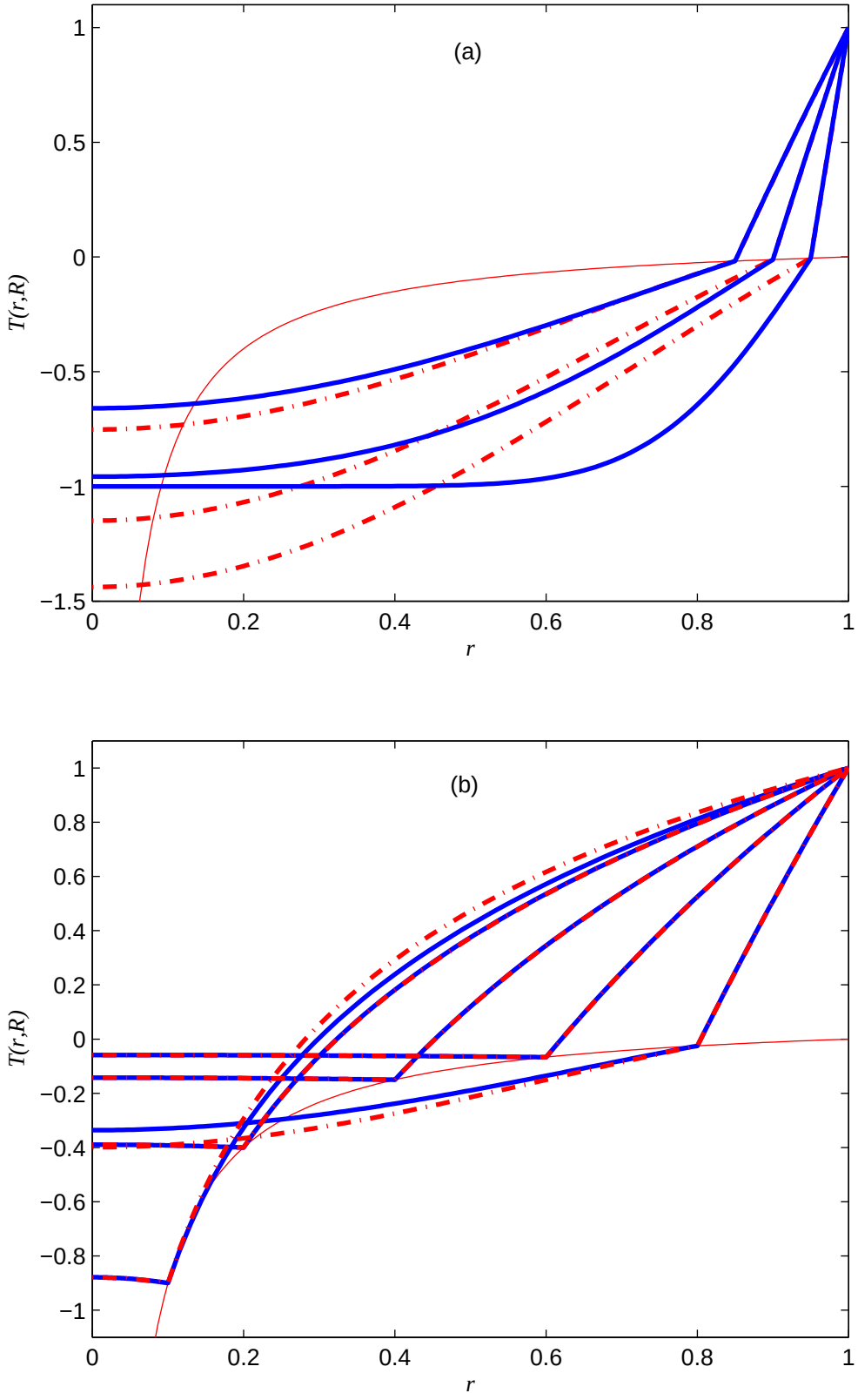

Figure 5.3: Temperature profiles for $\alpha = 10$, $\kappa = 1$, $\delta = 1$, $V = -1$, $\sigma = 0.1$ at different positions: (a) is for R=0.85, 0.90 and 0.95; (b) is for R=0.1, 0.2, 0.4, 0.6 and 0.8. The solid curves represent the numerical solution, while the dashed curves come from the large Stefan number asymptotics. The very thin curve denotes the melting temperature.

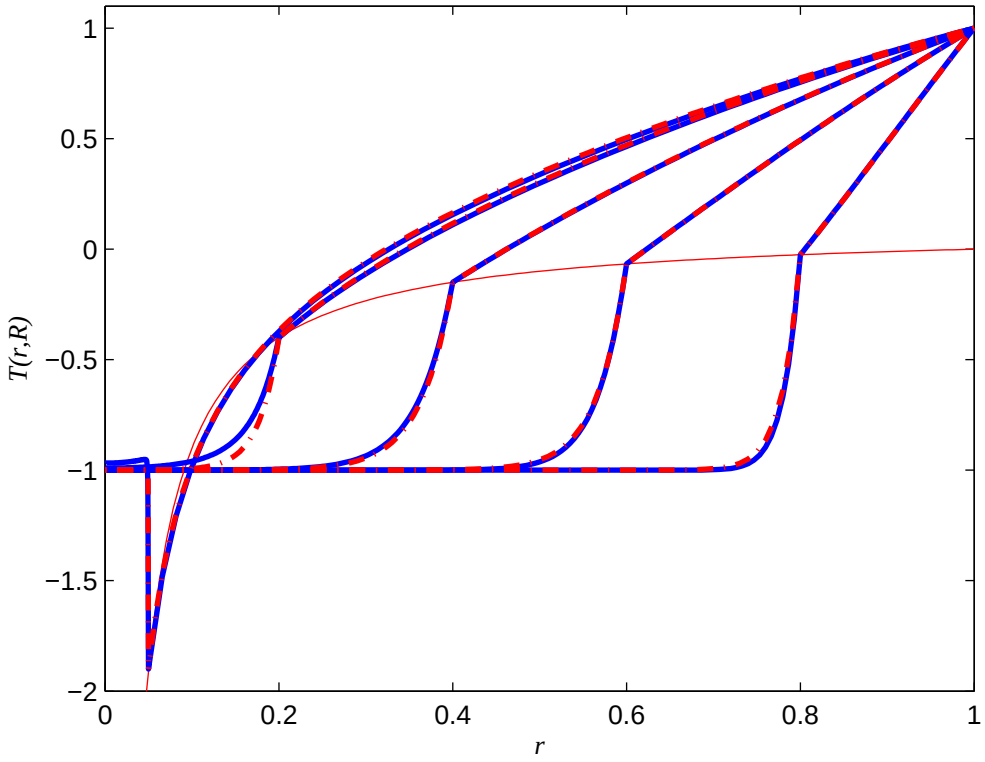

Figure 5.4: Temperature profiles for $\alpha = 1$, $\kappa = 0.05$, $\delta = 1$, $V = -1$, $\sigma = 0.1$ at different positions R=0.1, 0.2, 0.4, 0.6 and 0.8. The solid curves indicate the numerical solution to the full two-phase problem (4.1)-(4.7), while the dashed curves represent numerical solutions to the limiting one-phase problem derived in Chapter 3

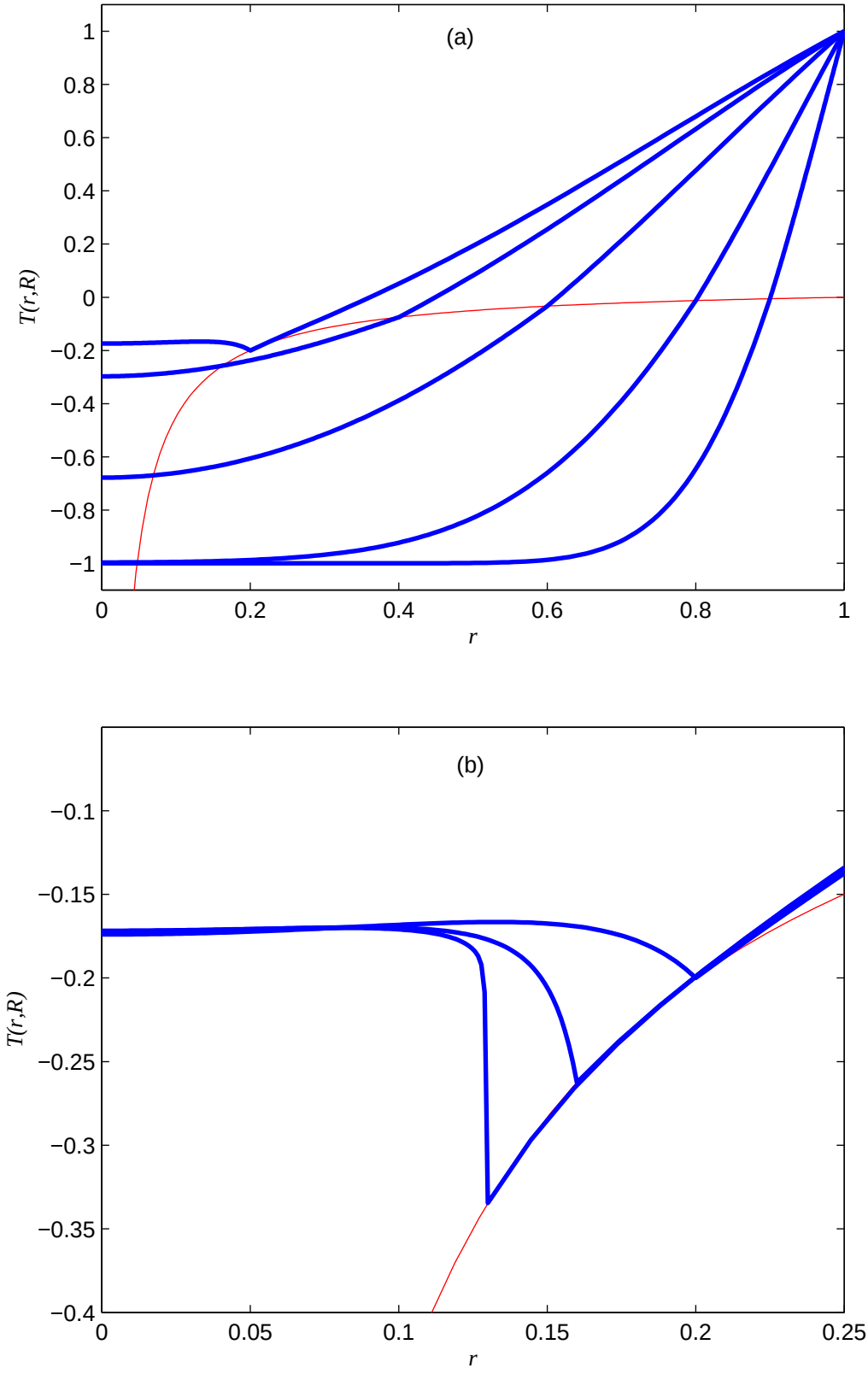

Figure 5.5: Temperature profiles for $\alpha = 0.1$, $\kappa = 1$, $\delta = 1$, $V = -1$, $\sigma = 0.05$. The thick curves represent the numerical solution, while the thin curve denotes the melting temperature. Part (a) is drawn for $R = 0.2$, 0.4, 0.6, 0.8 and 0.9, while part (b) is for $R = 0.13$, 0.16 and 0.2.

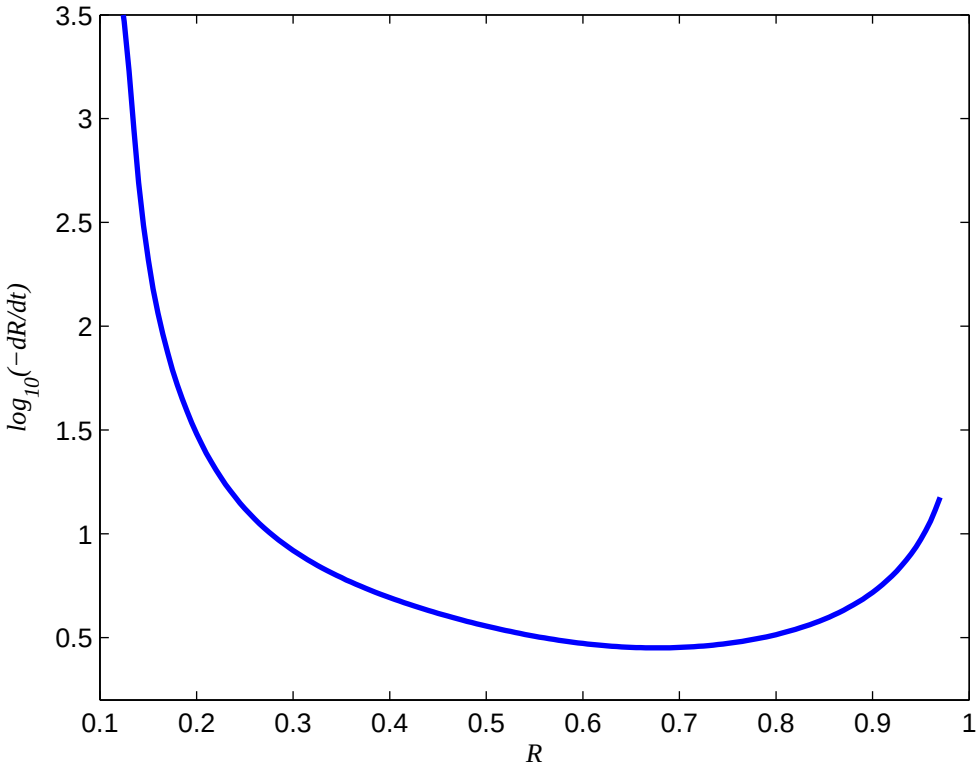

Figure 5.6: Plot of the interface speed $\dot{R}$ versus R for $\alpha = 0.1$, $\kappa = 1$, $\delta = 1$, $V = -1$, $\sigma = 0.05$.

Chapter 6

Concluding remarks

6.1 Summary

Based on the assumption that heat transfers only via conduction in a pure material, the melting or freezing of particles, especially nanoparticles, is investigated from the perspective of Stefan problems. Analytical or semi-analytical methods (small-time perturbation expansions, large Stefan number limit and integral iterative approach) and numerical schemes (enthalpy formulation and front-fixing method) are utilized to study the melting and freezing problems in a spherical or cylindrical domain. The results from these methods are in good agreement to some extent and show some interesting results.

6.1.1 Effect of the surface tension on the temperature distribution

The surface tension has a considerable effect on the temperature distribution. Chapter 2 investigates the classical two-phase solidification problem (the corresponding melting is equivalent). In this case, the temperature at the solid/liquid interface is equal to the fusion temperature and the temperature in the liquid phase is always higher than that in the solid phase. Moreover, the temperatures in the two phases are a monotone function of time and space.

However, when taking into account the effect of surface tension, the temperature at the solid/liquid interface decreases when the interface becomes close to the centre of the nanoparticle, see Chapters 3-5. In addition, the surface tension have a great effect on the temperature in the particle, especially in the solid phase. Take the problem studied in Chapters 3-5 for example. During the initial melting stage, the

particle absorbs heat and the temperature in both phases increases with time. When the solid/liquid interface moves inward, the temperature at the interface decreases leading to the decrease of the temperature in the solid phase near the interface. When the melting temperature continues to decrease, there is a point in time after which the particle is superheated, with the temperature everywhere greater than the melting temperature. This is called superheating phenomenon which has been confirmed in [112, 113, 114].

6.1.2 Effect of the surface tension on the interface speed

Chapter 3 shows that for the melting of nanoparticles, the varying surface tension does not have a significant effect on the speed of the solid/liquid interface in a small time. However, as the interface position R decreases, surface tension becomes more important and has a dramatic effect on the speed of the interface. Moreover, there exists a critical position with a radius R_c where a blow-up occurs and the speed of the interface becomes infinite. For the two -phase melting problem studied in in Chapters 4 and 5, it is still found that a finite blow-up will happen when the interface comes to a critical position R_c. This may explain the interesting phenomenon of "abrupt melting" observed in experiments [7].

6.1.3 Potential applications and future research

The study on size-dependent melting of nanoparticles is important not just from a fundamental point of view. It offers new possibilities for drug delivery and targeted destruction of cancer tumors: melted particles will release their drug load much faster than solid particles due to the higher diffusion coefficient of the drug molecules inside the liquid carrier. When solid particles circulating in the bloodstream reach a site where the temperature is higher than the melting temperature of the particle matrix e.g., due to an external warming of that sites they will suddenly melt and rapidly release their drug load. Such drug delivery systems require carrier particles with a narrow melting temperature range around approximately 39-40 °C.

This thesis mainly deals with nanoparticles with a spherical or cylindrical shape under certain assumptions, such as their density for the liquid phase is a constant, and the liquid phase does not flow away. Another important future issue is what

is the melting point when the particle size approaches zero. Thus, possible future research will be undertaken on the following topics:

1. Two/three dimensional melting of particles with arbitrary shapes;
2. Two/three dimensional melting of particles with contact angles on the substrates;
3. The melting of particles by considering the effect of density change (this means that the fluid flow cannot be ignored).

Appendices and References

Appendix A

Derivation of (2.30) in Chapter 2

The leading order behaviour of $\hat{T}(0;\beta)$ as $\beta \to \infty$ is determined by considering

$$\int_0^1 R(1-R)^2 \sum_{n=1}^{\infty} \exp\left\{n^2\pi^2\kappa\beta(1-R+\ln R)\right\} \mathrm{d}R, ,$$

which comes from combining (4.33) and (2.29). The argument of the exponential is maximum at the endpoint $R = 1$, but the infinite sum does not converge at this value. Thus some care must be taken.

We note that for $\beta \gg 1$ the maximum of the integrand occurs roughly at

$$R = 1 - \sigma, \quad \sigma = \frac{\sqrt{2}}{\pi\kappa^{1/2}\beta^{1/2}}.$$

Thus, in order to proceed, we divide the range of integration into two parts: the first is for R between 0 and $1-\sigma$, and the other for R between $1-\sigma$ and 1. For the first part, the major contribution arises near the upper limit $1-\sigma$. We cannot apply Laplace's method directly, as $1-\sigma$ is dependent on β. However, since $1-\sigma \to 1$ as $\beta \to \infty$, we may expand $1 - R + \ln R$ about $R = 1$, so that

$$\int_0^{1-\sigma} R(1-R)^2 \mathrm{e}^{n^2\pi^2\kappa\beta(1-R+\ln R)} \mathrm{d}R \sim \int_0^{1-\sigma} R(1-R)^2 \mathrm{e}^{-n^2\pi^2\kappa\beta(1-R)^2/2} \mathrm{d}R$$

$$\sim \frac{1}{\sqrt{2}\pi^3\kappa^{3/2}\beta^{3/2}} \left(\frac{2\mathrm{e}^{-n^2}}{n^2} + \frac{\pi^{1/2}}{n^3}(1 - \mathrm{erf}(n)) \right) \quad \text{as} \quad \beta \to \infty.$$

For the second part, we use the property (2.20) to write the integrand in terms of a rapidly converging series. By expanding the integrand about $R = 1$ we find

$$\int_{1-\sigma}^1 R(1-R)^2 \sum_{n=1}^{\infty} \mathrm{e}^{n^2\pi^2\kappa\beta(1-R+\ln R)} \, \mathrm{d}R \sim \frac{1}{\sqrt{2}\pi^3\kappa^{3/2}\beta^{3/2}} \left(\pi^{1/2} - \frac{2}{3} \right) \quad \text{as} \quad \beta \to \infty.$$

The result (2.30) follows.

Appendix B

High-order solutions for large Stefan number limit in Chapter 3

Here we present solutions associated with the large Stefan number expansions. For the spherical case the second-order solutions are

$$\begin{aligned}\hat{T}_2 &= \frac{R+\sigma(1-R)}{6rR^5}\left(\frac{1-r}{1-R}\right) \\ &\times \left\{\left(\frac{R+2\sigma(1-R)(1-R-3R^2)}{6} - R^3(\sigma(1-\delta)+\delta V(R))\right)\right. \\ &\times \left.\left[1-\left(\frac{1-r}{1-R}\right)^2\right] + \frac{R(4R-1)+2\sigma(1-R)(2R-1)}{20}\left[1-\left(\frac{1-r}{1-R}\right)^4\right]\right\}, \qquad \text{(B.1)}\\ \hat{t}_2 &= -\frac{(1-R)(2-R)}{45R} + \frac{1}{45(1-\sigma)}\left\{\sigma\ln R + \frac{1}{\sigma}\ln\left[\frac{R+\sigma(1-R)}{R}\right]\right\}, \qquad \text{(B.2)}\end{aligned}$$

while the first-order solutions for the cylindrical case are

$$\hat{T}_1 = \frac{R+\sigma(1-R)}{4R^4\ln^2 R}\left[\frac{R+\sigma(1-R)}{\ln R}+\sigma\right]\left\{1-r^2+\left[r^2-R^2-\frac{1-R^2}{\ln R}\right]\ln r\right\} \qquad \text{(B.3)}$$

$$\begin{aligned}\hat{t}_1 &= \frac{1}{4}\left[(1+R)^2+\frac{1-R^2}{\ln R}\right] - \sigma(1-\delta)\hat{t}_0 + \delta\int_R^1 \frac{\xi^2\ln\xi}{\xi+\sigma(1-\xi)}V(\xi)\mathrm{d}\xi \\ &+ \frac{\sigma}{4}\int_R^1\left[4\xi^2\ln\xi - 2\xi - 2\xi\ln\xi + \frac{\xi}{\ln\xi} - \frac{1}{\xi\ln\xi}\right]\frac{\mathrm{d}\xi}{\xi+\sigma(1-\xi)}. \qquad \text{(B.4)}\end{aligned}$$

This last integral may be simplified somewhat, but these details are not included here.

Appendix C

Functions for high-order iterations in Chapter 3

The following functions are used in the iteration scheme:

$$
\begin{aligned}
h_1 &= 3(R-1)^2[(R-1)^2(60R^2-8R+7)+3(r-1)^2(4R-1)]\sigma^2 \\
&+ (R-1)\{6R[(R-1)^2(60R^2-4R+7)+3(r-1)^2(2R-1)](\alpha-\sigma(1-\delta) \\
&- \delta V(R))+(R-1)^2(144R^2-R+7)-3(r-1)^2(12R^2-3R+1)\}\sigma \\
&+ 3R^2\{(R-1)^2[60R^2(\alpha-\sigma(1-\delta)-\delta V(R))^2+(48R-7)(\alpha-\sigma(1-\delta) \\
&- \delta V(R))+7]+3(r-1)^2[(1-4R)\beta-3]\}+3R^2(1-R)[\sigma(R-1)-R] \\
&\times[3(r-1)^2-7(R-1)^2]\delta\frac{dV(R)}{dR}, \qquad \text{(C.1)} \\
h_2 &= 135R^2(R-1)^3\sigma^3+3(R-1)^2[135(\alpha-\sigma(1-\delta)-\delta V(R))R^3+45R^2 \\
&+ R+1]\sigma^2+(R-1)[405(\alpha-\sigma(1-\delta)-\delta V(R))^2R^4+270(\alpha-\sigma(1-\delta) \\
&- \delta V(R))R^3+3(\alpha-\sigma(1-\delta)-\delta V(R))R^2+42R^2+6(\alpha-\sigma(1-\delta) \\
&- \delta V(R))R+2R+1]\sigma+3R^2[1+45R^3(\alpha-\sigma(1-\delta)-\delta V(R))^3 \\
&+ 45R^2(\alpha-\sigma(1-\delta)-\delta V(R))^2+(-1+14R)(\alpha-\sigma(1-\delta)-\delta V(R))] \\
&+ 3R^2(R-1)[(R-1)\sigma-R]\delta\frac{dV(R)}{dR}, \qquad \text{(C.2)} \\
h_3 &= 2(R-1)[(R-1)^2(-30R^2-4R+7)+3(r-1)^2(2R-1)]\sigma \\
&- R[(R-1)^2(12R+7)+3(r-1)^2(4R-1)]+60(\sigma(1-\delta) \\
&+ \delta V(R))R^3(R-1)^2, \qquad \text{(C.3)}
\end{aligned}
$$

$$\begin{aligned} h_4 &= [2R^3 \ln R - R^2 \ln R - 2R^2(\ln R)^3 - R^3 + R^2 + R - 1 - \ln R - 2R^3(\ln R)^2 \\ &+ 4(\ln R)^3 R^3]\sigma + 2R^3(\ln R)^2 - R + 4(\ln R)^3 R^3(\alpha - \sigma(1-\delta) - \delta V(R)) \\ &- 2R^3 \ln R + R^3. \end{aligned} \tag{C.4}$$

Appendix D

The numerical front-fixing method

As there are no exact analytical solutions available for the two-phase Stefan problem of nanoparticle melting, the numerical results are obtained by employing a front-fixing method. The idea of this approach is to fix the moving boundary by making the following Landau transformations [82]

$$\eta = \frac{r}{R(t)} \quad v(\eta, t) = T_s(r, t) \quad \text{(solid)}, \quad \zeta = \frac{r-1}{R(t)-1} \quad u(\zeta, t) = T_l(r, t) \quad \text{(liquid)},$$

so that for the liquid phase ($R(t) \leq r \leq 1$) $r = R(t)$ becomes $\zeta = 1$ and $r = 1$ becomes $\zeta = 0$, and for the solid phase ($0 \leq r \leq R(t)$) $r = R(t)$ becomes $\eta = 1$ and $r = 0$ becomes $\eta = 0$. The domains $0 \leq \eta \leq 1$ and $0 \leq \zeta \leq 1$ are divided into N_1 and N_2 sub-regions. By substituting the above transformations into equations (3.7) and (3.8), and then using forward finite differences and central differences for the temperature derivatives with respect to time and space respectively, straightforward formulations for the solid and liquid phases are easily obtained as follows

$$\begin{aligned} v_i^{k+1} &= v_i^k + \frac{\kappa F_1}{\delta R_k^2}(v_{i-1}^k - 2v_i^k + v_{i+1}^k) \\ &+ \frac{\Delta\eta F_1}{2R_k}\left[\eta_i \dot{R}_k + \frac{m\kappa}{\delta\eta_i R_k}\right](v_{i+1}^k - v_{i-1}^k), \end{aligned} \tag{D.1}$$

$$\begin{aligned} u_i^{k+1} &= u_i^k + \frac{F_2}{(R_k^2 - 1)}(u_{i-1}^k - 2u_i^k + u_{i+1}^k) \\ &+ \frac{\Delta\zeta F_2}{2(R_k - 1)}\left[\zeta_i \dot{R}_k + \frac{m}{1 + \zeta_i(R_k - 1)}\right](u_i^{k+1} - u_i^{k-1}), \end{aligned} \tag{D.2}$$

where $F_1 = \Delta t/\Delta\eta^2$ and $F_2 = \Delta t/\Delta\zeta^2$. At the origin and the surface of the particle, the temperatures are expressed by

$$v_1^{k+1} = v_1^k + \frac{m\kappa F_1}{\delta R_k^2}(v_2^k - v_1^k), \quad u_1^{k+1} = 1, \tag{D.3}$$

and at the solid-melt interface, the equilibrium temperature becomes

$$v_{N_1+1}^{k+1} = v_{N_2+1}^{k+1} = \sigma\left(1 - \frac{1}{R_{k+1}}\right). \tag{D.4}$$

The speed of the solid-melt interface is also expressed in terms of finite differences as

$$\frac{dR_k}{dt} = \left\{\frac{(1-\delta)\sigma}{R_k} - \alpha\right\}^{-1}\left\{\frac{3u_{N_2-1}^k - 4u_{N_2}^k + u_{N_2+1}^k}{2\Delta\zeta(R_k-1)} - \kappa\frac{3v_{N_1+1}^k - 4v_{N_1}^k + u_{N_1-1}^k}{2\Delta\eta R_k}\right\}. \tag{D.5}$$

We see that, given the interface position R_k and the temperature distributions u_i^k, v_i^k at a particular time step, we can obtain the interface position R_{k+1} through $R_{k+1} = R_k + \Delta t * dR_k/dt$ and the temperature profiles at the next time step using equations (D.1)-(D.4). By using the Von Neumann's method [100] a suitable time step is chosen to make the numerical scheme stable

$$\begin{aligned} \Delta t &\leq \frac{2R^2\Delta\eta^2\kappa/\delta}{4\kappa^2/\delta^2 + \Delta\eta^2R^2\left(\dot{R}^2 + m^2\kappa^2/[\delta^2\Delta\eta^2R^2]\right)}, \quad \text{(solid phase)} \\ \Delta t &\leq \frac{2(R-1)^2\Delta\zeta^2}{4 + \Delta\zeta^2(R-1)^2\left(\dot{R}^2 + m^2/R^2\right)}, \quad \text{(liquid phase)} \end{aligned} \tag{D.6}$$

where $m = 1$ and $m = 2$ are for cylindrical and spherical cases, respectively. As there is no liquid phase when the melting begins and the program needs the initial information of the solid and liquid phases, we create an "initial condition" by assuming that the solid/liquid interface moves forward a very small step. The time required and temperature distributions can be calculated using the small-time solutions so that the program can be run.

Bibliography

[1] V. Rodrigues, J. Bettini, A. R. Rocha, L. G. C. Rego and D. Ugarte, 2002 "Quantum conductance in silver nanowires: Correlation between atomic structure and transport properties", *Phys. Rev. B*, **65**, 153402.

[2] V. M. Rotello, editor, 2004 *Nanoparticles: building blocks for nanotechnology*, *Springer*.

[3] C. Q. Sun, Y. Shi, C. M. Li, S. Li and T. C. A. Yeung, 2006 "Size-induced undercooling and overheating in phase transitions in bare and embedded clusters", *Phys. Rev. B*, **73**, 075408.

[4] S. R. Sershen, S. L. Westcott, N. J. Halas and J. L. West, 2000 "Temperature-sensitive polymer-nanoshell composites for photothermally modulated drug delivery", in "World Biomaterials Congress 2000", pp. 15–20, Kamuela.

[5] F. B. Hsiao, C. P. Jen, D. B. Wang, C. H. Chuang, Y. C. Lee, C. P. Liu and H. J. Hsu, 2006 "An analytical modeling of heat transfer for laser-assisted nanoimprinting processes", *Comput. Mech.*, **37**, 173–181.

[6] D. P. O'Neal, L. R. Hirsch, N. J. Halas, J. D. Payne and J. L. West, 2004 "Photo-thermal tumor ablation in mice using near infrared-absorbing nanoparticles", *Cancer Letters*, **209**, 171–176.

[7] R. Kofman, Y. Lereah and A. Stella, 1999 "Melting of clusters approaching 0D", *Eur. Phys. J. D.*, **9**, 441–444.

[8] M. Takagi, 1954 "Electron-diffusion study of liquid-solid transition of thin metal films", *J. Phys. Soc. Jpn.*, **9**, 359–363.

[9] M. Blackman and A. E. Curzon, 1959 *Structure and properties of thin films*, *John Wiley*, New York.

[10] K. J. Hanszen, 1960 "Theoretische untersuchungen über den schmelzpunkt kleiner kügelchen ein beitrag zur thermodynamik der grenzflächen", *Zeitschrift für Physik*, **157**, 523–553.

[11] C. R. M. Wronski, 1967 "The size dependence of the melting point of small particles of tin", *Br. J. Appl. Phys.*, **18**, 1731–1737.

[12] P. A. Buffat and J. P. Borel, 1976 "Size effect on the melting temperature of gold particles", *Phys. Rev. A*, **13**, 2287–2298.

[13] C. L. Clevland, W. D. Luedtke and U. Landman, 1999 "Melting of gold clusters", *Phys. Rev. B*, **60**, 5065–5077.

[14] F. Ercolessi, W. Andreoni and E. Tosatti, 1991 "Melting of small gold particles: mechanism and size effects", *Phys. Rev. Lett.*, **66**, 911–914.

[15] W. Hu, S. Xiao, J. Yang and Z. Zhang, 2005 "Melting evolution and diffusion behaviour of vanadium nanoparticles", *Eur. Phys. J. B*, **45**, 547–554.

[16] L. J. Lewis, P. Jensen and J. L. Barrat, 1997 "Melting, freezing, and coalescence of gold nanoclusters", *Phys. Rev. B*, **56**, 2248–2257.

[17] S. Toxværd, 1983 "Size-dependent properties of a two-dimensional solid near melting", *Phys. Rev. Lett.*, **51**, 1971–1974.

[18] T. Bachels and H. J. Güntherodt, 2000 "Melting of isolated tin nanoparticles", *Phys. Rev. Lett.*, **85**, 1250–1253.

[19] S. L. Lai, J. Y. Guo, V. Petrova, G. Ramanath and L. H. Allen, 1996 "Size-dependent melting properties of small tin particles: nanocalorimetric measurements", *Phys. Rev. Lett.*, **77**, 99–102.

[20] E. A. Olson, M. Y. Efremov, M. Zhang, Z. Zhang and L. H. Allen, 2005 "Size-dependent melting of Bi nanoparticles", *J. Appl. Phys.*, **97**, 034304.

[21] Q. Jiang, J. C. Li and B. Q. Chi, 2002 "Size-dependent cohesive energy of nanocrystals", *Chem. Phys. Lett.*, **366**, 551–554.

[22] L. H. Liang, J. C. Li and Q. Jiang, 2003 "Modeling of melting enthalpy of organic nanowire", *Phys. Status Solidi(B)*, **236**, 583–588.

[23] P. R. Couchman and W. A. Jesser, 1977 "Thermodynamic theory of size dependence of melting temperature in metals", *Nature*, **269**, 481–483.

[24] R. R. Vanfleet and J. M. Mochel, 1995 "Thermodynamics of melting and freezing in small particles", *Surf. Sci*, **341**, 40–50.

[25] M. Wautelet, 1991 "Estimatiion of the variation of the melting temperature with the size of small particles, on the basis of a surface-phonon instability model", *J. Phys. D*, **24**, 343–346.

[26] L. I. Rubinstein, 1971 *The Stefan problem*, volume **27**, *Translations of Mathematical Monographs*, USA.

[27] S. C. Gupta, 2003 *The classical Stefan problem: basic concepts, modelling and analysis*, *Elsevier*, Amsterdam.

[28] J. M. Hill, 1987 *One-dimensional Stefan problems: an introduction*, *Longman Scientific and Technical*, Essex.

[29] K. O'Neill, 1983 "Boundary integral equation solution of moving boundary phase change problems", *Int. J. Numer. Methods Eng.*, **19**, 1825–1850.

[30] R. S. Gupta and D. Kumar, 1980 "A modified variable time step method for the one-dimensional Stefan problem", *Comput. Methods Appl. Mech. Eng.*, **23**, 101–109.

[31] V. Alexiades and A. D. Solomon, 1993 *Mathematical modeling of melting and freezing processes*, *Hemisphere Publishing Corporation*, Washington.

[32] J. Crank, 1984 *Free and moving boundary problems*, *Clarendon Press*, Oxford.

[33] H. S. Carslaw and J. C. Jaeger, 1959 *Conduction of heat in solids*, *Clarendon Press*, Oxford.

[34] L. N. Tao, 1980 "The analyticity of solutions of the Stefan problem", *Arch. Ration. Mech. Anal.*, **72**, 285–301.

[35] R. Fazio, 1998 "A similarity approach to the numerical solution of free boundary problems", *SIAM Review*, **40**, 616–635.

[36] J. M. Savino and R. Siegel, 1969 "An analytical solution for solidification of a moving warm liquid onto an isothermal cold wall", *Int. J. Heat Mass Transfer*, **12**, 803–809.

[37] Y. P. Shih and S. Y. Tsay, 1971 "Analytical solutions for freezing a saturated liquid inside or outside cylinders", *Chem. Eng. Sci.*, **76**, 809–816.

[38] Y. P. Shih and T. C. Chou, 1971 "Analytical solutions for freezing a saturated liquid inside or outside sphere", *Chem. Eng. Sci.*, **26**, 1787–1793.

[39] J. N. Dewynne, 1985 *On an integral formulation for heat-diffusion moving boundary problems*, Ph.D. thesis, *University of Wollongong*, NSW, Australia.

[40] T. R. Goodman, 1958 "The heat-balance integral and its application to problems involving a change of phase", *Trans. of the ASME*, **80**, 335–342.

[41] T. R. Goodman and J. J. Shea, 1960 "The melting of finite slabs", *J. Appl. Mech.*, **27**, 16–27.

[42] W. W. Yuen, 1981 "Application of the heat-balance integral to melting problems with initial subcooling", *Int. J. Heat Mass Transfer*, **23**, 1157–1160.

[43] D. S. Tsai and W. Strieder, 1986 "Application of heat balance integral in melting with initial subfreezing", *Int. Com. Heat Mass Transfer*, **13**, 265–280.

[44] D. S. Riley and P. W. Duck, 1977 "Application of the heat-balance integral method to the freezing of a cuboid", *Int. J. Heat Mass Transfer*, **20**, 294–296.

[45] C. Charach and P. Zoglin, 1985 "Solidification in a finite, initially overheated slab", *Int. J. Heat Mass Transfer*, **28**, 2261–2268.

[46] C. Konrad, Y. Zhang and Y. Shi, 2007 "Melting and resolidification of a subcooled metal powder particle subjected to nanosecond laser heating", *Int. J. Heat Mass Transfer*, **50**, 2236–2245.

[47] A. S. Wood, 2001 "A new look at the heat balance integral method", *Appl. Math. Model.*, **25**, 815–824.

[48] S. Ostrach and D. G. McConnell, 1965 "Melting ablation about decelerating spherical bodies", *A.I.A.A. Journal*, **3**, 1883–1889.

[49] T. Wu and Y. Z. Chen, 2003 "Analytical studies of gibbs-thomson effect on the diffusion controlled spherical phase growth in a subcooled medium", *Heat Mass Trans.*, **39**, 665–674.

[50] T. Wu, H. C. Liaw and Y. Z. Chen, 2002 "Thermal effect of surface tension on the inward solidification of spheres", *J. Heat Mass Transfer*, **45**, 2055–2065.

[51] G. B. Davis and J. M. Hill, 1982 "A moving boundary problem for the sphere", *IMA J. Appl. Math.*, **29**, 99–111.

[52] J. M. Hill and A. Kucera, 1983 "Freezing a saturated liquid inside a sphere", *Int. J. Heat Mass Transfer*, **26**, 1631–1637.

[53] V. Voller and M. Cross, 1981 "Accurate solutions of moving boundary problems using the enthalpy method", *Int. J. Heat Mass Transfer*, **24**, 545–556.

[54] R. I. Pedroso and G. A. Domoto, 1973 "Inward spherical solidification-solution by the method of strained coordinates", *Int. J. Heat Mass Transfer*, **16**, 1037–1043.

[55] D. S. Riley, F. T. Smith and G. Poots, 1974 "The inward solidification of spheres and circular cylinders", *Int. J. Heat Mass Transfer*, **17**, 1507–1516.

[56] C. L. Huang and Y. P. Shih, 1975 "A perturbation method for spherical and cylindrical solidification", *Chem. Eng. Sci.*, **30**, 897–906.

[57] K. Stewartson and R. T. Waechter, 1976 "On Stefan's problem for spheres", *Proc. R. Soc. Lond. A*, **348**, 415–426.

[58] A. M. Soward, 1980 "A united approach to Stefan's problem for spheres and cylinders", *Proc. R. Soc. Lond. A*, **373**, 131–147.

[59] S. Weinbaum and L. M. Jiji, 1977 "Singular perturbation theory for melting or freezing in finite domains initially not at the fusion temperature", *J. Appl. Mech.*, **3**, 25–30.

[60] L. M. Jiji, 1970 "On the application of perturbation of free-boundary problems in radial system", *Journal of Franklin Institute*, **289**, 281–290.

[61] M. Prud'homme and T. Nguyen, 1989 "Solutions par perturbations singulières pour un problème de Stefan généralisé", *Int. J. Heat Mass Transfer*, **32**, 1501–1515.

[62] J. Gammon and J. A. Howarth, 1996 "The inward solidification of spheres with a slightly perturbed temperature distribution at the boundary", *Int. Comm. Heat Mass Transfer*, **23**, 397–406.

[63] J. Gammon and J. A. Howarth, 1996 "The inward solidification of cylinders with a slightly perturbed temperature distribution at the boundary", *Int. Comm. Heat Mass Transfer*, **23**, 387–396.

[64] J. Gammon and J. A. Howarth, 1995 "The two-dimensional Stefan problem with slightly varying heat flux", *Int. Comm. Heat Mass Transfer*, **22**, 629–638.

[65] S. Kharche and J. A. Howarth, 2000 "The inward solidification of a liquid cylinder with periodic axial perturbation of the boundary temperature or heat flux", *Int. Comm. Heat Mass Transfer*, **27**, 903–912.

[66] S. Kharche and J. A. Howarth, 2000 "The inward solidification of a liquid cylinder with periodic axial perturbation of the boundary geometry, and constant boundary temperature or heat flux", *Int. Comm. Heat Mass Transfer*, **27**, 913–923.

[67] D. L. Feltham and J. Garside, 2001 "Analytical and numerical solutions describing the inward solidification of a binary melt", *Chem. Eng. Sci.*, **56**, 2357–2370.

[68] J. M. Hill and J. N. Dewynne, 1987 *Heat conduction*, *Blackwell Scientific Publications*, Oxford.

[69] R. M. Furzeland, 1980 "A comparative study of numerical methods for moving boundary problems", *IMA J. Appl. Math.*, **26**, 411–429.

[70] S. Kutluay, A. R. Bahadir and A. Özdes, 1997 "The numerical solution of one-phase classical Stefan problem", *J. Comput. Appl. Math.*, **81**, 135–144.

[71] C. Y. Li, S. V. Garimella and J. E. Simpson, 2003 "Fixed-grid front-tracking algorithm for solidification problems, part i: method and validation", *Numer. Heat Transfer*, **43**, 117–141.

[72] W. D. Murray and F. Landis, 1959 "Numerical and machine solutions of transient heat conduction problems involving melting and freezing", *J. Heat Transfer*, **81**, 106–112.

[73] L. C. Tao, 1967 "Generalized numerical solutions of freezing a saturated liquid in cylinders and spheres", *AIChE Journal*, **13**, 165–169.

[74] L. C. Tien and S. W. Churchill, 1985 "Freezing front motion and heat transfer outside an infinite, isothermal cylinder", *AIChE Journal*, **11**, 790–793.

[75] A. Lazaridis, 1970 "A numerical solution of the multidimensional solidification (or melting) problem", *Int. J. Heat Mass Transfer*, **13**, 1459–1477.

[76] D. Womble, 1989 "A front-tracking method for multiphase free boundary problems", *SIAM J. Numer. Anal.*, **26**, 380–396.

[77] H. G. Askar, 1987 "The front-tracking scheme for the one-dimensional freezing problem", *Int. J. Numer. Methods Eng.*, **24**, 859–869.

[78] N. R. Eyres, D. R. Hartree, J. Ingham, R. Jackson, R. J. Sarjant and J. B. Wagstaff, 1946 "The calculation of variable heat flow in solids", *Philos. Trans. R. Soc. Lond.*, **A240**, 1–57.

[79] A. S. Wood, S. J. Ritchie and G. E. Bell, 1981 "An efficient implementation of the enthalpy method", *Appl. Math. Modelling*, **17**, 301–305.

[80] K. H. Tacke, 1985 "Discretization of the explicit enthalpy method for planar phase change", *Int. J. Numer. Methods Eng.*, **21**, 543–554.

[81] A. A. Rostami, R. Greif and R. E. Russo, 1992 "Modified enthalpy method applied to rapid melting and solidification", *Int. J. Heat Mass Transfer*, **35**, 2161–2172.

[82] H. Landau, 1950 "Heat conduction in a melting solid", *Q. Appl. Math.*, **8**, 81–94.

[83] J. Crank, 1957 "Two methods for the numerical solution of moving boundary problems in diffusion and heat flow", *J. Mech. Appl. Math.*, **10**, 220–231.

[84] J. N. Dewynne and J. M. Hill, 1986 "Integral formulations and bounds for two phase Stefan problems initially not at their fusion temperature", *Acta Mech.*, **58**, 201–228.

[85] E. T. Whittaker and G. N. Watson, 1952 *A course in modern analysis*, *Cambridge University Press*, Cambridge, 4th edition.

[86] A. H. Nayfeh, 1973 *Perturbation Methods*, *Wiley*, New York.

[87] M. A. Herrero and J. J. L. Velázquez, 1997 "On the melting of ice balls", *SIAM J. Math. Anal.*, **28**, 1–32.

[88] J. R. King and J. D. Evans, 2005 "Regularization by kinetic undercooling of blow-up in the ill-posed Stefan problem", *SIAM J. Appl. Math.*, **65**, 1677–1707.

[89] J. D. Evans and J. R. King, 2000 "Asymptotic results for the Stefan problem with kinetic undercooling", *Q. J. Mech. Appl. Math.*, **53**, 449–473.

[90] J. Struckmeier and A. Unterreiter, 2001 "A singular-perturbed two-phase Stefan problem", *Appl. Math. Lett.*, **14**, 217–222.

[91] A. Kucera and J. M. Hill, 1986 "On inward solidifying cylinders and spheres initially not at their fusion temperature", *Int. J. Non-linear Mech.*, **21**, 73–82.

[92] M. Abramowitz and I. Stegun, 1965 *Handbook of mathematical funcions*, Dover Publications, New York.

[93] S. W. McCue, J. R. King and D. S. Riley, 2005 "The extinction problem for three-dimensional inward solidification", *J. Eng. Math.*, **52**, 389–409.

[94] J. M. Hill and A. Kucera, 1983 "The time to complete reaction or solidification of a sphere", *Chem. Eng. Sci.*, **38**, 1360–1362.

[95] J. N. Dewynne and J. M. Hill, 1984 "On an integral formulation for moving boundary problems", *Q. Appl. Math.*, **41**, 443–455.

[96] J. M. Hill and J. N. Dewynne, 1986 "On the inward solidification of cylinders", *Q. Appl. Math.*, **64**, 59–70.

[97] L. A. Herraiz, M. A. Herrero and J. J. L. Velázquez, 2001 "A note on the dissolution of spherical crystals", *Proc. Roy. Soc. Edin.*, **131**, 371–389.

[98] V. M. Entov and P. I. Etingof, 1991 "Bubble contraction in hele-shaw cells", *Q. J. Mech. Appl. Math.*, **44**, 507–535.

[99] S. W. McCue, J. R. King and D. S. Riley, 2003 "Extinction behaviour of contracting bubbles in porous media", *Q. J. Mech. Appl. Math.*, **56**, 455–482.

[100] G. D. Smith, 1985 *Numerical solution of partial differential equations: finite difference methods*, *Clarendon Press*, Oxford.

[101] A. S. Okhotin, L. I. Zhmakin and A. P. Ivanyuk, 1991 "The temperature dependence of thermal conductivity of some chemical elements", *Exp. Therm. Fluid Sci.*, **4**, 289–300.

[102] M. E. Gurtin, 1986 "On the two-phase Stefan problem with interfacial energy and entropy", *Arc. Rat. Mech. Anal.*, **96**, 199–241.

[103] S. W. McCue, J. R. King and D. S. Riley, 2003 "Extinction behaviour for two-dimensional solidification problems", *Proc. Roy. Soc. Lond. A*, **459**, 977–999.

[104] D. Andreucci, M. A. Herrero and J. J. L. Velázquez, 2001 "The classical one-phase Stefan problem: a catalog of interface behaviors", *Surv. Math. Ind.*, **9**, 247–337.

[105] M. E. Glicksman and A. Lupulescu, 2003 "Melting in microgravity", *J. Thermophys. Heat Trans.*, **17**, 69–76.

[106] A. Lupulescu, M. E. Glicksman and M. B. Koss, 2005 "Conduction-limited cystallite melting", *J. Cryst. Growth*, **276**, 549–565.

[107] A. Fasano and M. Primicerio, 1977 "General free boundary problems for the heat equation", *J. Math. Anal. Appl.*, **57**, 694–723.

[108] A. Fasano, M. Primicerio and A. A. Lacey, 1981 "New results on some classical parabolic free boundary problems", *Q. Appl. Math.*, **38**, 439–460.

[109] A. Fasano, M. Primicerio, S. D. Howison and J. R. Ockendon, 1990 "Some remarks on the regularization of supercooled one-phase Stefan problems in one dimension", *Q. Appl. Math.*, **48**, 153–168.

[110] M. A. Herrero and J. J. L. Velázquez, 1996 "Singularity formation in the one-dimensional supercooled Stefan problem", *Euro. J. Appl. Math.*, **7**, 119–150.

[111] T. Unruh, H. Bunjes and K. Westesen, 1999 "Observation of size-dependent melting lipid nanoparticles", *J. Phys. Chem. B*, **103**, 10373–10377.

[112] H. W. Sheng, G. Ren, L. M. Peng, Z. Q. Hu and K. Lu, 1996 "Superheating and melting-point depression of Pb nanoparticles embedded in Al matrices", *Philosophical Magazine Letters*, **73**, 179–186.

[113] J. Zhong, L. H. Zhang, Z. H. Jin, M. L. Sui and K. Lu, 2001 "Superheating of ag nanoparticles embedded in Ni matrix", *Acta Materialia*, **49**, 2897–2904.

[114] D. Schebarchov and S. C. Hendy, 2006 "Superheating and solid-liquid phase coexistence in nanoparticles with nonmelting surfaces", *Phys. Rev. Lett.*, **96**, 256101.

List of the author's publications

- S. W. McCue, B. Wu and J. M. Hill, 2007 "Classical two-phase Stefan problem for spheres", *Proceedings of the Royal Society A*, accepted for publication, doi:10.1098/rspa.2007.0315. (included in Chapter 2)

- B. Wu, S. W. McCue, P. Tillman and J. M. Hill, 2007 "Single phase limit for melting nanoparticles", *Applied Mathematical Modelling*, accepted for publication, 2007 . (included in Chapter 3)

- S. W. McCue, B. Wu and J. M. Hill, 2007 "Micro/nano particle melting with spherical symmetry and surface tension", *The IMA Journal of Applied Mathematics*, submitted for publication. (included in Chapter 4)

- S. W. McCue, B. Wu and J. M. Hill, 2008 "Melting of cylindrical nanoparticles", *International Journal of Heat and Mass Transfer*, in preparation. (included in Chapter 5)

- B. Wu, P. Tillman, S. W. McCue and J. M. Hill, 2007 "Nanoparticle melting as a Stefan moving boundary problem", *Journal of Nanoscience and Nanotechnology*, accepted for publication, 2007. (included in Appendix D)

- B. Wu, P. Tillman and J. M. Hill, 2006 "Mathematical Modelling of Nanoparticle Melting", *Proceedings of the 2006 International Conference on Nanoscience and Nanotechnology*, Brisbane, 3-7 July 2006, doi:10.1109/ICONN.2006.340704, 661-664.

- S. W. McCue, B. Wu and J. M. Hill,, 2008 "Asymptotic results for a Stefan problem with surface tension", *XXII International Congress of Theoretical and Applied Mechanics (XXII ICTAM)*, Adelaide, 25-29 August 2008, Australia.